



**UNIVERSIDADE DE BRASÍLIA  
INSTITUTO DE GEOCIÊNCIAS  
PROGRAMA DE PÓS-GRADUAÇÃO EM  
GEOLOGIA**

**CARACTERIZAÇÃO MINERALÓGICA, GEOQUÍMICA E  
POTENCIAL ECONÔMICO DE OCORRÊNCIAS DE TERRAS RARAS  
DO MACIÇO GRANÍTICO PEDRA BRANCA, GOIÁS.**

**TESE DE DOUTORADO**

**NIVIA OLIVEIRA DA COSTA**

**Orientador: Prof.Dr. Nilson Francisquini Botelho**

**BRASÍLIA/DF**

**2019**

Costa, Nivia  
CN735c      CARACTERIZAÇÃO MINERALÓGICA, GEOQUÍMICA E POTENCIAL  
ECONÔMICO DE OCORRÊNCIAS DE TERRAS RARAS DO MACIÇO GRANÍTICO  
PEDRA BRANCA, GOIÁS / Nivia Costa; orientador Nilson  
Botelho. -- Brasília, 2019.  
125 p.

Tese (Doutorado - Doutorado em Geologia) -- Universidade  
de Brasília, 2019.

1. ETRY. 2. Maciço Granítico Pedra Branca. 3. Adsorção  
Iônica. 4. Subprovincia Estanífera de Goiás. I. Botelho,  
Nilson , orient. II. Título.



**UNIVERSIDADE DE BRASÍLIA**

**INSTITUTO DE GEOCIÊNCIAS**

**PROGRAMA DE PÓS-GRADUAÇÃO EM  
GEOLOGIA**

**CARACTERIZAÇÃO MINERALÓGICA, GEOQUÍMICA E  
POTENCIAL ECONÔMICO DE OCORRÊNCIAS DE TERRAS RARAS  
DO MACIÇO GRANÍTICO PEDRA BRANCA, GOIÁS.**

**NIVIA OLIVEIRA DA COSTA**

**Área de concentração: Prospecção e Geologia Econômica**

**Orientador:**

Prof.Dr. Nilson Francisquini Botelho

**Banca examinadora:**

Prof. Dr. Artur Cezar Bastos Neto (UFRGS)

Prof<sup>a</sup>. Dr<sup>a</sup>. Lucy Takehara (CPRM)

Prof. Dr. José Affonso Brod (UFG)

Prof. Dr. Claudinei Gouveia de Oliveira (IGD/UnB-suplente)

**BRASÍLIA/DF  
2019**

*Aos meus pais José e Lindalva,*

*Nelma e Mjed*

## AGRADECIMENTOS

Primeiramente a Deus, por tudo que Ele representa em minha vida.

Aos meus pais José Paulino da Costa e Lindalva Oliveira da Costa pela minha formação como pessoa, a todos da minha família que torcem por mim, em especial a minha irmã Nelma Pacheco, o meu cunhado Geraldo Pacheco e ao meu marido Mjed Mofleh, por estarem sempre comigo, me apoiando nesta minha caminhada.

Ao meu orientador, Prof. Dr. Nilson Francisquini Botelho, pela transmissão de conhecimentos, pela sua compreensão, dedicação e principalmente sua paciência ao longo de todo este trabalho, pois sem o seu apoio seria impossível a finalização desta tese.

À todas as pessoas que contribuíram direta e indiretamente para ao desenvolvimento desta tese, em especial a Prof<sup>a</sup>. Dr<sup>a</sup>. Paola Ferreira Barbosa que não mediu esforços para me auxiliar no laboratório e pela sua colaboração enriquecedora para os artigos desta tese.

Ao Prof. Dr. Jérémie Garnier pelo seu auxílio no Laboratório de Geoquímica do IG/UnB, onde foram realizados os ataques químicos para extrações iônicas e sua colaboração nos resultados destas extrações.

Ao Prof. Dr. Valmir da Silva Souza pela sua ajuda e atenção sempre que precisei.

À Prof. Dra. Adriana Horbe, pela disponibilização do Laboratório de Difração de Raio-X, tanto para análises de Raio-X, quanto para utilização do laboratório para o peneiramento das minhas amostras, enquanto o Laboratório de Separação, chamado de Moinho estava em reforma.

À Prof<sup>a</sup>. Dr<sup>a</sup> Márcia Abrahão Moura, pelo seu apoio incondicional para o meu estabelecimento em Brasília e pela oportunidade de poder fazer parte como aluna de doutorado desta instituição.

Aos técnicos, Rafael Figueras do laboratório de Raios-X, Iris Santos e Jacqueline Machado do laboratório de Microsonda, Myller Tonhá do Laboratório de Geoquímica, Francisca Moraes e Edson Lima, da Oficina de Laminação, sempre disponíveis quando recorria seus préstimos.

À aluna Gisele Godim pela ajuda na preparação das amostras para as análises geoquímicas e microsonda.

A todos os funcionários de Geociências, como a secretária Eldna Pinheiro da pós-graduação, Sergio Brito (Serjão), Wesley Silva, Éderson Araújo (Jacaré), e em especial a Valdirene Lima, Sebastião Souza Filho (Tião), Luis Costa Filho e Maria Mendes, pela disposição em ajudar e resolver problemas burocráticos e pela amizade que me foi depositada.

À CAPES pela concessão de bolsa deste trabalho.

À Universidade de Brasília (UnB) e ao Instituto de Geociências (IG), por meio do Programa de Pós-Graduação em Geologia (PPGG), pela infraestrutura, ensinamentos recebidos e apoio oferecido.

Aos meus colegas da Pós-Graduação que compartilharam comigo momentos de descontração, em especial ao Gabriel Franco pela sua contribuição em ajudar a passar para o inglês o primeiro artigo, ao Hammel Macedo pela amizade sincera e pelo apoio mesmo de longe.

Ao Federico Cuadros que foi muito prestativo quando cheguei ao Instituto de Geociências, mostrando os laboratórios e os lugares importantes na UnB para resolver assuntos acadêmicos.

A todos, o meu muito obrigado.

*Baixem sobre mim as tuas misericórdias, para que eu viva,  
pois na tua lei está o meu prazer. Salmos 119:77*

## SUMÁRIO

AGRADECIMENTOS.....	ii
ÍNDICE DE FIGURAS.....	viii
ÍNDICE DE TABELAS.....	x
RESUMO.....	xi
ABSTRACT.....	xii
<b><u>CAPÍTULO I.....</u></b>	<b><u>1</u></b>
1. INTRODUÇÃO E JUSTIFICATIVAS.....	1
2. OBJETIVOS.....	2
3. CONTEXTO GEOLÓGICO.....	2
4. MATERIAS E MÉTODOS .....	10
4.1. <i>Amostragem de saprolitos e solos da Faixa Placha e arredores.....</i>	10
4.2. <i>Separação de Argila pelo Método de Peneiras .....</i>	10
4.3. <i>Separação da Fração Argila para Análises DRX.....</i>	10
4.4. <i>Difração de Raios-X análise do pó .....</i>	11
4.5. <i>Extrações e análises de troca iônica dos cátions .....</i>	11
4.5.1. <i>Extração em única etapa (fração argila e amostra total).....</i>	11
4.5.2. <i>Extração em 2 etapas .....</i>	12
4.5.2.1. <i>Óxidos de Fe e Mn Amorfos - Etapa 1.....</i>	12
4.5.2.2. <i>Óxidos de Fe e Mn - Etapa 2.....</i>	12
4.6. <i>Geoquímica de rocha total .....</i>	13
4.7. <i>Microsonda e Microscopia Eletrônica de Varredura .....</i>	13
4.8 <i>Desenvolvimento da Tese.....</i>	14
<b><u>CAPÍTULO II.....</u></b>	<b><u>15</u></b>
Abstract.....	15
1. Introduction.....	15

<b>2. Geological setting.....</b>	<b>16</b>
<b>3. The Faixa Placha tin deposit.....</b>	<b>17</b>
<b>4. Materials and methods.....</b>	<b>20</b>
4.1. EPMA and SEM analyses.....	20
4.2. Whole-rock geochemistry.....	20
<b>5. Results.....</b>	<b>21</b>
5.1. Mineralogical characterization.....	21
5.1.1. Zircon ( $ZrSiO_4$ ).....	21
5.1.2. Xenotime-(Y) ( $YPO_4$ ).....	25
5.1.3. Monazite-(Ce) ( $(Ce,La,Nd,Th)PO_4$ ).....	29
5.1.4. Apatite $Ca_5(PO_4)_3(OH,F,Cl)$ .....	29
5.1.5. Thorite ( $ThSiO_4$ ).....	34
5.1.6. REE oxyfluorides.....	34
5.1.7. Unidentified Nb-Y-REE mineral.....	37
5.2 - Whole-rock geochemistry.....	37
<b>6. Discussion and conclusions.....</b>	<b>42</b>
6.1. HREE-bearing minerals.....	42
6.2. LREE-bearing minerals.....	42
<b>7. Concluding remarks.....</b>	<b>44</b>
<b>8. References.....</b>	<b>45</b>

## **CAPÍTULO III.....48**

<b>Abstract.....</b>	<b>48</b>
<b>1. Introduction.....</b>	<b>49</b>
<b>2. Geological Context.....</b>	<b>50</b>
<b>3. Faixa Placha Tin Deposit.....</b>	<b>53</b>
<b>4. Materials and Methods.....</b>	<b>55</b>
4.1. Sampling of saprolites and soils of the Faixa Placha and nearby areas.....	55
4.2. Clay separation by the sieving method.....	55
4.3. Clay fraction separation for X-ray diffraction analysis.....	55
4.4. Powder XRD analysis.....	56
4.5. Cation extractions and ion exchange analysis.....	56
4.5.1. Single-step extraction (clay fraction and total sample).....	56
4.5.2. Two-step extraction.....	57

4.5.2.1. Amorphous oxides of Fe and Mn - Step 1.....	57
4.5.2.2. Fe and Mn oxides - Step 2.....	57
4.6. <i>Whole-rock geochemistry</i> .....	58
4.7. <i>Electron microprobe and scanning electron microscopy</i> .....	58
<b>5. Results</b> .....	<b>58</b>
5.1. <i>Comparisons between granites, greisen, saprolites and soils</i> .....	58
5.2. <i>Faixa Placha weathering profile</i> .....	65
5.3. <i>Geochemical results</i> .....	67
5.4. <i>Single-step ion exchange extraction</i> .....	71
5.5. <i>Two-step sequential extraction</i> .....	75
<b>6. Discussion and Conclusions</b> .....	<b>78</b>
6.1. <i>Comparison of REE enrichment between the Faixa Placha and nearby areas</i> .....	78
6.2. <i>Ion exchange extractions in the Faixa Placha weathering profile</i> .....	80
<b>7. Referências</b> .....	<b>84</b>
<b>5. CONCLUSÕES</b> .....	<b>88</b>
<b>6. REFERÊNCIAS</b> .....	<b>90</b>
<b>ANEXOS</b> .....	<b>93</b>

## ÍNDICE DE FIGURAS

<b>CAPÍTULO I.....</b>	<b>1</b>
Figura 1: Mapa geológico regional (Botelho, 1992).....	5
Figura 2: Mapa geológico simplificado do Maciço Pedra Branca (Botelho 1992).....	5
Figura 3: Amostragem de saprolito na Faixa Placha (A) e utilização do trado para amostragem de solo em superfície de aplainamento nas proximidades da Faixa Placha (B) e (C).....	10
<b>CAPÍTULO II.....</b>	<b>15</b>
<b>Fig. 1.</b> Geological Map of the northeastern portion of the Goiás Tin Province (GTP) showing the location of the Pedra Branca Massif and the distribution of REE occurrences in the A-type granites.....	17
<b>Fig. 2.</b> Geological map of the Pedra Branca Massif with the location of sampling (NC) and schematic geological cross-section (AB) in the region of the Faixa Placha and Bacia Zone.....	<b>Erro! Indicador não definido.</b>
<b>Fig. 3.</b> Aspects of the Faixa Placha Tin Deposit (FPTD). A: greisenized pb1b granite with greisen veinlets; B: abandoned area of ancient artisanal mining exploration; C: detail of the photo B showing black greisen hosted in fracture of the pb1b biotite granite.....	221
<b>Fig. 4.</b> Backscattered electron images (BSE) of REE-bearing minerals from the FPTD. (A) Primary euhedral zircon (Zrn) free of REE-rich minerals; (B to F) relationships between zircon, monazite (Mnz) and xenotime (Xnt); (D) zircon grain, with irregular and altered monazite inclusion, surrounded by secondary monazite agglomerate in a muscovite (Ms) and magnetite (Mgt) mass; (G and H) zircon and hydrothermal monazite from the biotite granite pb1b, associated with apatite rests (Ap), muscovite (Ms), quartz (Qtz), ilmenite (Ilm), and magnetite (Mgt).....	22
<b>Fig. 4 (extended).</b> (I and J) fluorapatite partially replaced by hydrothermal monazite on the edges and fractures; (K and L) Altered thorite (Thr) near zircon grains. Gn: galena; (M and N) Oxyfluorides (Oxf) associated with allanite and xenotime in a quartz-albite-muscovite mass. Aln: allanite; Fl: fluorite; (O) Unidentified Nb-Y-REE mineral.....	23
<b>Fig. 5.</b> Composition of zircons from different types of granites in the Faixa Placha Tin Deposit.....	24
<b>Fig. 6.</b> Concentration of Y <sub>2</sub> O <sub>3</sub> and HREE <sub>2</sub> O <sub>3</sub> in xenotime.....	25
<b>Fig. 7.</b> Domain of REE patterns in all analyzed granites and greisens from the FPTD. (chodrite normalization values of Sun & McDonough (1989)).....	40
<b>Fig. 8.</b> Chondrite normalized REE patterns of parent and altered granites. A and B: samples from the central part of the FPTD; C: samples from the southernmost border of the FPTD; (D): samples from the northern (NC10A) and southern (NC11A) parts of the FPTD.....	41
<b>CAPÍTULO III.....</b>	<b>48</b>
<b>Fig. 1.</b> Geological map of the northern part of the Goiás Tin Province, showing the location of the Pedra Branca Massif.....	52
<b>Fig.2.</b> Geological map of the Pedra Branca massif and schematic cross section (A-B) with detail of the central part of the Faixa Placha (modified from Botelho, 1992).....	54
<b>Fig. 3.</b> Sampling of saprolite in the Faixa Placha (A) and auger soil sampling in planing surface near the Faixa Placha (B) and (C).....	55

<b>Fig. 4.</b> Plot of granites of the Pedra Branca Massif in the Y + Nb versus Rb diagram (Pearce, 1996). VAG, volcanic-arc granite; ORG, ocean ridge granite; WPG, within plate granite, Syn-COLG, syn-collisional granite.....	59
<b>Fig. 5.</b> Chondrite-normalized REE patterns (Boynnton, 1984) of pb1b parental and greisenized granites and their corresponding soils, in the Faixa Placha (B) and nearby areas (A).....	61
<b>Fig. 6.</b> Photography and corresponding columnar section of the weathering profile sampled at the center of the Faixa Placha (NC 17).....	66
<b>Fig. 7.</b> Diagrams showing the variation of the relative REEY concentration in the whole-rock samples from the weathering profile of the Faixa Placha.....	68
<b>Fig. 8.</b> Chondrite-normalized REE patterns (Boynnton, 1984) of the saprolite, soil and laterite in samples from the upper zone (A) and lower zone (B) of the Faixa Placha weathering profile. Comparison with the greisenized granite (N6C) below the weathering profile).....	69
<b>Fig. 9.</b> Chondrite-normalized REE patterns (Boynnton, 1984) of ion-exchangeable from the single extraction in the clay fraction and in the whole-rock samples from the Faixa Placha saprolites and lateritic crust.....	74
<b>Fig. 10.</b> Chondrite-normalized REE patterns of the sequential extraction in amorphous Fe and Mn oxides and in Fe and Mn oxides from the Faixa Placha saprolites and lateritic crust (profile NC17).....	77
<b>Fig. 11.</b> Comparison of the REEY enrichment between the Faixa Placha and nearby areas.....	79
<b>Fig. 12.</b> Correlation between Zr and $(Yb / Ho)_{Gran}$ ratio in granites of the Faixa Placha and nearby areas.....	80
<b>Fig. 13.</b> Concretion of Fe and Mn oxide containing cerianite (CeO <sub>2</sub> ) in fissures.....	83

## ÍNDICE DE TABELAS

<b>CAPÍTULO I.....</b>	<b>1</b>
Tabela 1 Table 1: Extração de unica etapa usando a solução sulfato de amônia.....	12
Tabela 2 Table 2: Extração de 2 etapa.....	13
<b>CAPÍTULO II.....</b>	<b>15</b>
Table 1. EPMA analyses of zircon.....	26
Table 1 (extended). Number of ions on the basis of 16 (O, F).....	27
Table 2. EPMA analyses of xenotime .....	27
Table 3. EPMA analyses of primary monazite.....	30
Table 4. EPMA analyses of hydrothermal monazite.....	31
Table 5: EPMA analyses of fluorapatite .....	33
Table 6. EPMA analyses of thorite .....	34
Table 7. EPMA analyses of oxyfluorides.....	<b>Erro! Indicador não definido.</b>
Table 8. EPMA analyses for the unidentified Nb-Y-REE phase .....	37
Table 9: Chemical composition (major elements, traces and rare earths) of the parent granite, greisenized granites and greisen from Faixa Placha.....	39
<b>CAPÍTULO III.....</b>	<b>48</b>
<b>Table 1.</b> Mineralogy and petrography of granites from the Pedra Branca Suite (adapted from Botelho, 1992; Teixeira and Botelho, 1999; Zapata and Botelho, 2018; Vieira et al., 2019).....	51
<b>Table 2.</b> Experimental conditions of the single-step extraction using the ammonium sulfate solution.....	57
<b>Table 3.</b> Experimental conditions of the two-step extraction.....	57
<b>Table 4.</b> Whole-rock chemical analysis of the biotite granite, greisenized granite, greisen and soil of the Faixa Placha and nearby areas.....	62
<b>Table 5.</b> Chemical analysis of the laterite crust, soil, saprolites and greisenized granite of the Faixa Placha. ....	70
<b>Table 6</b> Results of the single step extraction showing extracted element concentrations (ppm) in the clay and in the whole-rock .....	73
<b>Table 7.</b> Results of the two - step extraction showing extracted element concentrations (ppm) in the amorphous Fe oxide and Mn and Fe and Mn oxide .....	76

## RESUMO

O presente estudo tem como principal enfoque os elementos terras raras (ETR) que ocorrem em importantes concentrações no maciço granítico Pedra Branca, situado na parte leste na Província Estanífera de Goiás, mais precisamente na Subprovíncia Estanífera Paranã. O maciço possui importantes depósitos de estanho e é constituído por granitos do Tipo A, metaluminosos a peraluminosos, com idade entre 1740 e 1769 Ma.

A Faixa Placha é o depósito de estanho mais importante do Maciço Pedra Branca e apresenta concentrações elevadas de ETRY, tanto no minério de Sn quanto no granito parental e nos granitos greisenizados com potencial para serem explorados economicamente como subproduto do estanho. Os valores ultrapassam 1000 ppm em ETRL e alcançam 500 ppm em ETRPY. Os minerais portadores de ETR no granito parental são allanita, monazita, xenotima, torita, apatita e zircão. Esses minerais, exceto zircão, são alterados, dando origem a monazita secundária, silicatos, fluorcarbonatos e oxifluoretos, que são responsáveis pela concentração de ETR nos granitos greisenizados e greisens e pela disponibilização desses metais para a fração argila dos saprolitos e solos. Análises de troca iônica nos saprolitos e solos de um perfil da Faixa Placha mostram que as extrações na fração argila são mais ricas em ETRY em relação às extrações em rocha total, apresentando valores entre 3425 e 36762 ppm e entre 2804 e 21689 ppm respectivamente. Os ETR encontram-se mais ricos na parte basal do perfil, principalmente os ETRL. A composição mineralógica e as concentrações de ETRY sugerem grande potencial econômico no depósito da Faixa Placha para recuperação de terras raras como subproduto da mineração de estanho. Adicionalmente, as concentrações de ETRs como íons trocáveis no perfil de intemperismo indicam potencial para que a Faixa Placha e áreas vizinhas constituam um importante depósito de ETRY do tipo adsorção iônica.

## ABSTRACT

The present study has as its main focus the rare earth elements (REE) that occur in important concentrations in the Pedra Branca granite massif, located in the eastern part of the Goiás Tin Province, more precisely in the Paranã Tin Subprovince. The massive has important tin deposits and consists of metaluminous to peraluminous A-type granites, aged between 1740 and 1769 Ma. The Faixa Placha is the most important tin deposit of the Pedra Branca Massif and presents high concentrations of REEY in the parental granite, in the greisenized granites and in the tin ore. The values are above 1000 ppm in LREE and reach 500 ppm in HREEY. The minerals with REE in the parental granite are allanite, monazite, xenotime, thorite, apatite and zircon. These minerals except zircon, are altered, giving rise to secondary monazite, REE-silicates, REE-fluorcarbonates and REE-oxyfluorides, which are responsible for the concentration of REE in greisenized granites and greisens and the availability of these metals to the clay fraction of soils and saprolite. Ion exchange analyses on saprolite and soil in a weathering profile of Faixa Placha, show that the extraction from the clay fraction are more enriched in REEY in relation to the extraction from whole rock, with values between 3425 and 36762 ppm and between 2804 and 21689 ppm respectively. The REE are more enriched in the basal part of the profile, especially the LREEs. Both the REEY concentrations and mineral compositions suggest an important economic potential of the Faixa Placha deposit for recovery of REE as by-product of tin mining. In addition, the exchangeable REEY concentrations in the weathering profile indicate the potential of the Faixa Placha and nearby areas to constitute an important REEY deposit of the ion-adsorption-type.

## CAPÍTULO I

### **1. INTRODUÇÃO E JUSTIFICATIVAS**

Nos últimos anos, a demanda e procura dos elementos terras raras (ETR) têm ficado cada vez mais críticas por causa de sua escassez no mercado mundial (Roskill, 2007; Sanematsu et al., 2009). Segundo Industrial Rare Metals (2008), o preço dos elementos terras raras pesados (ETRP) vem aumentando drasticamente em relação aos elementos terras raras leves (ETRL). Assim, a demanda mundial crítica é pelos ETRP, principalmente por disprósio, ítrio e európio, juntamente com o ETRL neodímio (Stone 2009; Service 2010, Garcia 2013). O problema não é somente pelo o aumento da demanda dos ETRP, mas também pelo suprimento limitado dos depósitos de minério. Atualmente, grande parte da oferta de ETRP é proveniente de depósitos do tipo adsorção iônica, localizados no distrito de Longnan, no sul da China (Sanematsu et al., 2009; Sanematsu & Watanabe, 2016; Hoshino *et al.*, 2016; Xu *et al.*, 2017). Entretanto, apesar da situação crítica projetada para o futuro, em 2015 houve uma redução significativa dos preços de ETR, decorrente de uma excessiva oferta, principalmente da China, que continua dominando o mercado mundial (USGS, 2016).

O presente trabalho tem os elementos terras raras (ETR) como foco de estudo, com a pretensão de se conhecer a concentração e o comportamento desses elementos nos granitos, greisens e solos que se encontram no Maciço Estanífero Pedra Branca (GO), principalmente na Faixa Placha, pertencente à Província Estanífera de Goiás (PEG).

O tema "elementos terras raras" tem sido abordado na PEG desde os trabalhos pioneiros de Marini et al. (1992) e Teixeira e Botelho (2002, 2006). Atualmente os ETR têm adquirido especial importância devido às concentrações econômicas no Maciço Serra Dourada, onde uma mina de classe mundial está sendo implantada (Rocha et al., 2013; Santana et al. 2015). Além disto, várias ocorrências foram investigadas como dissertações concluídas na Universidade de Brasília (Santana, 2015; Vieira, 2016 e Zapata, 2017).

O Maciço Pedra Branca contém o principal depósito de estanho da PEG e exibe concentrações anômalas de ETR, tanto nos granitos parentais quanto nas rochas mineralizadas em Sn (Marini et al., 1992; Botelho, 1992; Teixeira e Botelho, 2006). Assim, este maciço granítico constitui um excelente alvo para investigações de detalhe sobre ETR, com potencial para seu aproveitamento como subproduto do estanho ou mesmo depósito econômico destes elementos.

## 2. OBJETIVOS

O principal objetivo deste trabalho é a caracterização geoquímica, mineralógica dos elementos terras raras nos granitos, greisens e saprolitos na região do principal depósito de estanho do Maciço Pedra Branca, denominado de Faixa Placha e sua concentração no perfil de intemperismo do depósito, utilizando o método de extração na fração argila e em rocha total.

## 3. CONTEXTO GEOLÓGICO

A Província Estanífera de Goiás (PEG), localizada na porção norte de Goiás (Figura 1), compreende granitos com idades do Paleoproterozoico ao Neoproterozoico, divididos em quatro subprovíncias (Marini e Botelho, 1986), dentre as quais se destacam as subprovíncias estaníferas Tocantins (SPT) e Paranã (SPP), com pequena parte se estendendo para o estado de Tocantins. Estas subprovíncias são constituídas predominantemente por granitos tipo A mineralizados em Sn, subdivididos em duas suítes: Pedra Branca, com idades entre 1,74 e 1,77 Ga., e Serra Dourada, com idade de 1,58 Ga (Pimentel e Botelho, 2001). Os granitos de ambas subprovíncias apresentam alterações tardi- a pós-magmáticas como microclinização, albitização e greisenização, além de altos teores de álcalis, Sn, Y, Nb, Th, Rb, e ETR, que os definem como granitos tipo A.

A área de estudo está localizada no nordeste do estado de Goiás, no município de Nova Roma, na porção externa da Faixa Brasília. Esta região é alvo de muitos trabalhos por causa de seu potencial para ouro, estanho, índio, terras raras, urânio, gemas e rochas ornamentais. O estanho, além do urânio e ouro, tem sido o principal bem mineral pesquisado até agora.

O Maciço Pedra Branca constitui a área tipo da Suíte Pedra Branca e está localizado na SPP (Figura 2), onde os granitos do tipo A são intrusivos em paragneissos e micaxistos da Formação Ticunzal, que tem idade > 2,15 Ga., e também em milonitos graníticos, granitos e pegmatitos, alguns também estaníferos, da Suíte Aurumina (2,15 Ga.) (Figura 1) (Botelho *et al.* 1999, Lacerda Filho *et al.* 1999, Teixeira e Botelho, 2006). Este maciço é o mais importante da Subprovíncia Paranã, possuindo importantes zonas mineralizadas. Constituído por biotita granitos e leucogranitos das duas famílias de Suíte Pedra Branca, representadas pelas fácies: pb1 (pb1a, pb1b e pb1c), pb2 (pb2a, pb2b, pb2c e pb2d) (Botelho, 1992). O granito mais evoluído e mineralizador é o pb2d e as mineralizações mais importantes estão hospedadas em sua cúpula, na área denominada de Zona da Bacia, ou em zonas de fraturas nas suas proximidades, como é o caso da Faixa Placha.

A Faixa Placha representa a zona mineralizada mais importante do Maciço Pedra Branca, com extensão de 4 km e espessura variável entre 20 e 150 metros. Entretanto, a 100 metros de profundidade esta espessura se reduz a 10 metros (Figura 2). A mineralização que ocorre é toda pré-tectônica. Na parte central Faixa Placha, representando cerca de 1/4 de sua extensão, uma reserva de 15 kt de Sn foi bloqueada. A rocha mineralizada dominante é um topázio-Li-siderofilita-quartzo-greisen, chamado de " greisen preto" (Botelho e Rossi, 1988).

A maior concentração de garimpos de cassiterita ocorreu nesta parte central e mais rica da Faixa Placha. Os greisens são constituídos de topázio, quartzo, Li-siderofilita e cassiterita. A cassiterita desta zona contém 0,2 % de In. Em torno de 120 metros de profundidade, trabalhos de sondagens interceptaram, após a faixa principal, uma zona de 10 metros de espessura, rica em sulfetos, principalmente esfalerita com teor de 1% de In. Na parte NE, próxima da falha NS que delimita a parte central da Faixa Placha, ocorrem fraturas subparalelas, intensamente deformadas e catacladas, com atitudes de N30-40E e 70-80NW, mineralizadas.

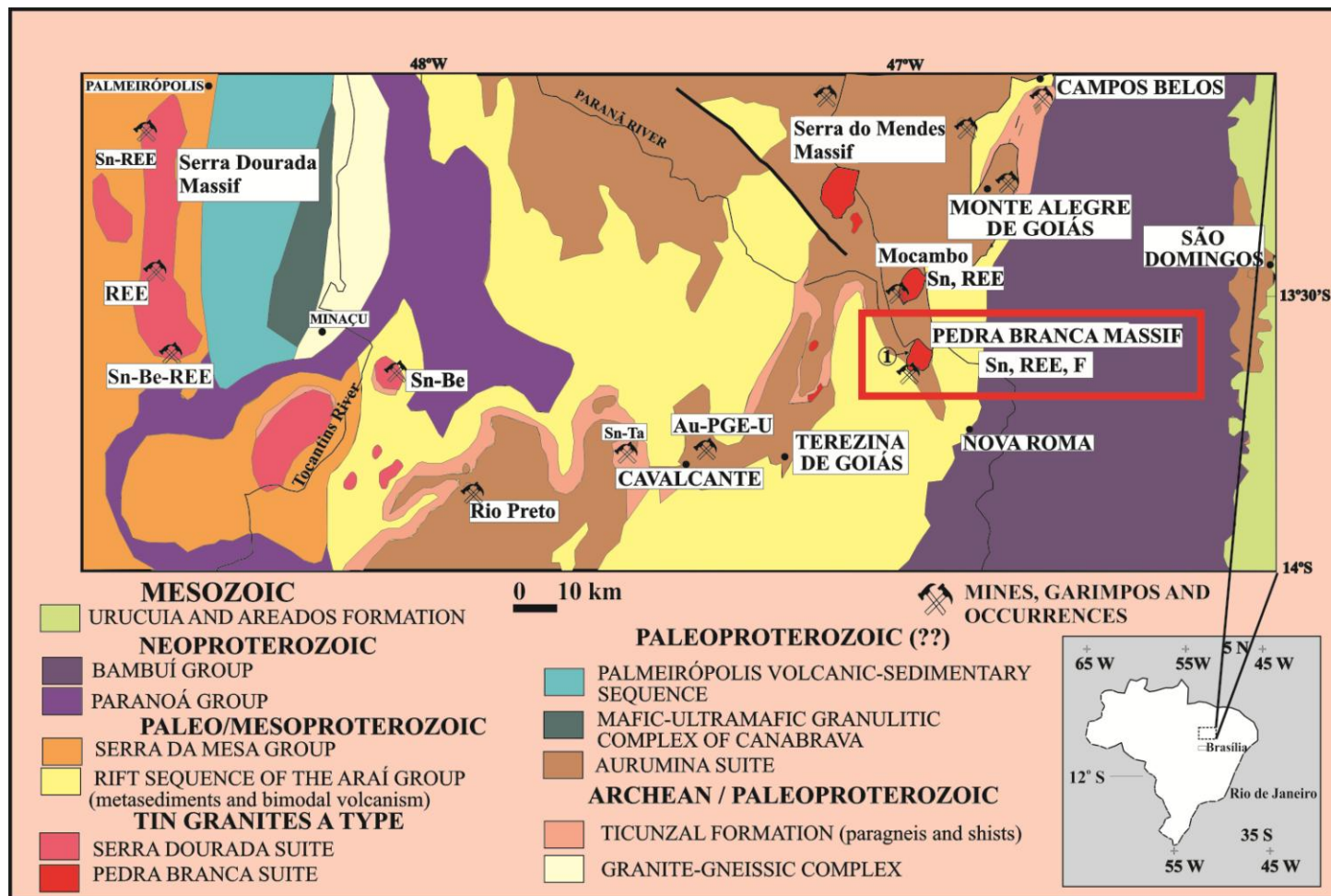


Figura 1: Mapa geológico regional da Província Estanífera de Goiás (Botelho, 1992).

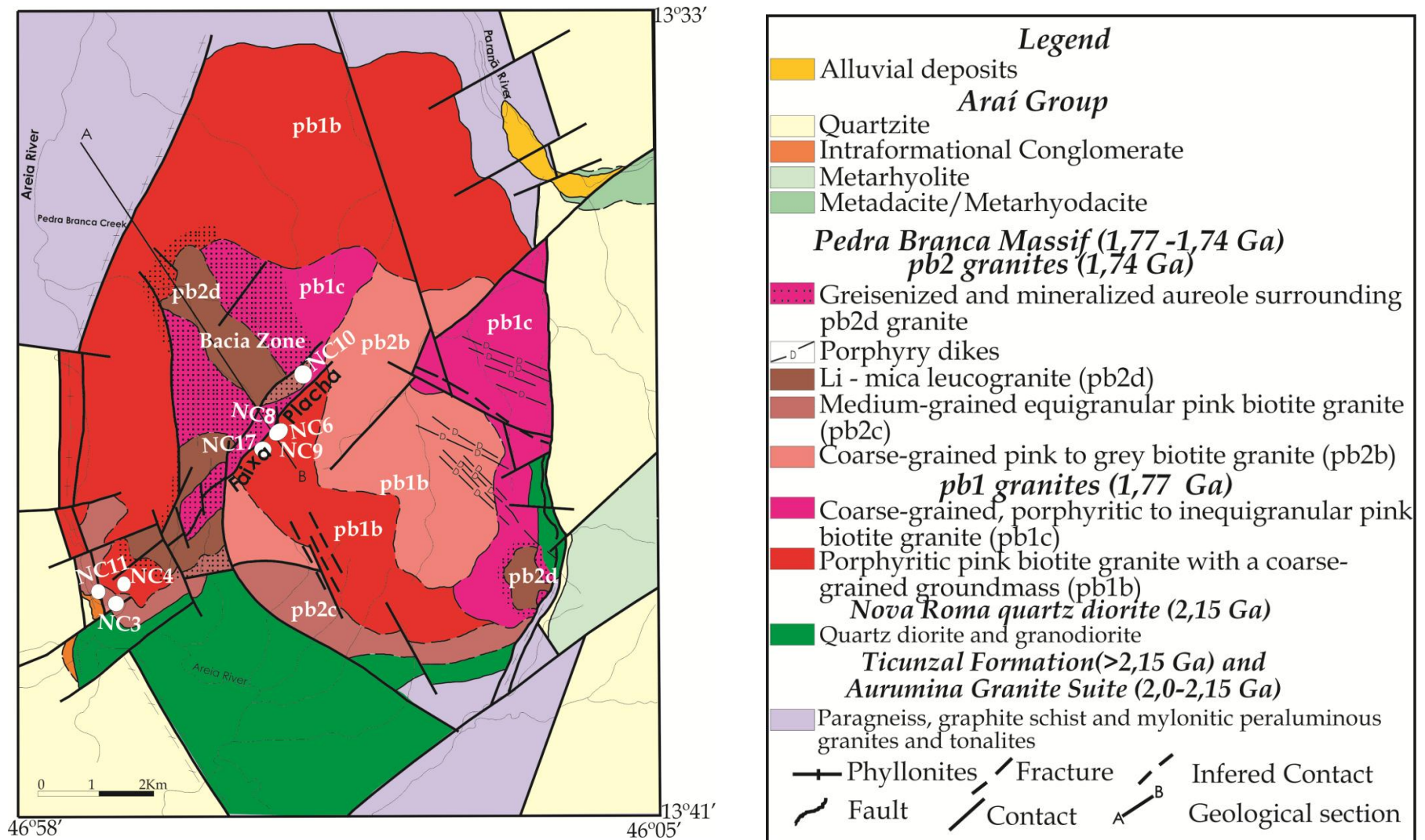


Figura 2. Mapa geológico simplificado do Maciço Pedra Branca (Botelho, 1992).

## 4. MATERIAIS E MÉTODOS

### 4.1. Amostragem de saprolitos e solos da Faixa Placha e arredores

As primeiras amostragens de saprolitos ocorreram em perfis de intemperismo da Faixa Placha, situados nas proximidades de uma lavra experimental para a extração do minério de estanho (Fig. 3A). Nesta área, há uma grande concentração de veios de greisens. Também foram amostrados solos (Fig.3B e C), em vários furos de trado, localizados na porção centro-sul do Maciço Pedra Branca para fim de comparação desses com a Faixa Placha.

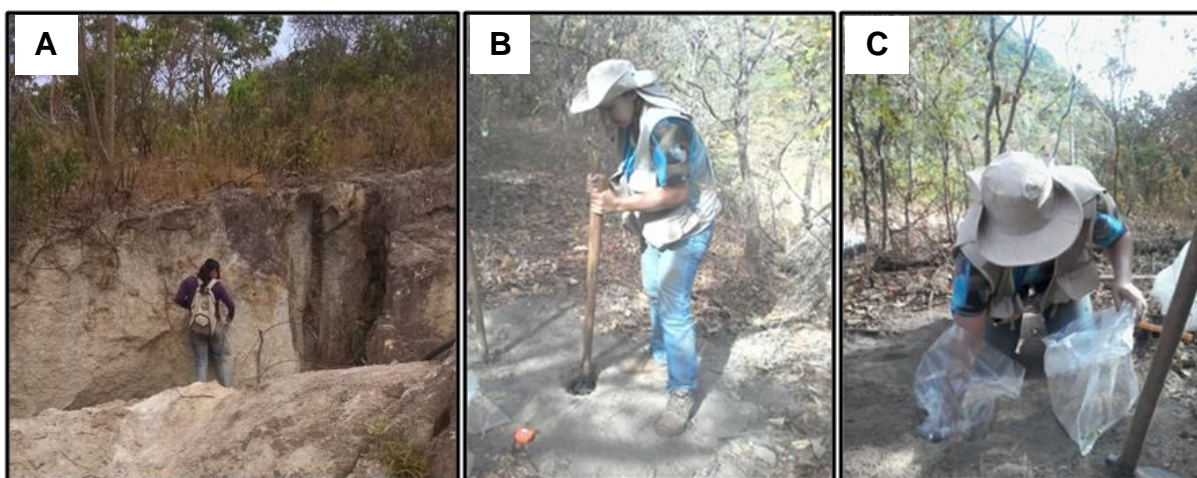


Figura 3: Amostragem de saprolito na Faixa Placha (A) e utilização do trado para amostragem de solo em superfície de aplainamento nas proximidades da Faixa Placha (B) e (C).

### 4.2. Separação de Argila pelo Método de Peneiras

Este trabalho foi executado no Laboratório de Difração de Raios-X do Instituto de Geociências da Universidade de Brasília (UnB). As amostras (NC17\_1 a NC17\_7 ) foram quarteadas e peneiradas em água, para a desagregação da argila, nas frações  $\geq 250$ ,  $\geq 125$ ,  $\geq 62$ ,  $\geq 45$ ,  $\geq 20$  e  $< 20$   $\mu\text{m}$ . Para análise de troca iônica, foi utilizada a fração argila  $< 20$   $\mu\text{m}$ .

### 4.3. Separação da Fração Argila para Análises DRX

A separação da fração argila da amostra total foi realizada no Laboratório de Difração de Raios-X do Instituto de Geociências da UnB. Foram realizadas três etapas; na primeira etapa, foram adicionados 2 gramas da mesma amostra e 50 ml de água destilada em dois tubos separados. As amostras foram centrifugadas, com rotação de 750 rpm (rotação por minuto) durante 7 min. Na segunda etapa, a fração argila em suspensão foi recuperada e recolocada em dois tubos, com 50 ml de água destilada, para nova centrifugação, em uma rotação de 3000 rpm, durante 30 min. . Em ambas as etapas a temperatura foi de 30° C. A última etapa

consistiu na recuperação da fração argila precipitada no fundo dos tubos e sua preparação para a análise por difração de Raios-X.

#### ***4.4. Difração de Raios-X análise do pó***

O trabalho foi desenvolvido no Laboratório de Difração de Raios-X do Instituto de Geociências da Universidade de Brasília (UnB). As análises incluíram rocha total e fração argila e foram realizadas em difratômetro da marca Rigaku - Ultima IV, pelo método do pó. As amostras foram pulverizadas em gral de ágata e o material analisado compreendeu 8 amostras totais, incluindo 5 saprolitos (NC17\_3 a NC17\_7), 2 solos (NC17\_1 e NC17\_2) e 1 laterita (NC17\_LC). O tratamento dos difratogramas foi obtido com auxílio do programa Jade 9, base Windows, com banco de dados PC-PFC executado pelo International Center for Diffraction Data – ICDD.

#### ***4.5. Extrações e análises de troca iônica dos cátions***

Antes de iniciar as extrações das amostras, os tubos foram enxaguados em água ultra pura, limpos por imersão em 1M HNO<sub>3</sub>, durante 24 h, e novamente enxaguados repetidamente em água ultra pura.

As extrações foram realizadas no Laboratório de Geoquímica da Universidade de Brasília e as análises de ICP-MS no Laboratório Actlabs no Canadá. Foram analisados 6 amostras do perfil de intemperismo da Faixa Placha, ponto 17 (5 saprolitos da camada 3 a 7 do perfil, e a crosta laterítica). As concentrações dos elementos extraídos foram determinadas pela High Resolution Inductively Coupled Plasma Mass Spectrometry (HRICP-MS).

##### ***4.5.1. Extração em única etapa (fração argila e amostra total)***

A extração em única etapa foi realizada em 11 amostras de perfil de intemperismo da Faixa Placha (NC17), sendo que 5 amostras (NC17\_3, 4, 5, 6 e 7) foram utilizadas para extração na fração argila e 6 amostras para extração na amostra total (NC17\_3, 4, 5, 6, 7 e LC). O procedimento realizado teve como base os trabalhos de Sanematsu et al (2015) e Sanematsu e Kon (2013).

Em um tubo de centrífuga de 50 ml foram adicionados 1 grama da amostra e 40 ml de uma solução de 0,5 M (6,6 peso%) de sulfato de amônia [(NH<sub>4</sub>)SO<sub>4</sub>] com pH ~5,7. O tubo foi agitado mecanicamente durante 24 horas em temperatura ambiente e em seguida foi centrifugado por 15 minutos a 4500 rpm, para separar o sólido da solução. Após isso, a

solução sobrenadante foi filtrada com um filtro de membrana do tipo celulose acetato ( $\phi = 0,22 \mu\text{m}$ ), pré-lavado com água ultra pura e acidificada usando 1% de ácido nítrico  $\text{HNO}_3$  (Tabela 1).

Table 1: Extração de unica etapa usando a solução sulfato de amônia.

Extraction Step	Reagent	pH	Reaction Time (hrs)	Dominantly reacting material
1	0.5M ammonium sulphate	5.7	24	Ion-exchangeable materials

#### 4.5.2. Extração em 2 etapas

##### 4.5.2.1. Óxidos de Fe e Mn Amorfos - Etapa 1

Nesta etapa e na etapa 2 somente as 6 amostras do material total (NC17\_3, 4, 5, 6, 7, LC) foram processadas (Tabela 2).

Com base no procedimento de Rauret et.al. (1999), 10 ml da mistura de 0,2M  $\text{NH}_4\text{C}_2\text{O}_4\text{H}_2\text{O}$  (oxilato de amônia) com 0,2M  $\text{C}_2\text{H}_2\text{O}_4$  (ácido oxiálico) foram adicionados ao sólido que ficou retido no tubo utilizado na extração em única etapa. A solução foi agitada mecanicamente durante 4 horas, em temperatura de 20°C. Após esse tempo, a solução foi centrifugada por 17 minutos, finalizando com a filtração da solução.

##### 4.5.2.2. Óxidos de Fe e Mn - Etapa 2

A etapa 2 consistiu na extração realizada com o resíduo sólido retido na etapa 1, utilizando 40 ml do reagente 1,24M de hidroxilamina ( $\text{NH}_2\text{OH}$ ), pH=1. A solução foi agitada por 16 horas, em temperatura ambiente, e em seguida centrifugada durante 20 minutos e filtrada com membrana de 0,22  $\mu\text{m}$  (Tabela 2).

Table 2: Extração de 2 etapas.

Extração	Reagentes	pH	Reação	Materiais que reagem
Etapas			Tempo (hrs)	de forma dominante
1	0,2M Oxalato de amônia e 0,2M ácido oxalático	1	4	Óxidos de Fe e Mn amorfos
2	1,24M Hidroxilamina	1	16	Óxidos de Fe e Mn

#### 4.6. Geoquímica de rocha total

As amostras para geoquímica foram pulverizadas em panela de ágata e enviadas para análise no Laboratório *Acme Analytical Laboratories Ltd.*, Canadá, totalizando 15 amostras, sendo que 5 amostras eram de saprolito, 4 de solo, 2 de granito parental, 2 de granito greisenizado, 1 de greisen e 1 de crosta laterítica. A rotina analítica adotada envolveu a fusão das amostras com metaborato de lítio, digestão ácida e leitura em ICP-ES para os elementos maiores e ICP-MS para elementos menores e traços.

#### 4.7. Microsonda e Microscopia Eletrônica de Varredura

As análises foram realizadas no equipamento JEOL JXA-8230, do Laboratório de Microsonda Eletrônica, do Instituto de Geociências da Universidade de Brasília (UnB), equipado com 5 espectrômetros com sistema de análise por dispersão de comprimento de onda (WDS) e um espectrômetro com sistema de análise por dispersão de energia (EDS) para análises qualitativas. Foram feitas duas etapas de análises: a primeira, utilizando os sistemas de imagens por elétrons secundários (SEM) e elétrons retroespalhados (BSE), junto com análises por EDS, para identificar os minerais enriquecidos em REE e Y. A segunda etapa consistiu nas análises quantitativas, obtidas por meio de dois programas analíticos. No primeiro programa, foram utilizados 15 kV de aceleração de voltagem, corrente de 10nA e 1 µm de diâmetro do feixe de elétrons para análise de Si, Al, F, P, Sr, Mn, Ti, Y, Ca e Fe. No segundo programa, foram analisados REE, Y, Na, Pb, K, Th, Zr, U e Ba, com aceleração de voltagem de 20kV, corrente de 50nA e 1 µm de diâmetro do feixe de elétrons. O tempo de contagem para todos os elementos foi de 10 segundos no pico e 5 segundos no *background*. As correções de interferência foram executadas em todos os casos necessários.

#### ***4.8. Desenvolvimento da Tese***

A tese foi redigida em forma de dois artigos. O primeiro artigo, submetido ao Journal of Geochemical Exploration, trata da caracterização mineralógica, geoquímica e do potencial econômico dos elementos terras raras nos granitos e greisens do depósito estanífero do Maciço Pedra Branca. O segundo artigo, que será submetido a Ore Geology Review, aborda a concentração dos elementos terras raras em granitos, greisens e saprolitos do depósito estanífero na Faixa Placha e seu potencial econômico para mineralização de ETRY do tipo adsorção iônica.

## CAPÍTULO II

### **MINERALOGICAL AND GEOMISTRY CHARACTERIZATION AND ECONOMIC POTENTIAL FROM RARE EARTH ELEMENTS IN GRANITES AND GREISENS OF THE A-TYPE PEDRA BRANCA GRANITE MASSIF TIN DEPOSIT, CENTRAL BRAZIL**

Costa N.O.<sup>1</sup>, Botelho N.F.<sup>1</sup>

<sup>1</sup>University of Brasília, Institute of Geosciences, Campus Darcy Ribeiro, 70919-970, Brasília-DF, Brazil

Corresponding author: Nivia Costa, email: nivia.costa@gmail.com

phone: +55 61983039537

#### **Abstract**

The Pedra Branca Massif is an A-type granitic pluton located in the Goiás Tin Province (GTP) in central Brazil, characterized by the presence of REE-bearing granites and tin deposits. The Pedra Branca Massif (PBM) is the type area of the 1,74-1,77 Ga Pedra Branca Granite Suite that hosts the Faixa Placha tin deposit (FPTD), the largest tin deposit in the GTP and in central Brazil. The PBM is constituted by at least seven different granite facies, ranging from biotite monzogranite to evolved Li-mica-albite granite. In the FPTD, the dominant rock type corresponds to biotite granite, where intensely greisenized granites and tin ore, hosted in topaz-Li-synderophyllite-quartz greisen, were developed. All of the FPTD rock types exhibit high concentrations of REE in relation to chondrite, reaching over 1000 times in LREE, and 500 times in HREE. The main HREE-bearing minerals found in the Faixa Placha are zircon, xenotime and thorite, and the main LREE-bearing minerals are monazite, apatite, allanite and oxyfluorides. The parental biotite granite, greisenized granite and greisen all display the same REE patterns and contents, indicating that there is no relevant change in concentration and fractionation of REE coeval with the hydrothermal evolution of the FPTD. Among the accessory minerals, the REEY enrichment in zircon and apatite are conspicuous. During greisenization, apatite disappears after being replaced by secondary monazite and oxyfluorides. HREEY concentration in zircon reaches up to 15 wt%, and the metamictization and alteration of zircon favor the concentration of HREEY in granites and greisen, reaching values above 500 ppm in some samples. Both the REEY concentrations and mineral compositions suggest an important economic potential of the Faixa Placha deposit for recovery of REE as by-product of tin mining. In addition, the area might also be prospected for REE deposits of ionic adsorption type in both the tin deposits and the weathering fronts of the granite massif.

#### **1. Introduction**

In recent years, the rare earth elements (REEs) have been in high demand in the world market because of their uses in technology, as well as of the Chinese monopoly that currently accounts for 70% of world production (USGS 2019). These elements have widespread use in the batteries of hybrid cars, high-efficiency magnets, superconductors, robotics, wind power generators and other clean energy applications.

The REEs are considered "strategic minerals" on account of their scarcity, and they are essential and/or critical for a country. According to the National Mining Plan 2030 (Brazil 2010), a mineral is deemed strategic if it meets three conditions: i) a commodity of which Brazil needs import an elevated percentage; ii) minerals that are bound to have increased importance in the next decades due to their uses in high technology industry; and iii) mineral resources for which the country has competitive advantages that are paramount for the economy and its regulation in the balance of trade.

Brazil has important REE reserves found in monazite-bearing placer deposits. However, for the most part, they are located in coastal zones, with several drawbacks that arise from environmental regulations. Brazilian carbonatites have sizeable contents of REE oxides. Amid these rocks, Araxá stands out with 4.4 wt% in the whole rock (Issa Filho *et al.* 1984) and 13.5% in gorceixite and goyazite ores (Mariano, 1989). Likewise, Catalão I has estimated reserves of approximately 2 Mton. However, the REE deposits hosted in carbonatites do not satisfy the Brazilian demand for heavy rare earth elements (HREEs), since carbonatites are richer in light rare earth elements (LREEs) (Dostal, 2017).

Out of all the REEs produced worldwide, less than 15% consists of HREEs. Nevertheless, HREEs provide 50% of the revenue because of their diverse technological applications. Outside of China, the majority of mines exploit LREEs. Hence, HREEs are in high demand worldwide, especially Dy, Y and Eu, as well as the LREE Nd (Stone, 2009; Service, 2010; Garcia, 2013; Hoshino *et al.*, 2016).

In the Goiás Tin Province (GTP), where Sn has been exploited for a long time, research is being conducted on the economic potential for REE exploitation in granites, greisens, alluvial deposits and saprolites. The results show economic potential, such as in the Serra Dourada Massif, where monazite- and xenotime-rich placer deposits are situated. Additionally, in the same location, an ion adsorption REE deposit is about to become a mine (Rocha *et al.*, 2013; Santana *et al.*, 2015; <https://revistamineros.com.br/mineracao-serra-verde/>, 2019).

The REE research described in this work was developed in the Pedra Branca Massif, which is also part of the GTP. Previous work has shown REE enrichment in the granites in this massif, with contents of LREEs and HREEs up to 1000 times and 500 times chondrite, respectively (Marini *et al.*, 1992).

This article presents the mineralogy and distribution of REEs and Y in granites, greisens and saprolites of the Faixa Placha, which is the largest Sn deposit exploited in the GTP.

## **2. Geological setting**

The study area is situated in the northern part of Goiás State in the Nova Roma municipality and in the external region of the Brasília fold belt (Fig 1). The potential for Au, Sn, In, REEs, U, gems and ornamental rocks has attracted interest in the region (Botelho and Moura, 1998; Moura *et al.*, 2014; Menez and Botelho, 2017). In addition to tin, uranium and gold has been important commodities researched thus far in the region of the Goiás Tin Province (GTP).

The GTP encompasses granites with ages from Paleoproterozoic to Neoproterozoic. The most noteworthy tin granites are situated in the northern part of the province (Fig. 1). Tin deposits are related to peraluminous granites of the 2.11-2.15 Ga Aurumina Suite (Botelho *et*

al. 1999; Cuadros et al., 2017) and to A-type granites subdivided into two suites, namely, Pedra Branca (1.74-1.77 Ga) and Serra Dourada (1.58 Ga) (Pimentel and Botelho, 2001). The A-type granites in both suites show late to postmagmatic alterations such as microclinization, albitization, and greisenization and host the most important tin mineralizations. Furthermore, these rocks are classified as A-type granites on account of their moderately alkaline character and high Sn, Ga, Nb, Rb, Y and REE contents (Lenharo et al., 2002).

The Pedra Branca massif is the type locality of the Pedra Branca Suite and is situated in the eastern part of the GTP, in the domains of the Araí rift (Araí Group). In this location, the granites intrude paragneisses and schists from the Ticunzal Formation, the oldest lithostratigraphic unit in the GTP (>2.15 Ga), and the mylonitic granites, granites and pegmatites from the Aurumina Suite. The Pedra Branca massif comprises biotite granites and leucogranites subdivided into two generations, pb1 (pb1a, pb1b and pb1c) and pb2 (pb2a, pb2b, pb2c and pb2d). The pb2d Li-mica leucogranite is the most evolved facies and the richest in tin. The most important ore-bearing zones are situated in the granite cupola, named the Bacia Zone, or in nearby fractures such as Faixa Placha.

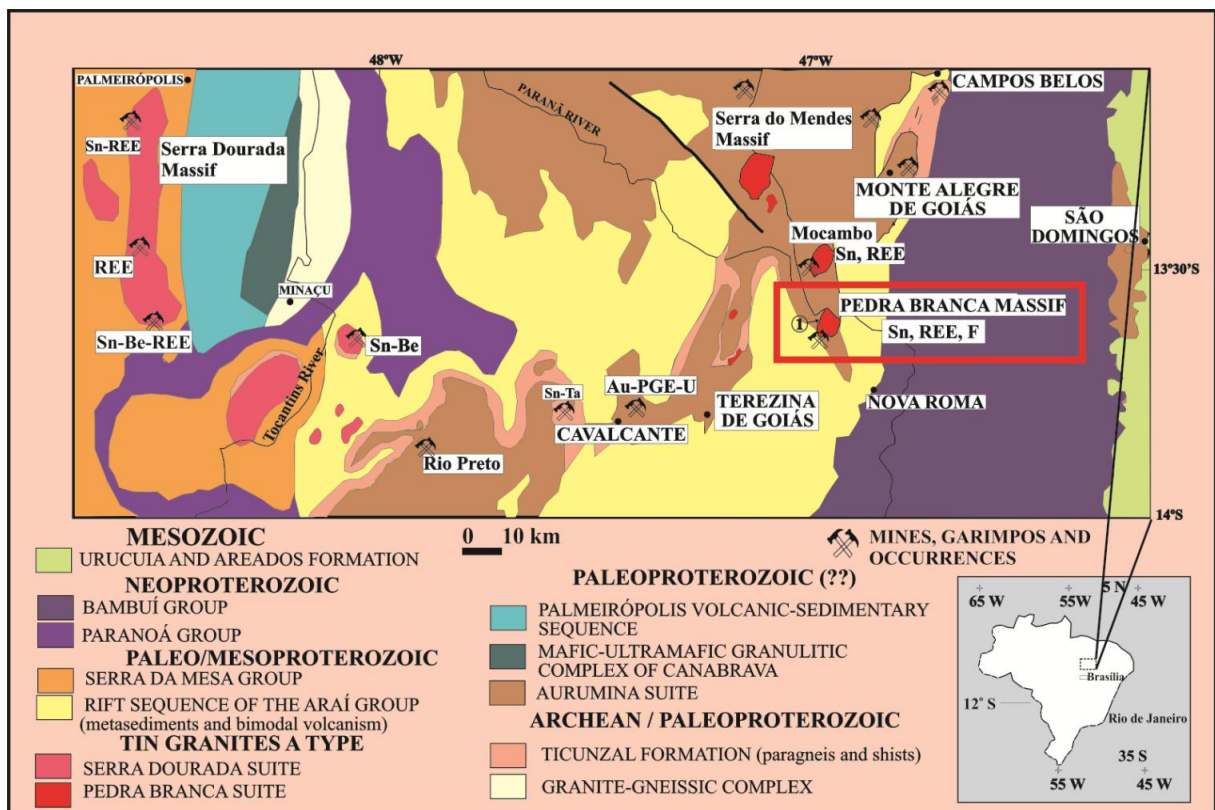


**Fig 1.** Geological Map of the northeastern portion of the Goiás Tin Province (GTP) showing the location of the Pedra Branca Massif and the distribution of REE occurrences in the A-type granites (Botelho, 2013).

### 3. The Faixa Placha tin deposit

The Faixa Placha tin deposit (FPTD) is the most significant mineralized zone in the Pedra Branca Massif and the main tin deposit in central Brazil. It is 4 km in length with widths ranging between 20 and 150 m. The Faixa Placha deposit trends roughly N30-40°E and dips 70-80°NW (Fig. 2). It is a highly deformed fracture zone that underwent intense cataclasis. The tin mineralization is completely pre-tectonic. A 15 kton Sn reserve is located

approximately in the center of this zone, representing 1/4 of its extent. Topaz-Li-siderophyllite-quartz-greisen, named black greisen (Botelho and Rossi, 1988), is the host rock (Fig. 3). The FPTD is also known, among other tin deposits in the GTP, to host anomalous indium concentrations (Botelho and Moura, 1998; Moura et al., 2014).

Intense cassiterite artisanal mining exploration happened in the 1970s and 1980s, in the central area of the FPTD, which is the portion richest in Sn (Fig. 3B). In this area, the indium concentration in cassiterite is approximately 0.2 wt% (Botelho and Moura, 1998). Drilling projects have found, in addition to the main region, a 10 m-thick zone at 120 m depth that hosts sulfides, especially sphalerite with 1 wt% of In. Currently, the deposit is owned and exploited by EDEM Projetos Ltd.

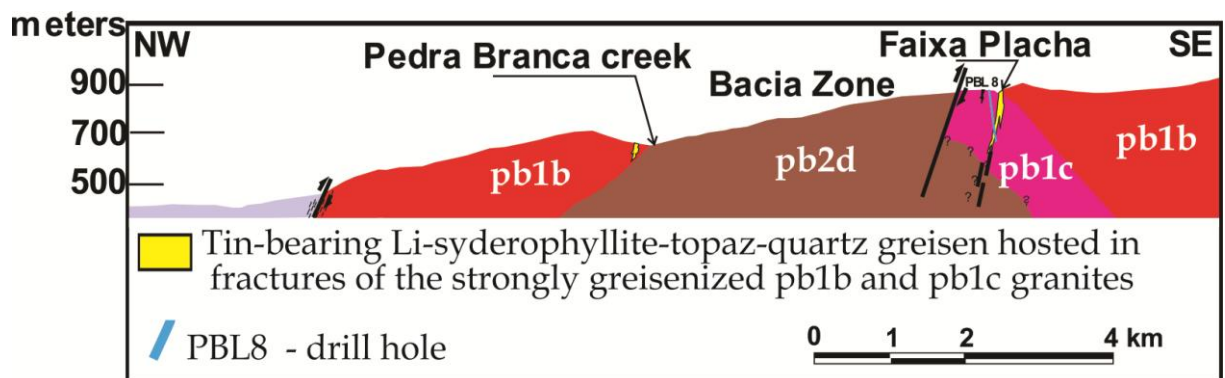
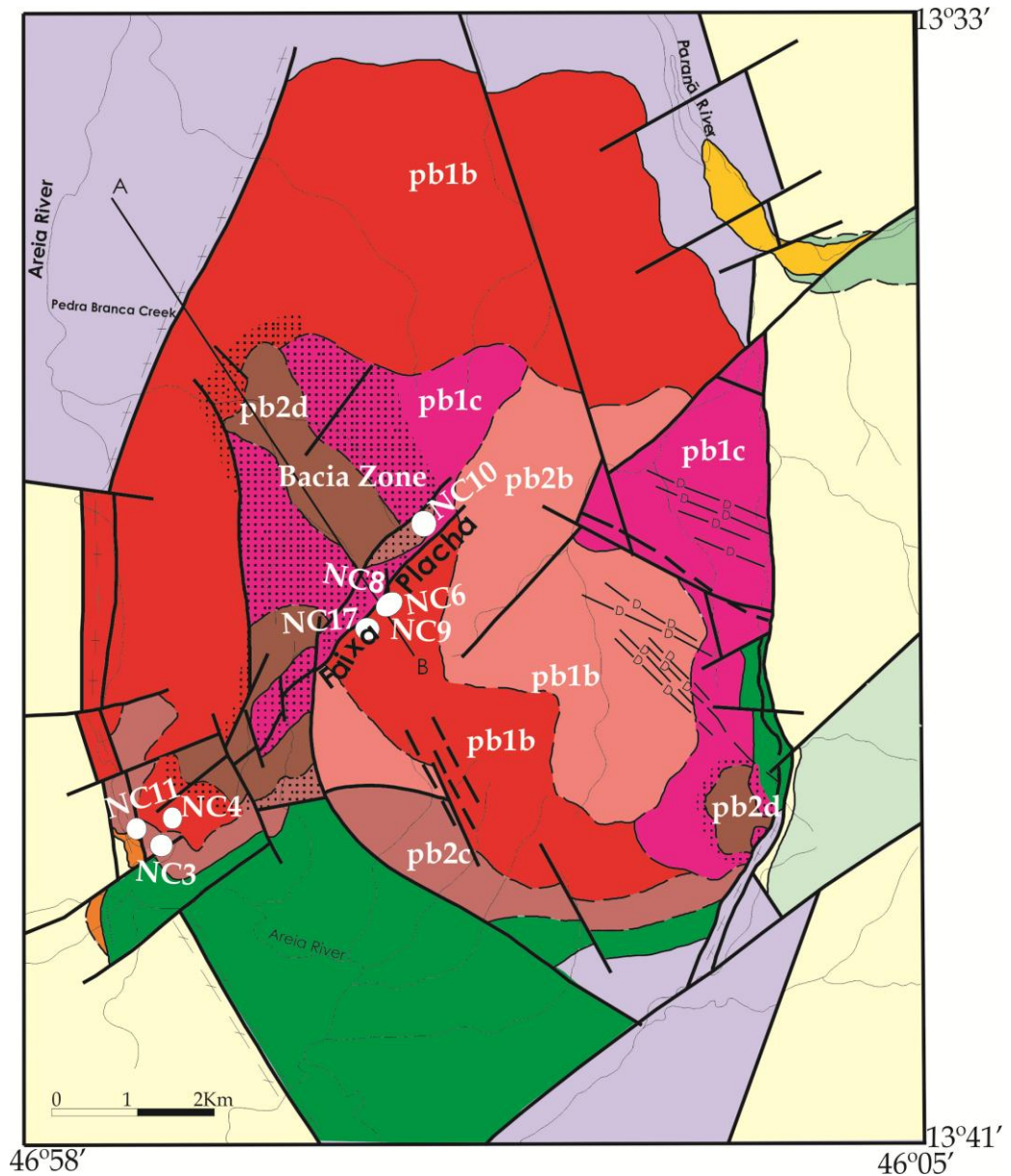


**Fig 2.** Geological map of the Pedra Branca Massif with the location of sampling (NC) and schematic geological cross-section (AB) in the region of the Faixa Placha and Bacia Zone.

#### 4. Materials and methods

The samples have undergone several procedures for analysis in the sample preparation laboratories (SPL) in the Institute of Geosciences of the University of Brasília. For mineral separation, the samples were first split in four portions and then sieved to separate 60, 90, 125, 200, 250, 300 and 500  $\mu\text{m}$  fractions. The best recovery of REE-bearing minerals grains was in the 200-125  $\mu\text{m}$  fraction. The minerals were preliminarily identified and hand-picked under a binocular stereo microscope to be assembled into sections with 100 grains.

##### 4.1. EPMA and SEM analyses

Microanalyses were undertaken using a JEOL JXA-8230 electron probe microanalyzer (EPMA) and an FEI-Quanta 450 scanning electron microscope (SEM) with a QEMSCAN system at the Institute of Geosciences in the University of Brasília. The probe is equipped with five vertical wavelength-dispersive spectrometers (WDS), one energy-dispersive spectrometer (EDS) and ZAF matrix correction. REE minerals were analyzed following the protocol of Scherrer *et al.* (2000). The advantage of this method is that no premeasured correction factors are needed and that spectral lines and background positions are set in order to avoid overlapping peaks. Analytical conditions were as follows: take-off angle of  $40^\circ$ , 25 kV acceleration voltage; 50 nA electron current and 3  $\mu\text{m}$  beam diameter. Counting times were 20 s for the REEs and 10 s for the other elements.  $K\alpha$ -lines were used for P, Al, Si, Ca and Fe.  $L\alpha$ -lines were considered for Y, La, Ce, Er, and Yb.  $L\beta$ -lines were used for Pr, Nd, Sm, Gd, Tb, Dy, and Ho. For U, Th, and Pb, we used  $M\beta$ ,  $M\alpha$  and  $M\beta$ , respectively. The standards for the REEs were synthetic glasses; for Y, a synthetic oxide of Fe and Y; for the elements U and Th, natural oxides; and for Pb, galena. The elements Ca and Si were standardized with wollastonite; and P, with apatite. For supplementary detailed information on the background positions and integration times, refer to Scherrer *et al.* (2000).

##### 4.2. Whole-rock geochemistry

Sixteen specimens were milled in agate mills and shipped for analysis in Acme Analytical Laboratories, Ltd., in Canada. Out of all sixteen samples, thirteen are greisenized granite, one is greisen, and two are granite saprolite.

The procedures included fusion with lithium metaborate, acidic digestion and reading in the ICP-ES for major elements and ICP-MS for minor and trace elements.

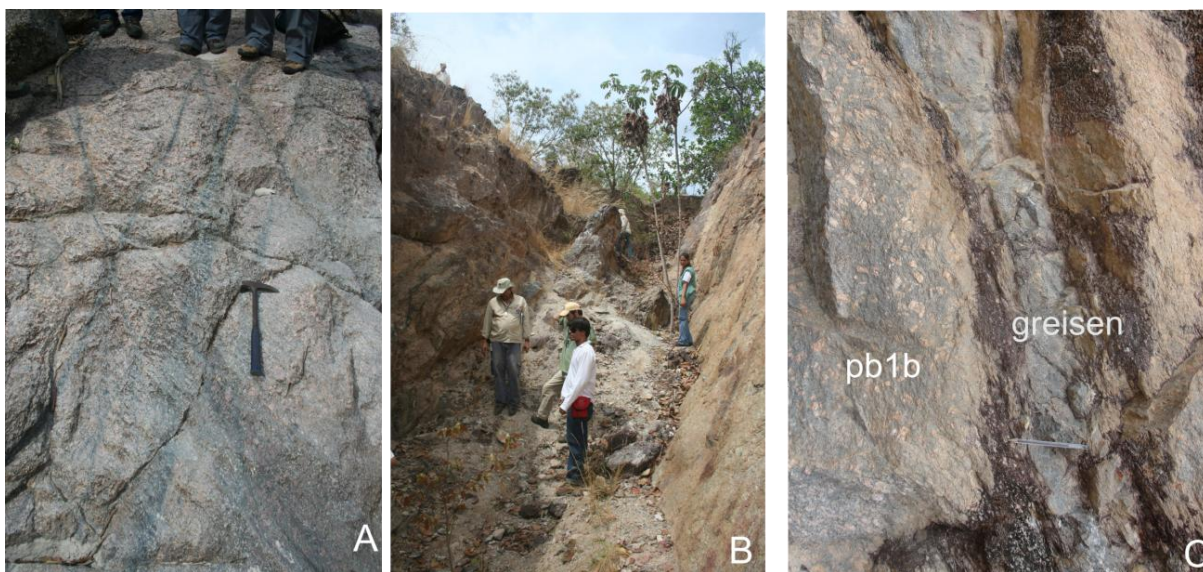


**Fig 3.** Aspects of the Faixa Placha Tin Deposit (FPTD). A: greisenized pb1b granite with greisen veinlets; B: abandoned area of ancient artisanal mining exploration; C: detail of the photo B showing black greisen hosted in fracture of the pb1b biotite granite.

## 5. Results

### 5.1. Mineralogical characterization

The REE-bearing minerals in the FPTD, listed in order of abundance, are REE oxyfluorides, zircon, xenotime, monazite, apatite, allanite and thorite. These minerals exhibit, some important characteristics and their REE contents are described below.

#### 5.1.1. Zircon ( $ZrSiO_4$ )

Zircon crystals from Faixa Placha are prismatic and euhedral to subhedral, with lengths ranging from 70 to 300  $\mu\text{m}$  and width-length ratios from 1:1 to 1:4. Their colors range from colorless to pinkish, white and dark brown. White and brown grains are translucent to almost opaque, indicating strong metamictization and are enriched in HREE (Fig. 4A-C). Zircon is one of the most important HREE-hosting phases, and the metamict crystals found in all the evolved granitic facies have HREE-rich mineral inclusions, in this case, xenotime-(Y) (Fig. 4a-C). HREE and LREE-rich minerals (xenotime, monazite and oxyfluorides) are also found in rims around zircon crystals, as can be observed in Figure 4a- (B-E).

EPMA analyses yield  $\text{SiO}_2$  contents between 20.09% and 33.6%,  $\text{ZrO}_2$  between 34% and 67.1%,  $\text{HfO}_2$  between 0.76% and 3.3%,  $\text{HREE}_2\text{O}_3$  up to 4.86% and  $\text{HREEY}_2\text{O}_3$  contents above 1% and up to 18.40% (Table 1).

The  $\text{Y}_2\text{O}_3$  and  $\text{REE}_2\text{O}_3$  concentration diagrams in zircon crystals show that the contents of these oxides are usually below 4% and 2%, respectively (Fig. 5A). Nevertheless, metamict zircons from pb1b and pb1c have  $\text{Y}_2\text{O}_3$  concentrations above 8% and  $\text{REE}_2\text{O}_3$  up to 6%. Some specimens with the same oxides above 10% and 19.4%, respectively, suggest fine xenotime inclusions. This interpretation is confirmed by the contents of  $\text{P}_2\text{O}_5$  higher than 8% and  $(\text{REE}_2\text{O}_3 + \text{Y}_2\text{O}_3)$  above 10% (Fig. 5B). However, for the most part,  $\text{P}_2\text{O}_5$  and  $(\text{Y}_2\text{O}_3 + \text{REE}_2\text{O}_3)$  are lower than 1.5% and 5%, respectively.

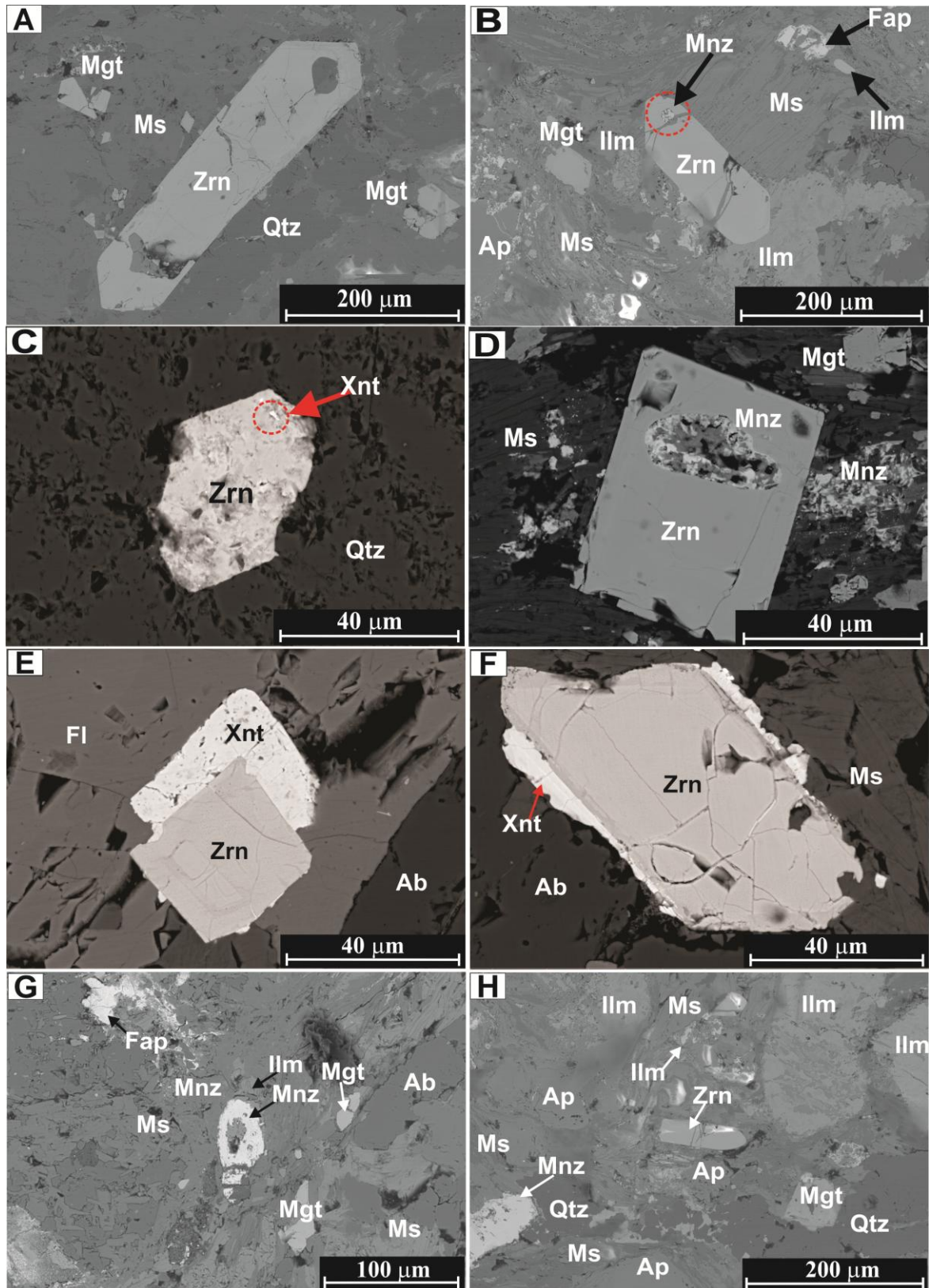


**Fig 4.** Backscattered electron images (BSE) of REE-bearing minerals from the FPTD. (A) Primary euhedral zircon (Zrn) free of REE-rich minerals; (B to F) relationships between zircon, monazite (Mnz) and xenotime (Xnt); (D) zircon grain, with irregular and altered monazite inclusion, surrounded by secondary monazite agglomerate in a muscovite (Ms) and magnetite (Mgt) mass; (G and H) zircon and hydrothermal monazite from the biotite granite pb1b, associated with apatite rests (Ap), muscovite (Ms), quartz (Qtz), ilmenite (Ilm), and magnetite (Mgt).

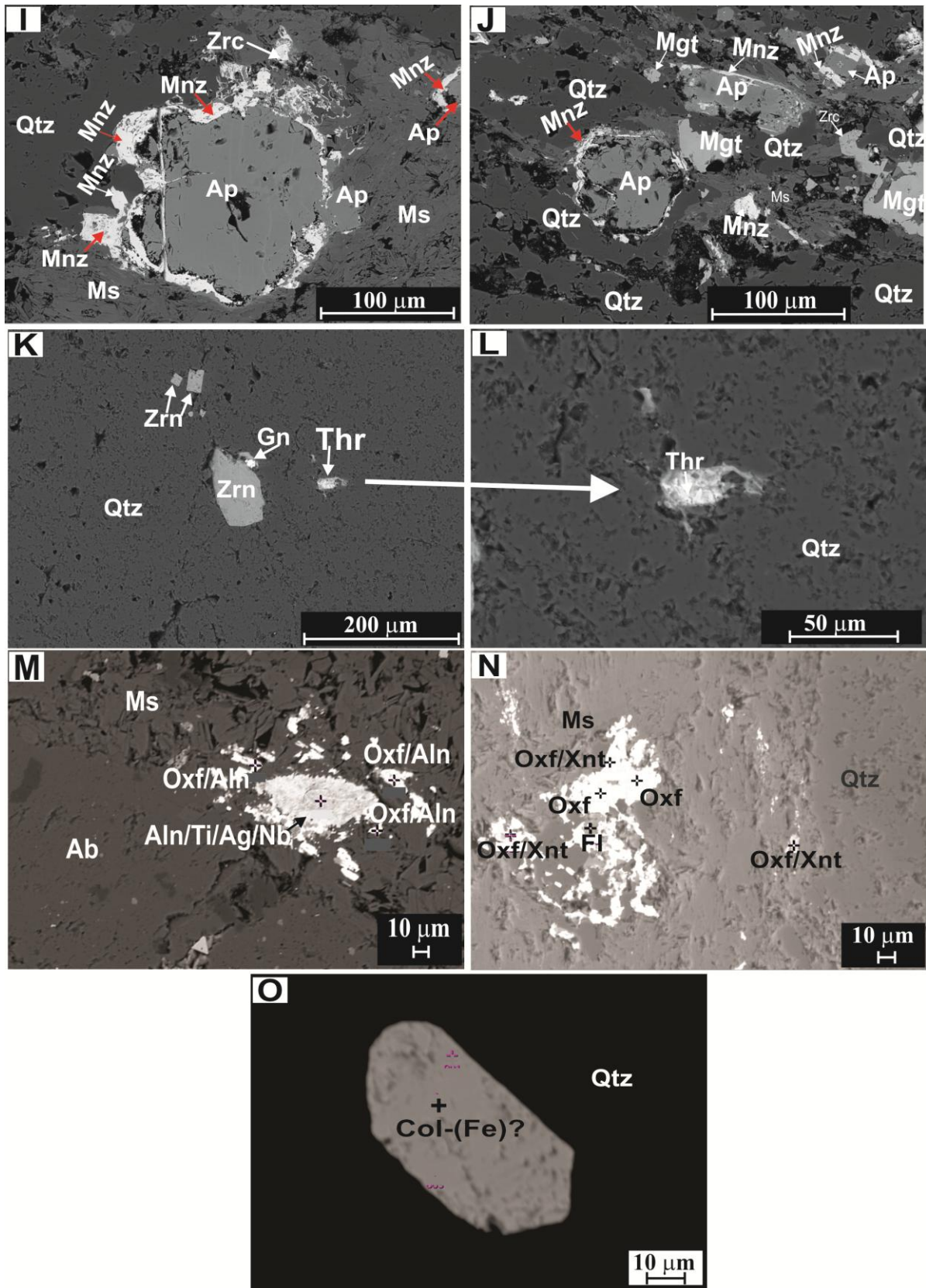


**Fig. 4 (extended).** (I and J) fluorapatite partially replaced by hydrothermal monazite on the edges and fractures; (**K and L**) Altered thorite (Thr) near zircon grains. Gn: galena; (**M and N**) Oxyfluorides (Oxf) associated with allanite and xenotime in a quartz-albite-muscovite mass. Aln: allanite; Fl: fluorite; (**O**) Unidentified Nb-Y-REE mineral.

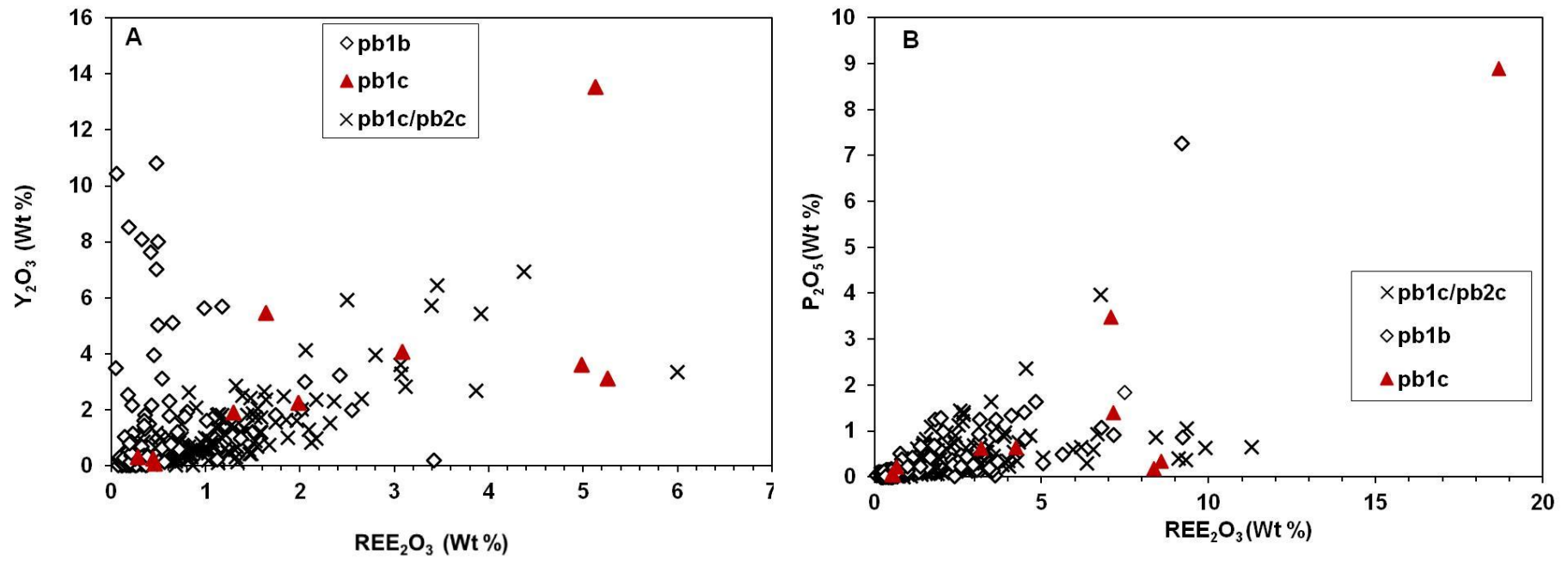


**Fig 5.** Composition of zircons from different types of granites in the Faixa Placha Tin Deposit.

### 5.1.2. Xenotime-(Y) (YPO<sub>4</sub>)

Xenotime from the FPTD is irregular to prismatic and usually occurs in close association with zircon, both as inclusions and as rims (Fig.4- C, E and F). It is characterized by a yellow hue and crystals that measure approximately 30  $\mu\text{m}$ .

Xenotime is a HREE mineral and a by-product in tin mines and to a lesser extent in placer deposits. In the xenotime from the FPTD, P<sub>2</sub>O<sub>5</sub> contents span an interval between 19.89% and 31.67%, Y<sub>2</sub>O<sub>3</sub> contents between 24.32% and 38.9% and HREE<sub>2</sub>O<sub>3</sub> between 3.72% and 23.58%, with HREERY<sub>2</sub>O<sub>3</sub> between 28% and 55.8% (Fig. 6). Dy<sub>2</sub>O<sub>3</sub> is the heavy rare earth oxide with highest contents of up to 8.4%. Yb<sub>2</sub>O<sub>3</sub> follows, spanning an interval between 0.83% and 7.62%, and Er<sub>2</sub>O<sub>3</sub> ranges between 0.83% and 5.34% (Table 2). The low analytical totals are due to variable degree of metamictization.

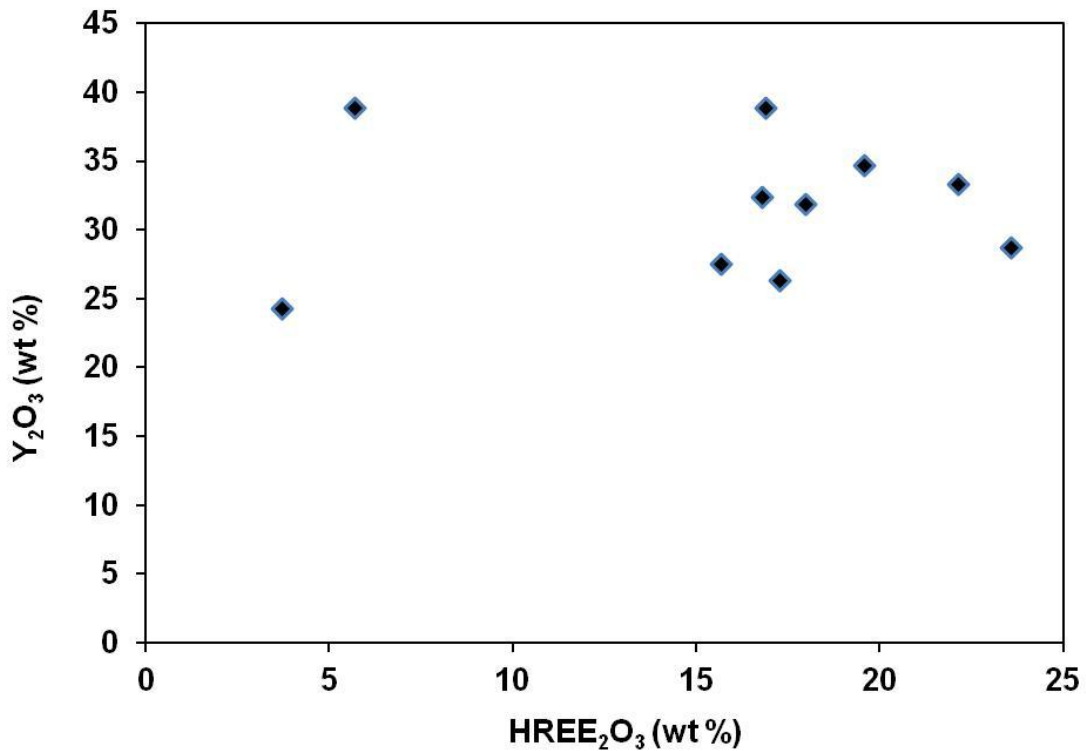


**Fig. 6.** Concentration of Y<sub>2</sub>O<sub>3</sub> and HREE<sub>2</sub>O<sub>3</sub> in xenotime.

Table 1. EPMA analyses of zircon

Facies	pb1/pb2			pb1b		pb1c		pb1b					
	NC3A (1)	NC3A (2)	NC3A (3)	NC4B (1)	NC4B (2)	NC9 (1)	NC9 (2)	NC10A (1)	NC10A (2)	NC10A (3)	NC10A (4)	NC10A (5)	NC10A (6)
(wt.%)													
SiO <sub>2</sub>	24,19	22,44	27,23	32,09	27,28	25,84	28,03	24,11	24,52	24,48	29,91	29,87	30,50
ZrO <sub>2</sub>	48,06	41,42	56,29	66,10	55,42	50,01	46,92	45,75	47,61	50,10	60,66	61,30	61,25
HfO <sub>2</sub>	1,01	1,42	3,28	1,34	2,77	2,26	2,00	1,63	1,82	2,50	0,76	0,95	1,74
Al <sub>2</sub> O <sub>3</sub>	1,65	0,96	0,12	0,01	0,69	0,49	0,41	2,63	1,59	0,37	0,02	0,00	0,00
P <sub>2</sub> O <sub>5</sub>	0,41	0,65	0,26	0,07	0,44	0,18	0,33	0,48	0,30	0,13	0,08	0,00	0,06
TiO <sub>2</sub>	0,01	0,00	0,00	0,05	0,02	0,20	0,19	0,03	0,00	0,09	0,13	0,00	0,09
FeO	0,77	1,24	0,51	0,31	0,90	0,86	1,12	1,36	1,99	0,72	0,03	0,04	0,00
CaO	0,66	0,72	0,64	0,08	0,53	0,25	0,40	1,02	0,85	0,30	0,00	0,25	0,00
MnO	0,33	0,17	0,00	0,00	0,93	1,33	0,46	0,00	0,10	0,08	0,00	0,04	0,04
Nb <sub>2</sub> O <sub>5</sub>	0,98	1,35	0,37	0,03	0,01	0,68	0,96	0,77	0,03	0,62	0,05	0,59	0,35
Ta <sub>2</sub> O <sub>5</sub>	0,02	0,25	0,00	0,02	0,15	0,16	0,24	0,00	0,08	0,00	0,17	0,00	0,12
PbO	0,24	0,00	0,00	0,00	0,00	0,37	0,85	0,00	0,00	0,00	0,00	0,00	0,00
ThO <sub>2</sub>	0,35	0,58	0,06	0,00	0,02	2,53	2,05	0,11	0,09	0,06	0,00	0,00	0,00
UO <sub>2</sub>	0,36	0,31	0,12	0,00	0,28	0,77	0,91	0,00	0,01	0,07	0,00	0,00	0,00
F	1,77	2,42	0,15	0,00	0,42	0,72	0,19	0,65	0,60	0,17	0,00	0,00	0,00
O=F	-0,75	-1,02	-0,06	0,00	-0,18	-0,30	-0,08	-0,27	-0,25	-0,07	0	0	0
Y <sub>2</sub> O <sub>3</sub>	5,71	6,92	0,86	0,22	1,93	3,11	3,61	3,21	2,99	1,80	0,08	0,04	0,00
La <sub>2</sub> O <sub>3</sub>	0,00	0,03	0,00	0,01	0,00	0,02	0,00	0,04	0,05	0,04	0,00	0,04	0,00
Ce <sub>2</sub> O <sub>3</sub>	0,08	0,22	0,06	0,04	0,11	1,29	0,17	0,34	0,25	0,21	0,05	0,04	0,01
Pr <sub>2</sub> O <sub>3</sub>	0,04	0,10	0,00	0,06	0,05	0,02	0,05	0,03	0,00	0,03	0,00	0,00	0,00
Nd <sub>2</sub> O <sub>3</sub>	0,02	0,09	0,00	0,00	0,01	0,06	0,03	0,16	0,13	0,06	0,00	0,00	0,00
Sm <sub>2</sub> O <sub>3</sub>	0,03	0,03	0,00	0,00	0,02	0,01	0,01	0,05	0,01	0,00	0,02	0,09	0,03
Eu <sub>2</sub> O <sub>3</sub>	0,00	0,01	0,00	0,00	0,03	0,04	0,00	0,00	0,10	0,00	0,04	0,00	0,00
Gd <sub>2</sub> O <sub>3</sub>	0,08	0,14	0,01	0,00	0,10	0,12	0,17	0,15	0,15	0,02	0,00	0,00	0,02
Tb <sub>2</sub> O <sub>3</sub>	0,00	0,00	0,00	0,00	0,00	0,00	0,00	0,00	0,00	0,00	0,00	0,00	0,03
Dy <sub>2</sub> O <sub>3</sub>	0,16	0,59	0,00	0,00	0,18	0,38	0,39	0,38	0,25	0,32	0,02	0,00	0,00
Ho <sub>2</sub> O <sub>3</sub>	0,37	0,11	0,00	0,02	0,00	0,12	0,21	0,06	0,00	0,08	0,05	0,00	0,00
Er <sub>2</sub> O <sub>3</sub>	0,75	0,88	0,10	0,00	0,09	0,72	0,94	0,42	0,36	0,37	0,05	0,00	0,03
Tm <sub>2</sub> O <sub>3</sub>	0,16	0,21	0,00	0,00	0,00	0,20	0,14	0,09	0,00	0,10	0,00	0,00	0,00
Yb <sub>2</sub> O <sub>3</sub>	1,49	1,70	0,09	0,01	0,22	2,02	2,45	0,64	0,62	0,53	0,00	0,00	0,00
Lu <sub>2</sub> O <sub>3</sub>	0,22	0,26	0,01	0,04	0,00	0,28	0,44	0,07	0,13	0,00	0,01	0,00	0,00
Total	90,67	86,24	90,22	100,50	92,78	95,34	93,75	84,45	84,88	83,32	92,13	93,25	94,27
REE <sub>2</sub> O <sub>3</sub>	3,40	4,37	0,27	0,18	0,80	5,26	4,99	2,42	2,05	1,75	0,24	0,17	0,11
REE <sub>2</sub> Y <sub>2</sub> O <sub>3</sub>	9,11	11,29	1,13	0,4	2,73	8,37	8,6	5,63	5,04	3,55	0,32	0,21	0,11
LREE <sub>2</sub> O <sub>3</sub>	0,17	0,47	0,06	0,11	0,22	1,43	0,26	0,62	0,54	0,34	0,11	0,17	0,04
HREE <sub>2</sub> O <sub>3</sub>	3,23	3,90	0,22	0,07	0,59	3,83	4,73	1,81	1,51	1,41	0,13	0,00	0,07
HREEY <sub>2</sub> O <sub>3</sub>	8,94	10,82	1,07	0,29	2,51	6,94	8,34	5,02	4,50	3,21	0,21	0,04	0,07
Zr/Hf	41,54	25,46	57,14	43,71	17,47	19,32	20,48	24,50	29,93	22,84	17,49	69,68	56,33

Table 1 (extended). Number of ions on the basis of 16 (O, F)

Si	3,47	3,43	3,79	3,94	3,72	3,62	3,90	3,59	3,66	3,74	3,98	3,94	3,98
Zr	3,36	3,09	3,82	3,95	3,68	3,42	3,19	3,33	3,47	3,73	3,94	3,95	3,89
Hf	0,05	0,07	0,15	0,05	0,13	0,11	0,09	0,08	0,09	0,13	0,03	0,04	0,08
Al	0,28	0,17	0,02	0,00	0,11	0,08	0,07	0,46	0,28	0,07	0,00	0,00	0,00
P	0,05	0,08	0,03	0,01	0,05	0,02	0,04	0,06	0,04	0,02	0,01	0,00	0,01
Ti	0,00	0,00	0,00	0,00	0,00	0,02	0,02	0,00	0,00	0,01	0,01	0,00	0,01
Fe	0,09	0,16	0,06	0,03	0,10	0,10	0,13	0,17	0,25	0,09	0,00	0,00	0,00
Ca	0,08	0,09	0,08	0,01	0,06	0,03	0,05	0,13	0,11	0,04	0,00	0,03	0,00
Mn	0,04	0,02	0,00	0,00	0,11	0,16	0,05	0,00	0,01	0,01	0,00	0,00	0,00
Nb	0,06	0,09	0,02	0,00	0,00	0,04	0,06	0,05	0,00	0,04	0,00	0,04	0,02
Ta	0,00	0,01	0,00	0,00	0,01	0,01	0,01	0,00	0,00	0,00	0,01	0,00	0,00
Pb	0,01	0,00	0,00	0,00	0,00	0,01	0,03	0,00	0,00	0,00	0,00	0,00	0,00
Th	0,01	0,02	0,00	0,00	0,00	0,08	0,06	0,00	0,00	0,00	0,00	0,00	0,00
U	0,01	0,01	0,00	0,00	0,01	0,02	0,03	0,00	0,00	0,00	0,00	0,00	0,00
F	0,80	1,17	0,07	0,00	0,18	0,32	0,08	0,31	0,28	0,08	0,00	0,00	0,00
Y	0,44	0,56	0,06	0,01	0,14	0,23	0,27	0,25	0,24	0,15	0,01	0,00	0,00
La	0,00	0,00	0,00	0,00	0,00	0,00	0,00	0,00	0,00	0,00	0,00	0,00	0,00
Ce	0,00	0,01	0,00	0,00	0,01	0,07	0,01	0,02	0,01	0,01	0,00	0,00	0,00
Pr	0,00	0,01	0,00	0,00	0,00	0,00	0,00	0,00	0,00	0,00	0,00	0,00	0,00
Nd	0,00	0,00	0,00	0,00	0,00	0,00	0,00	0,01	0,01	0,00	0,00	0,00	0,00
Sm	0,00	0,00	0,00	0,00	0,00	0,00	0,00	0,00	0,00	0,00	0,00	0,00	0,00
Eu	0,00	0,00	0,00	0,00	0,00	0,00	0,00	0,00	0,01	0,00	0,00	0,00	0,00
Gd	0,00	0,01	0,00	0,00	0,00	0,01	0,01	0,01	0,01	0,00	0,00	0,00	0,00
Tb	0,00	0,00	0,00	0,00	0,00	0,00	0,00	0,00	0,00	0,00	0,00	0,00	0,00
Dy	0,01	0,03	0,00	0,00	0,01	0,02	0,02	0,02	0,01	0,02	0,00	0,00	0,00
Ho	0,02	0,01	0,00	0,00	0,00	0,01	0,01	0,00	0,00	0,00	0,00	0,00	0,00
Er	0,03	0,04	0,00	0,00	0,00	0,03	0,04	0,02	0,02	0,02	0,00	0,00	0,00
Tm	0,01	0,01	0,00	0,00	0,00	0,01	0,01	0,00	0,00	0,00	0,00	0,00	0,00
Yb	0,07	0,08	0,00	0,00	0,01	0,09	0,10	0,03	0,03	0,02	0,00	0,00	0,00
Lu	0,01	0,01	0,00	0,00	0,00	0,01	0,02	0,00	0,01	0,00	0,00	0,00	0,00
Total	8,90	9,20	8,13	8,02	8,33	8,51	8,31	8,48	8,47	8,17	8,00	8,01	8,00



### 5.1.3. Monazite-(Ce) ((Ce,La,Nd,Th)PO<sub>4</sub>)

Monazite is an accessory mineral commonly found in granitic rocks and, together with allanite and apatite, the main LREE-hosting phase, with sizable contents of U and Th and low HREE and Y (Hinton e Paterson 1994, Bea *et al.* 1994, Bea 1996, Chang *et al.* 1996, Deer *et al.* 1997, Teixeira e Botelho 2002).

In the FPTD, monazite is found in prismatic hypidiomorphic (Fig. 4a – D, G and H) or irregular crystals rimming apatite grains (Fig. 4b – I and J). It has yellow to red colors, and sizes range between 10 and 30 µm. Monazite is classified as primary and hydrothermal. The primary crystals come from the least weathered evolved granitic rock, while hydrothermal monazite crystals are found in greisens and greisenized granites related to pb1b. The primary monazite has Ce<sub>2</sub>O<sub>3</sub> concentrations between 22.57% and 44.29%, La<sub>2</sub>O<sub>3</sub> between 6.17% and 24.92%, Pr<sub>2</sub>O<sub>3</sub> between 1.56% and 3.17%, Y<sub>2</sub>O<sub>3</sub> between 0.22% and 1.01%, LREE<sub>2</sub>O<sub>3</sub> from 37.50% to 74.97%, HREEY<sub>2</sub>O<sub>3</sub> from 0.42% to 2.58% and ThO<sub>2</sub> from 0.38% to 3.35% (Table 3). On the other hand, the hydrothermal monazite shows Ce<sub>2</sub>O<sub>3</sub> concentrations ranging from 39.03% to 33.16%; La<sub>2</sub>O<sub>3</sub>, 8.35% to 13.69%; Pr<sub>2</sub>O<sub>3</sub>, 2.44% to 3.55%; Y<sub>2</sub>O<sub>3</sub>, 0.08% to 1.49%; LREE<sub>2</sub>O<sub>3</sub>, 58.75% to 68.65%; (HREEY<sub>2</sub>O<sub>3</sub>), 0.86% to 3.78%; and ThO<sub>2</sub>, 0.98% to 2.70% (Table 4). These results indicate that primary monazite is richer in Ce<sub>2</sub>O<sub>3</sub>, La<sub>2</sub>O<sub>3</sub>, and ThO<sub>2</sub> and poorer in Pr<sub>2</sub>O<sub>3</sub>, HREE<sub>2</sub>O<sub>3</sub> and Y<sub>2</sub>O<sub>3</sub>, corroborating the observations of Teixeira & Botelho (2002).

### 5.1.4. Apatite Ca<sub>5</sub>(PO<sub>4</sub>)<sub>3</sub>(OH,F,Cl)

Apatite is one of the most abundant nonsilicate minerals in the crust. It is an important REE-bearing mineral across several settings and rock types and can be the main REE-bearing phase in granites.

In the FPTD, apatite is found especially in the parent biotite granite pb1b as 20 to 200 µm prismatic and irregular crystals. The studied apatite shows alteration and substitution, mainly by monazite observed at the edges (Fig. 4a-G and H) and (Fig. 4b – I and J) or in the fractures of the grains (Fig. 4b- I). The P<sub>2</sub>O<sub>5</sub> contents range between 31.66% and 41.80%; Y<sub>2</sub>O<sub>3</sub>, from 0.12% and 2.87%; and LREE<sub>2</sub>O<sub>3</sub> contents, between 0.49% and 5.25%. Among LREE, Ce<sub>2</sub>O<sub>3</sub> is the most abundant with contents ranging between 0.22% and 2.52%, followed by Nd<sub>2</sub>O<sub>3</sub> ranging between 0.6% and 1.48%. Likewise, for the HREE (0.34% to 4.05%), Gd<sub>2</sub>O<sub>3</sub> is the most abundant with contents of 0.07% and 0.88% and is followed by Dy<sub>2</sub>O<sub>3</sub> from 0.04% to 0.66%. The HREE<sub>2</sub>O<sub>3</sub>+Y<sub>2</sub>O<sub>3</sub> contents range between 0.34% and 5.25% (Table 5).



Table 4. EPMA analyses of hydrothermal monazite

Facies		Greisen (1A) and greisenized pblb granite (NC4B)								Number of ions on the basis of 16 (O, F)									
Sample	1A (1)	1A (2)	1A (3)	1A (4)	1A (5)	1A (6)	NC4B (1)	NC4B (2)	NC4B (3)										
(wt %)																			
P <sub>2</sub> O <sub>5</sub>	24,73	24,36	26,33	24,54	25,51	25,37	25,25	25,91	25,88	P	3,57	3,56	3,70	3,65	3,70	3,75	3,51	3,68	3,62
CaO	0,63	0,13	0,00	0,22	0,00	0,28	0,00	0,00	0,25	Ca	0,12	0,02	0,00	0,04	0,00	0,05	0,00	0,00	0,04
ThO <sub>2</sub>	1,99	2,18	1,78	1,06	0,98	1,39	2,70	1,73	2,31	Th	0,08	0,09	0,07	0,04	0,04	0,06	0,10	0,07	0,09
SiO <sub>2</sub>	0,39	0,50	0,88	0,23	0,59	0,18	0,28	0,24	0,73	Si	0,07	0,09	0,15	0,04	0,10	0,03	0,05	0,04	0,12
Y <sub>2</sub> O <sub>3</sub>	1,49	0,20	0,38	0,23	1,18	0,92	0,08	0,21	0,73	Y	0,14	0,02	0,03	0,02	0,11	0,09	0,01	0,02	0,06
ZrO <sub>2</sub>	0,60	0,83	0,67	0,54	0,80	0,55	0,70	0,78	0,60	Zr	0,05	0,07	0,05	0,05	0,07	0,05	0,06	0,06	0,05
FeO	0,15	0,09	0,19	0,26	0,45	0,60	0,80	0,12	0,20	Fe	0,02	0,01	0,03	0,04	0,06	0,09	0,11	0,02	0,03
PbO	0,13	0,18	0,14	0,01	0,03	0,11	0,10	0,00	0,13	Pb	0,01	0,01	0,01	0,00	0,00	0,01	0,00	0,00	0,01
UO <sub>2</sub>	0,22	0,00	0,00	0,02	0,18	0,16	0,01	0,04	0,00	U	0,01	0,00	0,00	0,00	0,01	0,01	0,00	0,00	0,00
F	1,19	1,289	1,658	1,344	1,135	1,044	1,711	1,32	0,948	F	0,64	0,70	0,87	0,75	0,62	0,58	0,89	0,70	0,49
O=F	-0,50	-0,54	-0,70	-0,57	-0,48	-0,44	-0,72	-0,56	-0,40	La	0,84	0,53	0,72	0,80	0,80	0,77	0,72	0,85	0,72
La <sub>2</sub> O <sub>3</sub>	13,34	8,35	11,81	12,35	12,69	12,04	11,87	13,69	11,77	Ce	2,21	2,16	2,20	2,29	2,12	2,12	2,35	2,10	2,23
Ce <sub>2</sub> O <sub>3</sub>	35,29	34,22	36,16	35,54	33,71	33,17	39,03	34,30	36,94	Pr	0,15	0,22	0,17	0,17	0,16	0,16	0,20	0,20	0,19
Pr <sub>2</sub> O <sub>3</sub>	2,44	3,55	2,83	2,68	2,59	2,47	3,38	3,21	3,23	Nd	0,54	0,94	0,57	0,60	0,51	0,55	0,70	0,68	0,67
Nd <sub>2</sub> O <sub>3</sub>	8,94	15,26	9,66	9,54	8,33	8,85	11,99	11,40	11,44	Sm	0,10	0,16	0,07	0,11	0,10	0,11	0,10	0,09	0,10
Sm <sub>2</sub> O <sub>3</sub>	1,70	2,68	1,14	1,76	1,66	1,90	1,82	1,60	1,71	Eu	0,03	0,04	0,04	0,03	0,02	0,02	0,03	0,03	0,03
Eu <sub>2</sub> O <sub>3</sub>	0,49	0,60	0,63	0,50	0,36	0,33	0,57	0,48	0,53	Gd	0,06	0,07	0,03	0,06	0,06	0,07	0,03	0,04	0,05

Gd <sub>2</sub> O <sub>3</sub>	1,13	1,15	0,54	1,03	1,00	1,14	0,48	0,73	0,92	Tb	0,01	0,00	0,00	0,00	0,00	0,00	0,00	0,00	0,00
Tb <sub>2</sub> O <sub>3</sub>	0,16	0,00	0,00	0,00	0,00	0,00	0,00	0,00	0,00	Dy	0,03	0,01	0,00	0,01	0,04	0,04	0,00	0,02	0,00
Dy <sub>2</sub> O <sub>3</sub>	0,46	0,20	0,00	0,16	0,78	0,67	0,00	0,32	0,08	Ho	0,00	0,00	0,00	0,00	0,01	0,01	0,00	0,01	0,01
Ho <sub>2</sub> O <sub>3</sub>	0,09	0,05	0,00	0,00	0,11	0,12	0,07	0,26	0,13	Er	0,01	0,00	0,00	0,00	0,01	0,01	0,01	0,01	0,00
Er <sub>2</sub> O <sub>3</sub>	0,23	0,09	0,02	0,08	0,22	0,22	0,10	0,25	0,09	Tm	0,00	0,00	0,00	0,01	0,00	0,00	0,01	0,01	0,00
Tm <sub>2</sub> O <sub>3</sub>	0,09	0,08	0,02	0,19	0,00	0,07	0,12	0,10	0,07	Yb	0,00	0,00	0,00	0,00	0,00	0,00	0,00	0,00	0,00
Yb <sub>2</sub> O <sub>3</sub>	0,07	0,01	0,00	0,00	0,06	0,00	0,00	0,03	0,04	Lu	0,00	0,00	0,00	0,00	0,00	0,00	0,00	0,00	0,00
Lu <sub>2</sub> O <sub>3</sub>	0,06	0,00	0,00	0,00	0,00	0,06	0,00	0,01	0,00	Total	8,69	8,70	8,70	8,71	8,55	8,56	8,89	8,63	8,53
Total	95,17	95,11	93,50	91,38	92,66	90,85	100,03	95,88	98,26										
REE <sub>2</sub> O <sub>3</sub>	64,48	66,23	62,81	63,84	61,50	61,02	69,42	66,37	66,96										
LREE <sub>2</sub> O <sub>3</sub>	62,19	64,66	62,23	62,37	59,33	58,75	68,65	64,67	65,63										
HREE <sub>2</sub> O <sub>3</sub>	2,29	1,57	0,58	1,47	2,17	2,27	0,77	1,70	1,33										
HREE <sub>2</sub> O <sub>3</sub> +Y <sub>2</sub> O <sub>3</sub>	3,78	1,76	0,96	1,70	3,34	3,19	0,86	1,91	2,06										

Table 5: EPMA analyses of fluorapatite

Facies Sample	Biotite granite pblb																
	NC10 (1)	NC10 (2)	NC10 (3)	NC10 (4)	NC10 (5)	NC10 (6)	NC10 (7)	NC10 (8)	NC10 (9)	NC10 (10)	NC10 (11)	NC10 (12)	NC10 (13)	NC10 (14)	NC10 (15)	NC10 (16)	NC10 (17)
(wt%)																	
P <sub>2</sub> O <sub>5</sub>	37,80	41,03	38,87	41,80	40,05	40,29	38,43	41,26	31,66	38,75	38,11	39,69	36,66	36,77	36,53	39,24	39,50
SiO <sub>2</sub>	2,05	0,33	2,05	0,36	0,26	0,87	1,69	0,79	6,52	1,97	4,03	0,76	2,27	1,76	1,67	0,55	0,36
ThO <sub>2</sub>	0,01	0,03	0,03	n.d.	n.d.	n.d.	0,04	0,03	0,24	0,09	n.d.	0,04	0,03	n.d.	n.d.	0,03	n.d.
UO <sub>2</sub>	n.d.	n.d.	0,02	n.d.	n.d.	n.d.	n.d.	n.d.	n.d.	n.d.	n.d.						
Y <sub>2</sub> O <sub>3</sub>	1,00	0,31	0,97	0,12	0,25	0,21	0,43	0,15	0,91	0,42	1,38	1,13	2,87	2,21	2,01	0,54	0,30
La <sub>2</sub> O <sub>3</sub>	0,23	0,09	0,22	0,25	0,02	0,30	0,30	0,18	0,59	0,52	0,05	0,10	0,28	0,13	0,14	0,18	0,32
Ce <sub>2</sub> O <sub>3</sub>	0,91	0,33	0,73	0,64	0,22	1,11	1,58	0,79	2,52	1,45	0,41	0,34	0,81	0,86	0,84	0,73	0,61
Pr <sub>2</sub> O <sub>3</sub>	0,09	n.d.	0,10	0,20	n.d.	0,11	0,55	0,38	0,32	0,28	0,52	0,52	n.d.	n.d.	n.d.	0,41	0,10
Nd <sub>2</sub> O <sub>3</sub>	0,62	0,16	0,56	0,32	0,25	0,43	0,84	0,53	1,48	0,74	0,60	0,49	0,87	0,86	0,81	0,42	0,39
Sm <sub>2</sub> O <sub>3</sub>	0,19	0,08	0,33	0,10	n.d.	0,03	0,27	0,08	0,34	0,20	n.d.	n.d.	0,51	n.d.	0,09	0,09	0,34
Eu <sub>2</sub> O <sub>3</sub>	n.d.	n.d.	n.d.	n.d.	n.d.	n.d.	n.d.	n.d.	n.d.	n.d.	0,06	n.d.	0,07	0,07	n.d.	0,03	0,06
Gd <sub>2</sub> O <sub>3</sub>	0,50	0,15	0,44	0,12	0,07	0,13	0,21	0,20	0,55	0,21	n.d.	0,40	0,16	0,88	0,48	n.d.	n.d.
Dy <sub>2</sub> O <sub>3</sub>	0,30	0,04	0,37	0,10	0,11	0,11	0,16	0,09	0,38	0,03	0,22	0,19	0,66	0,40	0,47	0,07	n.d.
Er <sub>2</sub> O <sub>3</sub>	n.d.	n.d.	n.d.	n.d.	n.d.	n.d.	n.d.	n.d.	n.d.	n.d.	0,31	n.d.	n.d.	0,31	0,04	0,49	0,31
Yb <sub>2</sub> O <sub>3</sub>	0,15	0,08	0,14	n.d.	0,02	0,07	0,13	0,01	0,14	0,08	0,14	0,15	0,21	0,25	0,17	0,06	n.d.
CaO	49,77	53,15	50,64	53,75	52,72	53,38	51,24	53,75	44,61	51,17	50,36	51,90	49,28	50,37	50,03	52,78	53,33
F	5,97	6,09	5,41	5,56	6,32	5,13	5,26	4,49	5,05	5,78	4,20	4,78	3,79	3,81	4,46	4,14	3,95
MnO	n.d.	n.d.	n.d.	n.d.	n.d.	n.d.	n.d.	n.d.	n.d.	n.d.	0,16	0,23	0,28	0,17	0,17	0,22	0,10
FeO	n.d.	n.d.	n.d.	n.d.	n.d.	n.d.	n.d.	n.d.	n.d.	n.d.	0,25	0,13	0,33	0,31	0,39	0,20	0,21
Na <sub>2</sub> O	n.d.	n.d.	n.d.	n.d.	n.d.	n.d.	n.d.	n.d.	n.d.	n.d.	0,03	0,01	0,01	n.d.	n.d.	n.d.	n.d.
Total	99,61	101,88	100,87	103,32	100,30	102,18	101,11	102,75	95,30	101,69	100,83	100,85	99,10	99,17	98,31	100,19	99,90
O=F	-2,52	-2,57	-2,28	-2,34	-2,66	-2,16	-2,21	-1,89	-2,13	-2,43	-1,77	-2,01	-1,60	-1,60	-1,88	-1,74	-1,66
Total	97,10	99,31	98,59	100,98	97,64	100,02	98,90	100,86	93,17	99,26	99,06	98,83	97,51	97,56	96,43	98,45	98,24

### 5.1.5. Thorite ( $ThSiO_4$ )

Thorite is found solely in a few biotite granite pb1c and greisenized granite samples, where crystals with sizes of 20  $\mu m$  are close to zircon grains (Fig. 4b - K and L).

SEM analyses show thorite and xenotime "intergrowths" as evident from the high  $P_2O_5$  and  $Y_2O_3$  contents, spanning intervals of 0.84%-1.52% and 5.54%-9.10%, respectively. The REE contents are between 2.86% and 3.63%, with HREE between 2.33% and 3.14%, which are higher than 0.49% to 0.57% found for LREE. HREE+ $Y_2O_3$  span an interval from 12.24% to 8.37% (table 6).

Table 6. EPMA analyses of thorite

Facies	biotite granite pb1c									
	Sample	NC11A	NC3A	NC3A	NC3A	Sample	NC11A	NC3A	NC3A	NC3A
(wt%)		(1)	(2)	(3)	(wt%)		(1)	(2)	(3)	
ThO <sub>2</sub>	62,58	53,63	54,78	47,71	La <sub>2</sub> O <sub>3</sub>	0,11	0,08	0,02	0,02	
Al <sub>2</sub> O <sub>3</sub>	0,72	1,65	0,23	0,25	Ce <sub>2</sub> O <sub>3</sub>	0,36	0,26	0,26	0,18	
SiO <sub>2</sub>	17,06	12,16	11,78	11,04	Pr <sub>2</sub> O <sub>3</sub>	0,05	0,06	0	0,07	
Nb <sub>2</sub> O <sub>5</sub>	0	3,14	3,88	2,84	Nd <sub>2</sub> O <sub>3</sub>	0,21	0,14	0,11	0,13	
P <sub>2</sub> O <sub>5</sub>	1,16	1,18	1,52	1,12	Sm <sub>2</sub> O <sub>3</sub>	0,08	0	0,07	0,06	
Y <sub>2</sub> O <sub>3</sub>	2,26	6,18	9,1	6,64	Eu <sub>2</sub> O <sub>3</sub>	0,14	0	0,02	0,07	
Ta <sub>2</sub> O <sub>5</sub>	0	0,006	0,26	0	Gd <sub>2</sub> O <sub>3</sub>	0,21	0,1	0,28	0,17	
TiO <sub>2</sub>	0	1,63	0,74	0,41	Dy <sub>2</sub> O <sub>3</sub>	0,12	0,44	0,57	0,5	
CaO	1,07	0,29	0,21	0,57	Yb <sub>2</sub> O <sub>3</sub>	0	1,09	1,08	0,71	
MnO	0	0,12	0,03	0	Ho <sub>2</sub> O <sub>3</sub>	0,21	0,16	0,22	0,01	
FeO	3,48	2,49	2,52	1,19	Er <sub>2</sub> O <sub>3</sub>	0,20	0,75	0,79	0,63	
ZrO <sub>2</sub>	0	1,12	0,82	0,56	Tm <sub>2</sub> O <sub>3</sub>	0	0,03	0,01	0,06	
PbO	0,23	0	0	0,1	Tb <sub>2</sub> O <sub>3</sub>	0	0	0	0	
F	1,20	1,75	3,23	4,36	Lu <sub>2</sub> O <sub>3</sub>	0	0,21	0,2	0,25	
UO <sub>2</sub>	0,95	0,77	1,27	1,27	REE	1,68	3,33	3,63	2,86	
BaO	0,04	0	0	0,06	LREE	0,94	0,55	0,49	0,52	
					HREE	0,73	2,78	3,14	2,33	
					HREE+Y <sub>2</sub> O <sub>3</sub>	2,99	8,97	12,24	8,97	
					<b>Total</b>	<b>92,43</b>	<b>89,44</b>	<b>93,98</b>	<b>80,99</b>	
					-O=F	-0,50	-0,74	-1,36	-1,84	
					<b>Total</b>	<b>91,93</b>	<b>88,7</b>	<b>92,62</b>	<b>79,15</b>	

### 5.1.6. REE oxyfluorides

REE oxyfluorides are found widespread or as prismatic crystals in the samples studied. Their sizes range between 2 and 30  $\mu m$ . Additionally, anhedral aggregates have sizes of 70  $\mu m$ . Oxyfluoride grains or aggregates are common near, zircon, xenotime and fluorite crystals. Aggregates of oxyfluorides and allanite (Fig. 4b - M) or xenotime (Fig. 4b - N) can also be observed.

The oxyfluoride compositions vary according to the host rock. In the biotite granite, the oxyfluoride has 8.40% F, 2.49%  $Y_2O_3$  and 2.17%  $ThO_2$ , whereas in the greisenized granite, the contents vary between 4.95 and 8.31% F, 0.24 and 5.36%  $Y_2O_3$ , and 4.11 and 8.99%  $ThO_2$ . In the greisen, the oxyfluoride compositions have 7.15 to 16.55% F, 1.51 to 2.07%  $Y_2O_3$  and 4.11 to 8.99%  $ThO_2$ . The highest REE contents, between 43.84 and 79.87%, are observed in the oxyfluorides from the greisenized granite, with  $Ce_2O_3$  as the most abundant REE oxide with a range of 30.09% to 41.63%.  $HREE_2O_3+Y_2O_3$  span an interval from 0.44% to 14.41%, also with higher concentrations in the greisenized granites related to oxyfluoride and xenotime aggregates.  $Gd_2O_3$  is the most abundant HREE, with contents ranging between 0.03% and 4.44% (Table 7).

Table 7. EPMA analyses of oxyfluorides

Facies	pblb Greisen		Greisenized pblb granite																	pblb Biotite granite	
	1A (1)	NC4A (2)	NC4B (1)	NC4B (2)	NC4B (3)	NC4B (4)	NC4B (5)	NC4B (6)	NC4B (7)	NC4B (8)	NC4B (9)	NC4B (10)	NC4B (11)	NC4B (12)	NC4B (13)	NC4B (14)	NC4B (15)	NC4B (16)	NC4B (17)	NC10A (1)	
(wt %)																					
F	7,15	16,56	7,45	5,80	6,37	5,99	4,95	4,88	6,15	5,71	7,94	8,31	8,18	5,95	7,41	4,69	6,18	7,47	6,50	8,40	
Al <sub>2</sub> O <sub>3</sub>	0,24	0,04	0,01	0,04	0,00	0,00	0,02	0,00	0,07	0,00	0,04	0,04	0,00	0,05	0,07	0,04	0,01	0,00	0,03	0,30	
SiO <sub>2</sub>	2,34	0,26	0,09	0,33	0,06	0,49	0,30	0,28	1,07	0,02	0,15	0,00	0,01	0,02	0,20	0,15	0,14	0,04	0,10	1,26	
P <sub>2</sub> O <sub>5</sub>	0,24	0,16	0,02	0,16	0,00	0,06	0,03	0,00	0,32	0,00	7,34	0,00	0,05	0,09	0,00	0,03	0,00	0,04	0,01	0,26	
CaO	3,23	17,43	0,90	1,25	0,18	0,15	0,11	0,05	1,90	0,00	1,15	2,13	1,40	0,28	0,20	0,29	0,23	0,53	0,66	2,57	
TiO <sub>2</sub>	0,21	0,14	0,29	0,11	0,15	0,06	0,01	0,09	0,03	0,00	0,00	0,00	0,00	0,00	0,09	0,00	0,00	0,00	0,07	0,00	
MnO	0,21	0,00	0,13	0,08	0,04	0,12	0,11	0,13	0,00	0,00	0,00	0,21	0,11	0,00	0,03	0,01	0,02	0,06	0,05	0,00	
FeO	18,93	0,13	0,05	0,38	0,52	1,36	0,07	0,14	1,41	0,57	2,09	0,58	0,08	0,87	0,16	0,07	0,89	0,27	0,00	1,12	
Y <sub>2</sub> O <sub>3</sub>	1,51	2,07	0,27	0,24	0,29	0,31	0,00	0,39	1,31	0,30	0,42	0,90	0,71	0,14	1,48	5,36	0,28	1,89	0,32	2,49	
ZrO <sub>2</sub>	0,50	0,19	0,00	0,00	0,00	0,62	0,00	0,00	1,14	0,00	0,16	0,00	0,00	0,00	0,00	0,00	0,00	0,00	0,00	0,05	
Ta <sub>2</sub> O <sub>5</sub>	0,07	0,00	0,12	0,00	0,00	0,00	0,00	0,06	0,32	0,00	0,17	0,00	0,04	0,13	0,05	0,00	0,10	0,16	0,00	0,01	
ThO <sub>2</sub>	8,99	4,11	2,63	2,85	1,19	1,14	0,29	0,51	6,72	8,03	2,54	3,57	0,26	3,43	2,04	0,62	0,85	2,33	2,25	2,17	
UO <sub>2</sub>	0,10	0,19	0,07	0,02	0,00	0,04	0,00	0,04	0,19	0,13	0,08	0,07	0,01	0,10	0,00	0,00	0,01	0,07	0,05	0,06	
SrO	0,33	0,26	0,36	0,30	0,13	0,14	0,00	0,00	0,22	0,47	0,33	0,33	0,10	0,58	0,18	0,10	0,03	0,13	0,39	0,07	
La <sub>2</sub> O <sub>3</sub>	11,92	9,73	18,53	18,17	19,74	17,97	17,47	16,04	16,25	13,37	12,43	12,79	15,86	16,78	11,24	10,10	17,22	13,97	15,73	11,11	
Ce <sub>2</sub> O <sub>3</sub>	11,14	26,54	41,63	40,99	39,78	39,16	41,13	39,57	34,48	37,75	34,65	31,93	38,82	39,25	33,20	30,09	40,46	37,74	39,38	27,28	
Pr <sub>2</sub> O <sub>3</sub>	3,40	2,84	3,50	3,05	2,86	3,18	3,15	3,66	2,73	3,16	3,31	3,05	3,47	3,28	3,44	2,94	3,26	3,21	3,04	2,22	
Nd <sub>2</sub> O <sub>3</sub>	13,32	12,14	12,27	10,78	10,05	12,16	11,12	15,17	9,58	11,64	14,09	13,23	15,13	12,99	15,12	13,55	12,80	12,55	11,15	9,57	
Sm <sub>2</sub> O <sub>3</sub>	2,42	2,46	1,46	1,48	1,05	1,93	1,40	2,64	1,08	2,13	2,90	2,69	2,54	1,95	3,56	3,83	1,97	2,55	1,66	1,36	
Eu <sub>2</sub> O <sub>3</sub>	0,72	0,47	0,56	0,58	0,47	0,49	0,61	0,55	0,50	0,53	0,55	0,45	0,61	0,53	0,59	0,42	0,52	0,55	0,39	0,41	
Gd <sub>2</sub> O <sub>3</sub>	0,67	2,28	0,43	0,03	0,00	0,36	0,11	1,62	0,26	0,77	1,41	1,52	1,60	0,74	3,81	4,44	0,58	1,64	0,49	1,04	
Tb <sub>2</sub> O <sub>3</sub>	0,00	0,16	0,08	0,00	0,00	0,00	0,00	0,03	0,00	0,00	0,00	0,00	0,11	0,00	0,31	0,51	0,00	0,00	0,06	0,00	
Dy <sub>2</sub> O <sub>3</sub>	0,00	0,84	0,00	0,00	0,00	0,00	0,10	0,24	0,13	0,00	0,09	0,14	0,29	0,00	1,37	3,03	0,00	0,49	0,00	0,41	
Ho <sub>2</sub> O <sub>3</sub>	0,00	0,00	0,15	0,11	0,12	0,00	0,01	0,21	0,29	0,00	0,00	0,06	0,21	0,01	0,19	0,40	0,24	0,02	0,00	0,09	
Er <sub>2</sub> O <sub>3</sub>	0,21	0,26	0,11	0,01	0,11	0,00	0,12	0,12	0,14	0,08	0,18	0,08	0,12	0,04	0,20	0,39	0,06	0,08	0,03	0,15	
Tm <sub>2</sub> O <sub>3</sub>	0,05	0,09	0,05	0,05	0,00	0,06	0,12	0,03	0,03	0,04	0,05	0,14	0,11	0,07	0,22	0,13	0,08	0,09	0,11	0,10	
Yb <sub>2</sub> O <sub>3</sub>	0,00	0,07	0,07	0,00	0,05	0,00	0,00	0,00	0,00	0,00	0,00	0,00	0,03	0,00	0,00	0,05	0,00	0,01	0,00	0,09	
Lu <sub>2</sub> O <sub>3</sub>	0,00	0,08	0,04	0,00	0,00	0,00	0,00	0,00	0,04	0,00	0,00	0,05	0,03	0,10	0,09	0,09	0,00	0,02	0,02	0,00	
Total	87,60	99,50	91,27	86,81	83,16	85,79	81,21	86,44	86,35	84,69	92,07	82,27	89,87	87,35	85,25	81,34	85,94	85,91	82,49	72,59	
-O=F	-3,01	-6,97	-3,14	-2,44	-2,68	-2,52	-2,08	-2,06	-2,60	-2,40	-3,34	-3,50	-3,44	-2,50	-3,12	-1,98	-2,60	-3,15	-2,74	-3,54	
Total	84,60	92,53	88,13	84,40	80,48	83,27	79,13	84,38	83,75	82,29	88,73	78,77	86,43	84,85	82,13	79,36	83,34	82,76	79,75	69,05	
REE	43,84	57,94	78,87	75,24	74,23	75,31	75,32	79,87	65,50	69,46	69,66	66,13	78,92	75,71	73,34	69,98	77,20	72,92	72,06	53,83	
LREE	42,92	54,17	77,95	75,04	73,95	74,89	74,87	77,62	64,62	68,57	67,93	64,15	76,42	74,76	67,15	60,94	76,24	70,57	71,35	51,95	
HREE	0,93	3,77	0,92	0,20	0,28	0,42	0,45	2,24	0,89	0,89	1,73	1,98	2,50	0,95	6,19	9,04	0,96	2,35	0,71	1,88	
HREE+Y <sub>2</sub> O <sub>3</sub>	2,44	5,84	1,19	0,44	0,57	0,73	0,45	2,63	2,20	1,19	2,16	2,88	3,21	1,08	7,67	14,41	1,24	4,24	1,03	4,36	

### 5.1.7. Unidentified Nb-Y-REE mineral

During MEV and EPMA analytical procedures, some opaque prismatic grains revealed a Nb-, Y, and REE-rich composition (Fig. 4b - O). Nb<sub>2</sub>O<sub>5</sub> and Y<sub>2</sub>O<sub>3</sub> contents are as high as 41.7% and 12.5%, respectively. REE oxides range between 4.24 and 9.3%, with approximately 3 to 7% HREE<sub>2</sub>O<sub>3</sub> and 1.3% to 2.3% LREE<sub>2</sub>O<sub>3</sub>. HREE<sub>2</sub>O<sub>3</sub>+Y<sub>2</sub>O<sub>3</sub> contents are between 5.3% and 19.5% (Table 8). Other elements in concentrations greater than 1% (wt% oxides) are Si, Ti, Fe, Ta, Th, U, and Pb. This mineral has a composition near that of some niobates, such as yttracolumbite-(Y), but its complete identification requires additional investigation.

Table 8. EPMA analyses for the unidentified Nb-Y-REE phase

Facies Sample (wt%)	pb1b granite				
	NC3A (1)	NC3A (2)		NC3A (1)	NC3A (2)
F	0,97	0,08	La <sub>2</sub> O <sub>3</sub>	0,31	0,19
Al <sub>2</sub> O <sub>3</sub>	0,34	0,49	Ce <sub>2</sub> O <sub>3</sub>	1,14	0,63
SiO <sub>2</sub>	5,87	4,76	Pr <sub>2</sub> O <sub>3</sub>	0,12	0,02
Nb <sub>2</sub> O <sub>5</sub>	33,84	41,69	Nd <sub>2</sub> O <sub>3</sub>	0,42	0,25
P <sub>2</sub> O <sub>5</sub>	0	0	Sm <sub>2</sub> O <sub>3</sub>	0,24	0,12
Y <sub>2</sub> O <sub>3</sub>	12,52	2,32	Eu <sub>2</sub> O <sub>3</sub>	0,05	0,04
Ta <sub>2</sub> O <sub>5</sub>	2,39	2,75	Gd <sub>2</sub> O <sub>3</sub>	0,47	0,15
TiO <sub>2</sub>	2,78	7,09	DY <sub>2</sub> O <sub>3</sub>	1,76	0,79
CaO	0,9	0,28	Yb <sub>2</sub> O <sub>3</sub>	1,94	0,87
MnO	0,26	0,59	Ho <sub>2</sub> O <sub>3</sub>	0,63	0,09
FeO	4,06	15,36	Er <sub>2</sub> O <sub>3</sub>	1,88	0,9
ZrO <sub>2</sub>	0,38	0,07	Tm <sub>2</sub> O <sub>3</sub>	0,27	0,12
PbO	6,28	7,18	Tb <sub>2</sub> O <sub>3</sub>	0	0
ThO <sub>2</sub>	2,45	1,56	Lu <sub>2</sub> O <sub>3</sub>	0,07	0,06
UO <sub>2</sub>	1,64	1,84	REE <sub>2</sub> O <sub>3</sub>	9,27	4,24
BaO	0	0,15	LREE <sub>2</sub> O <sub>3</sub>	2,27	1,26
Total	63,89	75,44	HREE <sub>2</sub> O <sub>3</sub>	7	2,98
			HREE <sub>2</sub> O <sub>3</sub> +Y <sub>2</sub> O <sub>3</sub>	19,52	5,3

### 5.2 - Whole-rock geochemistry

The geochemical analyses show that the parental biotite granite pb1b is more enriched in light rare earth elements (LREE) than in heavy rare earth elements (HREE). The LREE range between 580 and 954 ppm, especially Ce with the highest values between 230 and 461 ppm. On the other hand, the HREE display values between 88.3 and 150 ppm; nevertheless, the sum of HREE+Y spans an interval between 221.5 and 366 ppm. Among the HREE, Dy and Gd have the highest enrichments with concentrations from 23.7 to 39.7 ppm and from 26.9 to 35.9 ppm, respectively.

The greisenized granite samples also display higher LREE enrichment in comparison with HREE, with contents ranging between 180 and 1223 ppm. Likewise, in the parental granite, Ce displays the highest contents, ranging between 156 and 491 ppm, followed by La with 30 to 310 ppm and Nd with 36 to 279 ppm. The HREE contents span an 83 to 210 ppm interval. Nevertheless, some samples have higher HREE+Y than LREE, above 500 ppm, whereas the LREE contents are as high as 448 ppm. Among HREE, Y, Gd and Dy have the highest concentrations and vary between 119 and 296 ppm, 20 and 56 ppm and 21 and 59 ppm, respectively.

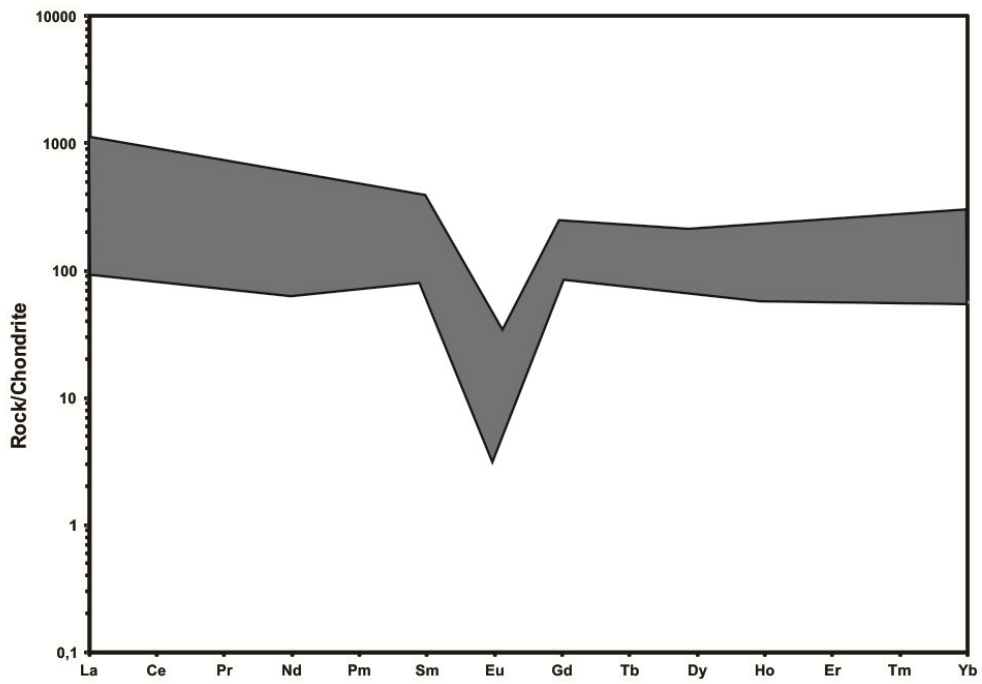
The only analyzed greisen with tin mineralization displays higher LREE concentrations than HREE, akin to the biotite granites and greisenized granites. The LREE in this sample have a total concentration of 1198 ppm. Ce, La and Nd are especially noteworthy, with 514 ppm, 306 ppm and 259 ppm concentrations, respectively. The HREE show a total concentration of 126 ppm, with Gd, Dy and Yb as major contributors at 34.7 ppm, 29.8 ppm and 23.8 ppm, respectively. The Y content is 292 ppm, and the HREE+Y content is 417.9 ppm (Table 9).

REE patterns are crucial for analysis of both the concentration and the behavior of these elements during magmatic differentiation as well as hydrothermal alteration. Normalized LREE contents show enrichments reaching 1000 times and HREE higher than 100 times the chondritic values (Fig. 7). These values reflect high enrichment and indicate economic potential for exploitation of these metals, according to similar data reported for granites in the literature (Wang *et al.*, 2015, Xu *et al.* 2017).

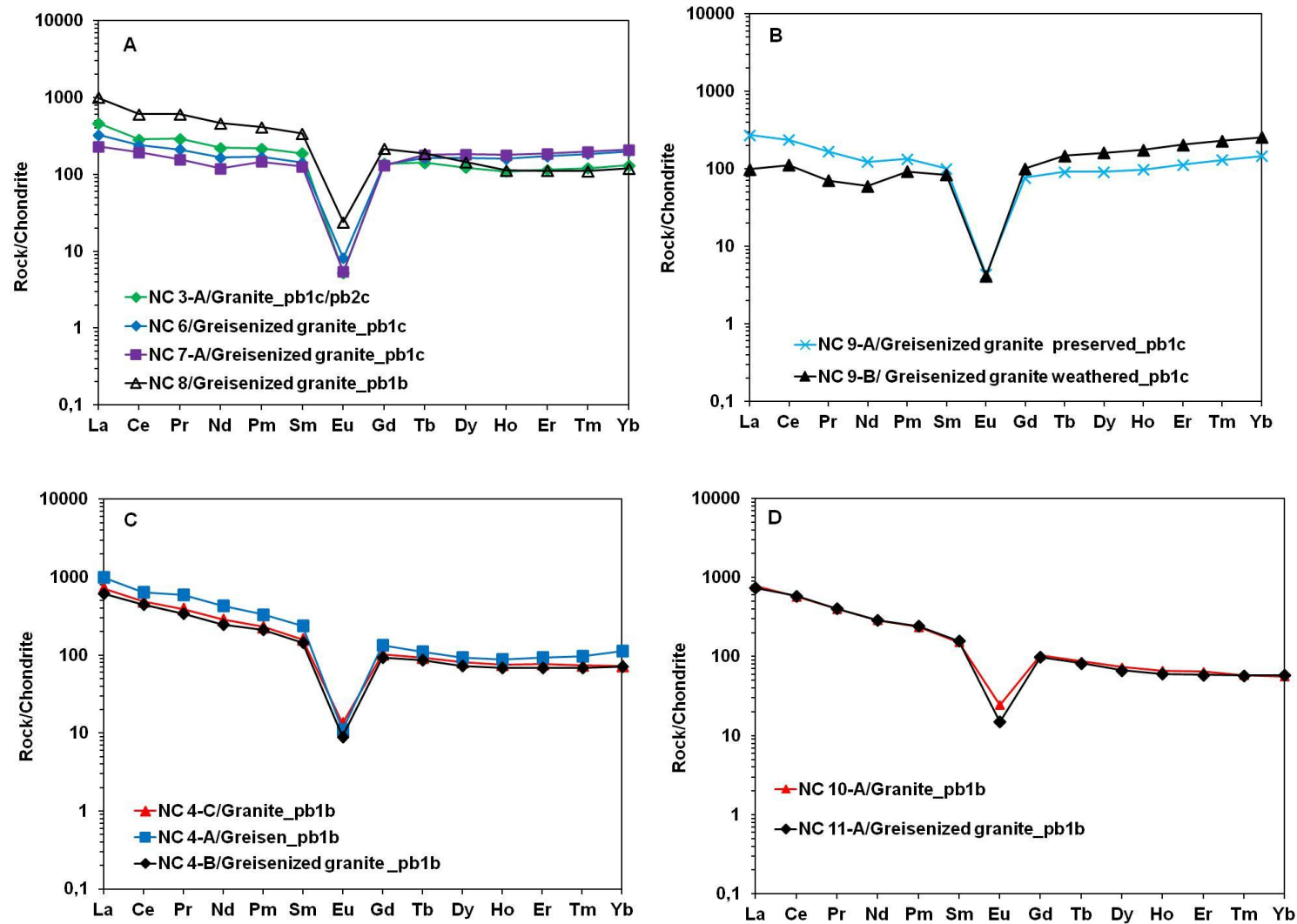
The REE patterns in granite, greisenized granite and greisen from Faixa Placha show behaviors of differentiated rocks, which match their evolution. Strongly differentiated granite pb1c is enriched in LREE and slightly depleted in HREE but still higher than 100 times the concentrations in chondrites (sample NC3A, Fig. 8A). In the greisenized granites of the pb1c facies (NC6 and NC7), LREE and HREE are enriched as much as 300 times that of chondrites. Greisenized granite NC8 also belongs to the Pb1c facies with enrichments in LREE and HREE of 1000 and 100 times relative to chondrites, respectively. The weathered greisenized granite Pb1c presents enrichment in HREE and depletion in LREE when compared to the pristine greisenized granite (Fig. 8B). In the pb1b facies, the parental biotite granite, greisenized granite and greisen have the same REE patterns. A weak enrichment in both LREE and HREE is observed in the greisen, but this enrichment could be related to the normal variation in REE concentrations in the pb1b granite (Fig. 8C). The same behavior is observed in the pb1b parental and greisenized granites, situated far from each other (Fig. 8D). In this case, NC10A and NC11A samples represent the core and the edge of the granite intrusion, respectively, but have the same REE patterns and contents, indicating that there is no relevant change in concentration and fractionation of REE during greisenization. The same REE behavior has been observed in other greisenized areas of the Pedra Branca Massif and in the FPTD by Teixeira and Botelho (2006).

Table 9: Chemical composition (major elements, traces and rare earths) of the parent granite, greisenized granites and greisen from Faixa Placha.

Rocks	Biotite granite			Greisenized granite								Greisen
	pb1c/pb2c	pb1b	pb1b	pb1c/pb2c	pb1b	pb1c	pb1c	pb1c	pb1c	pb1c	pb2b	
Facies	NC3A	NC4C	NC10A	NC3B	NC4B	NC6	NC7A	NC8	NC9A	NC9B	NC11A	NC4A
Sample												
(%)												
SiO <sub>2</sub>	75,42	72,9	74,34	73,85	88,18	76,79	74,6	65,19	76,87	68,89	71,94	70,37
TiO <sub>2</sub>	0,05	0,22	0,33	0,03	0,19	0,04	0,04	0,04	0,05	0,08	0,23	0,18
Al <sub>2</sub> O <sub>3</sub>	12,51	12,57	11,77	13,67	3,91	11,35	12,44	10,38	11,83	15,99	12,62	11,63
Fe <sub>2</sub> O <sub>3</sub>	1,47	2,21	3,62	1,24	3,11	1,18	1,45	1,3	1,33	3,06	2,56	6,43
MnO	0,01	0,06	0,03	0,02	0,01	0,01	0,02	0,02	0,03	0,05	0,03	0,08
MgO	0,09	0,11	0,18	0,04	0,07	0,1	0,15	0,51	0,07	0,23	0,13	0,06
CaO	0,88	1,27	0,88	0,15	1,02	1,14	0,78	11,36	0,86	0,34	1,61	3,21
Na <sub>2</sub> O	3,11	1,98	2,58	3,51	0,01	2,64	2,38	1,23	2,51	1,35	1,87	0,03
K <sub>2</sub> O	4,98	6,2	4,83	5,21	1,19	4,64	5,2	4,71	5,03	6,78	6,25	3,51
P <sub>2</sub> O <sub>5</sub>	<0,01	0,03	0,08	<0,01	0,03	<0,01	<0,01	<0,01	<0,01	<0,01	0,03	0,03
P.F.	1,1	1,9	1	1,8	1,5	1,5	2,3	4,8	1	2,8	2,2	3,9
(ppm)												
Be	4	7	6	7	1	15	16	5	6	37	10	5
Rb	621,7	635,7	253	628,2	409,7	430,5	574,7	527,9	472,2	871,1	323,5	1131,6
Cs	7	4,9	5,8	5,5	5	5	3,7	3,4	2,5	5,1	3	12,2
Ba	50	434	896	40	45	202	166	185	179	301	557	56
Sr	13,2	35,3	96,7	8,5	24,1	13,5	10,8	15,2	22,3	15,6	44,3	23,5
Ga	41,7	30,2	25,2	46,5	22,6	34,9	39,8	32,4	33,2	58,9	28	46,7
Sn	18	15	9	22	124	7	467	30	25	103	29	785
Ta	12,4	7,2	2,5	23,4	5,4	10,2	11,7	9,5	13,1	14,5	6,6	5
Nb	98,4	60,7	40,4	108,8	37,9	83,8	93	74,1	105,4	111,9	54,3	50,9
Th	71,8	61,9	35,3	49,9	58	59,3	45,9	46	66,9	75,3	65,2	58
U	9,5	3,8	5,3	6,5	5,9	8,5	19,6	10,5	16,9	32,7	11	7,7
Zr	164	388,5	496,1	83,8	364,5	120,4	95,2	99,4	156,9	178,7	375,6	345,3
Hf	10,1	13	15,1	5,8	12,4	7	5,4	5,4	8,6	9,8	12,5	13,2
Sc	6	6	6	6	7	7	7	6	6	15	6	8
Cu	6,3	46,6	152,1	20,9	100,7	74,1	101,6	135,9	151,8	133,2	24	71,6
Zn	51	707	204	104	2584	79	80	68	45	56	71	403
Pb	17,9	26,6	62,9	14,7	14,2	78	29,3	123,4	102,7	133,2	24	9,6
La	144,3	221,9	240,4	176	192,6	102	72	310,1	84,2	30,4	229,3	305,7
Ce	229,7	391,6	460,6	215,2	357,9	192,3	156,4	491,1	189,4	88,7	466,2	514
Pr	35,81	47,18	49,07	40,53	41,26	25,87	19,01	74,62	20,38	8,53	49,5	72,37
Nd	132,6	170,5	172,8	141,5	146,9	99,7	71,6	279,4	73,5	35,9	172,8	259,4
Sm	36,86	30,86	29,67	34,31	28,12	27,98	24,79	66,37	19,59	16,34	30,76	46,37
Eu	0,39	0,98	1,8	0,24	0,66	0,6	0,4	1,77	0,32	0,3	1,1	0,8
Gd	35,88	26,69	26,86	30,51	24,28	34,83	33,86	56,03	19,77	25,88	25,56	34,65
Tb	6,8	4,39	4,12	5,76	4,06	7,72	8,56	8,85	4,31	6,99	3,91	5,23
Dy	39,65	26,01	23,74	34,3	23,27	53,1	59,12	46,9	29,3	51,82	21,48	29,77
Ho	7,67	5,29	4,64	6,63	4,79	11,28	12,6	7,96	6,85	12,25	4,23	6,14
Er	24,2	16,16	13,59	19,99	14,44	36,53	39,3	23,49	23,66	42,9	12,3	19,55
Tm	3,92	2,41	1,89	3,37	2,21	6	6,45	3,57	4,23	7,41	1,86	3,12
Yb	27,87	15,26	11,8	23,57	14,86	41,99	44,15	25,24	30,75	53,36	12,24	23,82
Lu	4,2	2,27	1,67	3,43	2,13	6,02	5,95	3,73	4,44	7,87	1,81	3,7
Y	215,6	149,1	133,2	168,9	140,7	285,1	291,2	289,3	160,9	295,9	119,1	291,9
Total	99,62	99,45	99,64	99,52	99,22	99,39	99,36	99,54	99,58	99,57	99,47	99,43
LREE	579,66	863,02	954,34	607,78	767,44	448,45	344,2	1223,36	387,39	180,17	949,66	1198,64
HREE	150,19	98,48	88,31	127,56	90,04	197,47	209,99	175,77	123,31	208,48	83,39	125,98
HREEY	365,79	247,58	221,51	296,46	230,74	482,57	501,19	465,07	284,21	504,38	202,49	417,88
REEY	945,45	1110,6	1175,85	904,24	998,18	931,02	845,39	1688,43	671,6	684,55	1152,15	1616,52



**Fig. 7.** Domain of REE patterns in all analyzed granites and greisens from the FPTD. (chondrite normalization values of Sun & McDonough (1989).



**Fig. 8.** Chondrite normalized REE patterns of parent and altered granites. A and B: samples from the central part of the FPTD; C: samples from the southernmost border of the FPTD; (D): samples from the northern (NC10A) and southern (NC11A) parts of the FPTD.

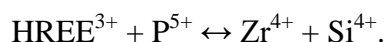
## 6. Discussion and conclusions

The main discussion of this work is related to the concentrations of REE in parental granitic rocks and their accessory and secondary minerals (zircon, xenotime, monazite, thorite, apatite, and oxyfluorides), as well as their concentrations in the greisenized and tin-mineralized rocks of the Faixa Placha tin deposit .

### 6.1. HREE-bearing minerals

Zircon is the main HREE-bearing accessory mineral in the studied granites. In the parental granite, the concentrations of HREE in the zircon are low, but in greisenized granites, the HREE contents are high, reaching up to 5.3% as observed in greisenized pb1c granite. The highest concentrations are related to metamict zircons from all studied granite facies. Tiny inclusions of xenotime are observed in some zircon grains and are probably the cause of  $P_2O_5$  and  $Y_2O_3$  values higher than 8% and 10%, respectively.

Teixeira and Botelho (1999) showed that there is a progressive enrichment in  $Y_2O_3$ ,  $HREE_2O_3$ ,  $ThO_2$  and  $UO_2$  in zircons from the Pedra Branca massif as magmatic evolution takes place. Pupin (2000) reported that zircons of the late magmatic phase are generally enriched in incompatible elements such as U, Hf, and/or Y and that at this stage,  $UO_2$  enrichment above 2000 ppm is remarkable. This result confirms that the zircons of the Faixa Placha were largely formed in the last magmatic stage, since this mineral shows  $UO_2$  values of up to 3800 ppm in the biotite granite. However the higher  $UO_2$  values near 1% observed in the greisenized granites are associated with high Y and REE concentrations and are probably due to hydrothermal alteration during which the chemical composition of magmatic zircon is altered. According to Förster (2006), the HREE are preferably incorporated into zircon by the substitution:



However, this author suggests that a continuous solid solution between zircon and xenotime is unlikely to exist.

Xenotime is the main source of Y, and in the Faixa Placha, this mineral occurs both as isolated grains and as inclusions or on the edges of zircon crystals. Xenotime presents  $Y_2O_3$  concentrations that reach 39%, and the sum of HREE+Y oxides reaches 56%. The highest concentration of  $HREE_2O_3$  in xenotime is found in the greisenized pb1b and pb1c granites, with contents up to 23.6%, but xenotime containing 22.1%  $HREE_2O_3$  is observed in a better preserved pb1b granite sample.

HREE-bearing thorite occurs in the pb1b facies, in the most evolved rocks, which corroborates the suggestion of Botelho (1992) that thorium becomes compatible at the end of the Pedra Branca magmatic evolution, giving rise to thorite.

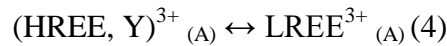
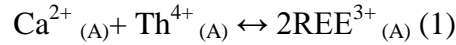
Thorite grains found as inclusions in zircon have the higher  $Y_2O_3$  and  $HREE_2O_3$  contents, reaching 9.1 and 3.6% respectively.

### 6.2. LREE-bearing minerals

The LREE-bearing minerals occurring in or near the Faixa Placha are monazite, apatite and oxyfluorides. Allanite is also a very common accessory mineral in the Pb1b granite, but in the Faixa Placha domain, this mineral was completely destabilized, giving rise to monazite and oxyfluorides. During the hydrothermal alteration, allanite, and to a lesser extent apatite, is

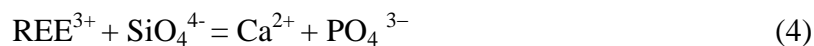
not stable; they are destroyed and release P, Ca and REE, which have great affinity with F, a common element in the hydrothermal fluids associated with the A-type tin granites in the Goiás Tin Province (GTP). During these alterations, Ca gives rise to fluorite, while P and REE form monazite. Similar alterations are described by Zapata and Botelho (2018) in the Serra do Mendes massif, situated nearby the Pedra Branca massif and also related to the A-type granites of the GTP.

The studied monazite was separated into primary and hydrothermal types, the first one coming from evolved and less altered granite rock and the second from greisens and greisenized granites. Both monazites are classified as Ce-monazite. The hydrothermal monazite contains the highest LREE concentrations up to 68.6% LREE<sub>2</sub>O, while in the primary monazites, these values reach 64.5%. This difference is due to the substitution of REE by Ca, Th and U. The compositional variations of monazite can be explained by substitutions involving cheralite (CaTh(PO<sub>4</sub>)<sub>2</sub>), huttonite (ThSiO<sub>4</sub>), coffinite (USiO<sub>4</sub>) and xenotime (Y(PO<sub>4</sub>)), according to the following equations:



Apatite occurs in less abundance in the FPTD, identified mainly in the granite Pb1b. The HREE values reach 6.32%, with the LREE more enriched in relation to the HREE reaching 5.3%; meanwhile, the HREE show maximum values of approximately 1.84%, and the sum of the HREE+Y shows values up to 4.05%. According to the work of Hoshiro et al. (2015), Hugher et al. (1991) and Roeder et al. (1987, apatite crystals may incorporate up to 21% REE<sub>2</sub>O<sub>3</sub>. The REE+Y-bearing apatite from the FPTD is partially to completely replaced by monazite, oxyfluorides and fluorite in the altered granites.

The studied apatite exhibits chemical substitutions that occur between components in the vast field of chemical composition of the apatite supergroup (Pan and Feet, 2002) that could be explained according to the following substitutions (Felsche, 1972; Fleet and Pan, 1995; Comodi et al., 1999; Cherniak, 2000; Serret et al., 2000; Chen et al., 2002a, b):



According to Pan & Fleet (2002), in these coupled substitutions, mechanisms (1) and (2) are reported only in a synthetic compound with the apatite structure and not in natural apatite. On the other hand, (3) and (4) are generally observed in nature and are related to minerals of the apatite supergroup possessing REE as major elements, e.g., belovite (Na(Ce,La)Sr<sub>3</sub>(PO<sub>4</sub>)<sub>3</sub>F) and britholite ((Ce,Y,Ca)<sub>5</sub>(SiO<sub>4</sub>)<sub>3</sub>OH). These two minerals, together with apatite, constitute groups within the apatite supergroup, i.e., the apatite group, belovite

group and britholite group (Hughes and Rakovan, 2015). These authors suggest that the coupled substitutions (3) and (4) are important for incorporation of REE in natural apatite.

Substitution (3) is well established on the basis of compositional data for natural apatite (Comodi et al., 1999; Peng et al., 1997; Roeder et al., 1987; Rønsbo, 1989). The incorporation of REE within apatite by substitution (3) results from apatite that contains high concentrations of alkaline elements as in the case of Na. Therefore, substitution (3) is often observed in apatite from alkaline rocks, including carbonatites.

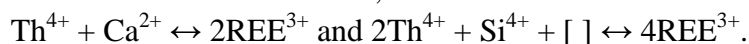
Substitution (4) is largely proven in natural apatite (Comodi et al., 1999; Roeder et al., 1987; Rønsbo, 1989) and is supported by the complete solid solution between hydroxyapatite and britholite-(Y) (Ito, 1968; Khudolozhkin et al., 1973). This substitution leads to the final member  $\text{Ca}_4\text{REE}_6(\text{SiO}_4)_6\text{F}_2$ , which has been synthesized with compositions involving La, Ce, Nd, and Y (Ito, 1968; Mayer et al., 1974).

The apatite containing Ce and Y is of the britholite type. Therefore, both LREE-rich and HREE-rich apatites form via substitution (4). Britholite typically occurs in the metamictic state in alkaline rocks and pegmatites.

According to Pan and Fleet (2002), the incorporation of REE into natural apatite is caused by the type of substitution by belovite or britholite and may be related to the alkalinity and silica saturation in the melt (Roeder et al., 1987; Watson and Green, 1981). Replacement of the britholite type is important for the incorporation of HREE, Th and U into apatite.

According to this information and the presented chemical data, the fluorapatite from granites of the Pedra Branca Massif shows a substitution of the britholite type, and this reaction is due to the alkalinity of the hydrothermal fluids in the FPTD.

The oxyfluorides found in the Pedra Branca Massif are concentrated mainly in the FPTD related to the hydrothermally altered rocks. The  $\text{REE}_2\text{O}_3$  concentrations reach approximately 80% in the greisenized granite with La, Ce and Nd as the elements with the highest values up to 18.5, 41.6 and 15.5%, respectively. According to the work of Teixeira (2002), the substitution of REE in the Pedra Branca Massif is due to the joint entry and intersubstitution between the REE as the main active substitutions, as in the case:



An unidentified mineral rich in Nb, Y and REE is found as accessory in the biotite granite, included in the quartz mass. This mineral could be REE+Y-rich columbite, but its identification needs more detailed studies.

## 7. Concluding remarks

All the granites from the Faixa Placha tin deposit are enriched in REE with highest values more than 1000 times the chondritic value, and this enrichment is due mainly to magmatic evolution. Although LREE are more abundant than HREE, contents of HREE up to 500 times the concentration in chondrites have been found. Parental granites, greisenized granites and greisens have the same REE patterns and contents, indicating that there is no relevant change in concentration and fractionation of REE coevally with the hydrothermal evolution of granites in the Pedra Branca Massif.

The results obtained to date suggest that the Pedra Branca Massif has a dominant REE+Y-rich granite due to the presence of allanite, monazite, xenotime, thorite, zircon and

apatite. In the parental granites, greisenized granites and greisens, metamictized and altered zircons favor the concentration of HREE+Y, which reaches values above 500 ppm in some samples. The REE+Y concentrations and the mineral compositions suggest an economic potential in the Faixa Placha deposit, the main tin deposit in central Brazil, for recovery of REE as by-products. In addition, the area is also favorable for REE deposits of the ionic adsorption type in both the tin deposits and the weathered surfaces of the granite massif.

## 8. References

- Bea, F., Pereira M.D., Corretge L.G., Fershtater G.B., 1994. Differentiation of strong peraluminous, perphosphorous granites: The Pedrobernardo pluton, central Spain. *Geochimica et Cosmochimica Acta* 58 (12), 2609-2627.
- Bea, F., 1996. Residence of REE, Y, Th, and U in granites and crustal protoliths, implications for the chemistry of crustal melts. *Journal of Petrology* 37 (3), 521-552.
- Botelho, N.F., 1992. Les ensembles granitiques subalcalins a peralumineux mineralisés en Sn et In de la sous-province Paranã, état de Goiás, Brésil. Université de Paris VI, Paris, Thèse de Doctorat, 344p.
- Botelho N.F., Moura M.A. 1998. Granite-ore deposit relationships in Central Brazil. *Journal of South American Earth Sciences* 11 (5), 427-438.
- Botelho, N.F., Rossi, G., 1988. Depósito de estanho da Pedra Branca, Nova Roma, Goiás. Principais Depósitos Brasileiros - Metais Básicos Não Ferrosos, Ouro e Alumínio. DNPM 3, 1431.
- Botelho, N.F., Alvarenga, C.J.S., Menezes, P.R., D'el Rey, S. L. J. H., 1999. Suíte Aurumina: uma suíte de granitos paleoproterozóicos, peraluminosos e sintectônicos na Faixa Brasília. In: SBG/Núcleo Centro Oeste e Minas Gerais, Simp.Geol. Centro Oeste, 7, Brasília, Boletim de Resumos, v. 1. p. 49-49.
- Botelho, N.F., 2013. Potencial Econômico para Terras Raras em Granitos tipo-A da Província Estanífera de Goiás. XIII Simpósio de Geologia do Centro-Oeste, SBG, Cuiabá, Palestras.
- Brasil. Plano Nacional de Mineração 2030 (PNM – 2030). Brasil, Ministério de Minas e Energia. Brasília, MME, 2010.
- Chang, L., Howie, R.A., Zussman, J., 1996. Rock forming minerals - volume 5B - Non Silicates - sulphates, carbonates, phosphates and halides. 2 ed. London, Longman Group Limited, 383p.
- Chen, N., Pan, Y., Weil, J.A., 2002a. Electron paramagnetic resonance spectroscopic study of synthetic fluorapatite: part I. Local structural environment and substitution mechanism of Gd at the Ca2 site. *American Mineralogist* 87, 37-46.
- Chen, N., Pan, Y., Weil, J.A., Nilges, M.J., 2002b. Electron paramagnetic resonance spectroscopic study of synthetic fluorapatite: part II. Gd<sup>3+</sup> at the Ca1 site, with a neighboring Ca2 vacancy. *American Mineralogist* 87, 47-55.
- Cherniak, D.J., 2000. Rare earth element diffusion in apatite. *Geochimica et Cosmochimica Acta* 64, 3871-3885.
- Comodi, P., Liu, Y., Stoppa, F., Woolley, A.R., 1999. A multi-method analysis of Si-, S- and REE-rich apatite from a new kind of kalsilite-bearing leucitite (Abruzzi, Italy). *Mineralogical Magazine* 63(5), 661-672.
- Cuadros, F.A., Botelho, N.F., Fuck, R.A., Dantas, E.L., 2017. The peraluminous Aurumina Granite Suite in central Brazil: An example of mantle-continental crust interaction in a Paleoproterozoic cordilleran hinterland setting?. *Precambrian Research* 299, 75-100.
- Deer, W.A., Howie, R.A., Zussman, J., 1997. Rock Forming Minerals - Volume 1B - Disilicates and Ring Silicates, London, The Geological Society, 629p.
- Dostal, J., 2017. Rare Earth Element Deposits of Alkaline Igneous Rocks. *Resources*, V.6, 12pp.
- Felsche, F., 1972. Rare earth silicates with apatite structure. *J. Solid State Chem.* 5, 266-275.
- Fleet, M.E., Pan, Y., 1995. Site preference of rare earth elements in fluorapatite. *American Mineralogist* 80, 248-258.
- Förster, H.J., 2006. Composition and origin of intermediate solid solutions in the system thorite-xenotime-zircon-coffinite. *Lithos* 88, 35-55.
- Garcia, M.D.M., 2013. O projeto ETR da mina Pitinga. Apresentação no Ministério da Ciência e Tecnologia. Brasília, julho de 2013.

- Hinton, R.W., Paterson, B.A., 1994. Crystallisation history of granitic magma; evidence from trace element zoning. *Mineralogical Magazine* 58(A), 416-417.
- Hoshino, M., Sanematsu, K., Watanabe, Y., 2016. REE mineralogy and Resources. In: Bünzli Jean-Claude and Pecharsky Vitalij K (eds.) *Handbook on the Physics and Chemistry of Rare Earths*, vol. 49, p.129 -291
- Issa Filho, Lima, P.R.A., Souza, O.M., 1984. Aspectos da geologia do complexo carbonatítico do Barreiro, Araxá MG, Brasil. In *Complexos Carbonatíticos do Brasil: geologia*. São Paulo. CBMN, p. 21-44.
- Ito, J., 1968. Silicate apatites and oxyapatites. *American Mineralogist* 53, 890-907.
- Khudolozhkin, V.O., Urosov, V.S., Tobelko, K.I., Vernadskiy, V.I., 1973. Dependence of structural ordering of rare earth atoms in the isomorphous series apatite-britholite (abukumalite) on composition and temperature. *Geochemistry International* 10, 1171-1177.
- Lenharo, S.L.R., Moura, M.A., Botelho, N.F., 2002. Petrogenetic and mineralization processes in Paleo- to Mesoproterozoic rapakivi granites: example from Pitinga and Goiás, Brazil. *Precambrian Research* 119, 277-299.
- Mariano, A., 1989. Nature of economic mineralization in carbonatites and related rocks. In Keit. B. (ed). *Carbonatites, Genesis and Evolution*, p. 149-176.
- Marini, O. J., Botelho, N. F., Rossi, PH., 1992. Elementos terras raras em granitóides da província estanífera de Goiás. *Revista Brasileira de Geociências* 22, 61-72.
- Mayer, I., Roth, R.S., Brown, W.E., 1974. Rare earth substituted fluoride-phosphate apatites. *J. Solid State Chem.* 11, 33-37.
- Menez, J., Botelho, N.F., 2017. Ore characterization and textural relationships among gold, selenides, platinum-group minerals and uraninite at the granite-related Buraco do Ouro gold mine, Cavalcante, Central Brazil. *Mineralogical Magazine* 81(3), 463-475.
- Moura, M.A., Botelho, N.F., Olivo, G.R., Kyser, K., Pontes, R.M., 2014. Genesis of the Proterozoic Mangabeira tin-indium mineralization, Central Brazil: Evidence from geology, petrology, fluid inclusion and stable isotope data. *Ore Geology Reviews* 60, 36-49.
- Pan, Y., Fleet, M.E., 2002. Compositions of the apatite-group minerals: substitution mechanisms and controlling factors. In: Kohn, M.J., Rakovan, J., Hughes, J.M. (Eds.), *Phosphates-Geochemical, Geobiological, and Materials Importance*. vol.48. *Rev. Mineral. Geochem.*, Washington, DC, pp. 13-49.
- Pimentel, M.M, Botelho, N.F., 2001. Sr and Nd isotopic characteristics of 1.77-1.58 Ga rift-related granites and volcanics of the Goiás tin province, Central Brazil. *Anais da Academia Brasileira de Ciências* 73, 263-276.
- Pupin, J.P., 2000. Granite genesis related to geodynamics from Hf-Y in zircon. *Earth Sciences* 91, 245-256.
- Rocha, A., Schissel, D., Sprecher, A., Tarso, P., Goode, J., 2013. Process Development for the Serra Verde Weathered Crust Elution-deposited Rare Earth Deposit in Brazil. In *Rare Earth Elements –Proceedings of the 52nd Conference of Metallurgists (COM 2013)*, Edited by I. London, J. Goode, G. Moldoveanu and M. Rayat. Metallurgical Society of the Canadian Institute of Mining, Metallurgy and Petroleum (MetSoc-CIM), Montreal, Canada, 2013.
- Roeder, P. L., MacArthur, D., Ma, X.P., Palmer, G.R., 1987. Cathodoluminescence and microprobe study of rare-earth elements in apatite. *American Mineralogist* 72, 801-811.
- Rønsbo, J.G., 1989. Coupled substitution involving REEs and Na and Si in apatite in alkaline rocks from the Illimaussaq intrusion, South Greenland, and the petrological implications. *American Mineralogist* 74, 896-901.
- Santana I. V., Wall F., Botelho N. F. 2015. Occurrence and behaviour of monazite-(Ce) and xenotime-(Y) in detrital and saprolitic environments related to the Serra Dourada granite, Goiás/Tocantins State, Brazil: potential for ETR deposits. *Journal of Geochemical Exploration* 155, 1–13.
- Scherrer, N.C., Engi, M., Gnos, E., Jacob, V., Liechti, A., 2000. Monazite analysis; from sample preparation to microprobe age dating and REE quantification. *Schweiz. Mineral. Petrogr. Mitt.* 80, 93-105.
- Serret, A., Cabañas, M.V., Vallet-Regí, M., 2000. Stabilization of calcium oxyapatites with lanthanum(III)-created anionic vacancies. *Chem. Mater.* 12, 3836-3841.
- Service, R. F., 2010. Nations move to head off shortages of rare earths. *Science* 327 (5973), 1596–1597.
- Stone, R., 2009. As China's rare earth R&D becomes ever more rarefied, others tremble. *Science* 325, 1336-1337.

- Sun, S.S., McDonough, W.F., 1989. Chemical and isotopic systematics of oceanic basalts; implications for mantle composition and processes. In: Saunders, A.D. and Norry, M.J. (Editors) *Magmatism in the ocean basins.*, Geological Society of London 42, 313-345.
- Teixeira, L.M., Botelho, N.F., 1999. Comportamento dos elementos terras raras pesadas em zircão, xenotíma e torita de granitos e greisens da subprovíncia estanífera Paranã, Goiás. *Revista Brasileira de Geociências* 29(4), 549-556.
- Teixeira, L.M., Botelho, N.F., 2002. Comportamento cristaloquímico de monazita primária e hidrotermal durante a evolução de granitos e greisens: Exemplos das subprovíncias Tocantins e Paranã, Goiás. *Revista Brasileira de Geociências* 32(3), 335-342.
- Teixeira, L.M., Botelho, N.F., 2006. Comportamento Geoquímico de ETR durante evolução magmática e alteração hidrotermal de granitos: Exemplos da Província Estanífera de Goiás. *Revista Brasileira de Geociências* 36(4), 679-691.
- Wang, L., Xu, C., Zhao, Z., Song, W., Kynicky, J., 2015. Petrological and geochemical characteristics of Zhaibei granites in Nanling region, Southeast China: Implications for REE mineralization. *Ore Geology Reviews* 64, 569–582.
- Watson, E.B., Green, T.H., 1981. Apatite/liquid partition coefficients for the rare earth elements and strontium. *Earth Planet. Sci. Lett.* 56, 405-421.
- Xu, C., Kynicky, J., Smith, M.P., Kopriva, A., Brtnicky, M., Urubek, T., Yang, Y., Zhao, Z., He, C., Song, W., 2017. Origin of heavy rare earth mineralization in South China. *Nature Communications*, Open Access, DOI: 10.1038/ncomms14598, p. 1-7.
- Zapata, A. M., & Botelho, N. F. 2018. Mineralogical and geochemical characterization of rare-earth occurrences in the Serra do Mendes massif, Goiás, Brazil. *Journal of Geochemical Exploration*, 188, 398-412.

### CAPÍTULO III

#### **CONCENTRATION OF RARE EARTH ELEMENTS IN THE FAIXA PLACHA TIN DEPOSIT, PEDRA BRANCA A-TYPE GRANITIC MASSIF, CENTRAL BRAZIL, AND ITS POTENTIAL FOR ION-ADSORPTION-TYPE REEY MINERALIZATION.**

Costa N. O.<sup>1</sup>, Botelho N. F.<sup>1</sup>

<sup>1</sup>University of Brasília, Institute of Geosciences, Campus Darcy Ribeiro, 70919-970, Brasília-DF, Brazil

Corresponding author: Nilson Botelho, email: nilsonfb@unb.br

phone: +55 (61) 99756150

#### **Abstract**

The Goiás Tin Province (GTP) in Brazil has great potential for rare earth element (REE) deposits associated with A-type granites, such as the Pedra Branca Massif, which contains several Sn deposits and REE anomalies, hosted in its cupola and fracture greisens. The Faixa Placha is the most important tin deposit in the Pedra Branca Massif and has high REEY concentrations, both in the Sn ore and parent granite, as well as greisenized granites with the potential to be economically used as a byproduct of tin. The values exceed 1000 ppm in light rare earth elements (LREEs) and 500 ppm in heavy rare earth elements (HREEs)+Y. The REE-bearing minerals in the parent granite are allanite, monazite, xenotime, thorite, apatite, and zircon. These minerals, except zircon, are altered to secondary monazite, silicates, fluorcarbonates, and oxyfluorides, which are responsible for the concentration of REE in greisenized granites and greisens and the availability of these metals for the clay fraction of saprolites and soils. Ion exchange analyses in the saprolites and soils of a Faixa Placha profile show that the extractions in the clay fraction are more enriched in REEY compared to the whole-rock extractions, with values between 3.425 and 36.762 ppm and between 2.804 and 21.689 ppm, respectively. The REEs are more enriched in the basal part of the profile, especially the LREEs. These exchangeable REEY concentrations indicate the potential of the Faixa Placha and nearby areas to constitute an important REEY deposit of the ion-adsorption-type.

**Key words: REE, Ion Adsorption, Faixa Placha, Tin deposit, Pedra Branca Massif**

## 30 **1. Introduction**

31 In recent years, the demand for rare earth elements (REEs) has become increasingly critical  
32 because of their scarcity in the world market (Roskill, 2007; Sanematsu et al., 2009). The  
33 price of heavy rare earth elements (HREEs) has been drastically increasing compared to that  
34 of light rare earth elements (LREEs) (Naumov, 2008). Thus, the critical global demand is for  
35 HREEs, primarily dysprosium, yttrium, and europium, along with the LREE neodymium  
36 (Stone, 2009; Service, 2010; Garcia, 2013). The problem is not only the increased demand for  
37 HREE but also the limited supply of ore deposits. Currently, much of the HREE supply  
38 comes from ion-adsorption deposits located in the Longnan District in southern China  
39 (Sanematsu *et al.*, 2009; Hoshino et al., 2016; Xu et al., 2017). However, despite the critical  
40 situation projected for the future, a significant reduction in REE prices was observed in 2017  
41 due to excessive supply that was mainly from China, which continues to dominate the world  
42 market (Roskill, 2018; USGS, 2019).

43 In Brazil, the best-known REE deposits are associated with carbonatites, and only more  
44 recently has attention been paid to the potential of granite rocks for the concentration of these  
45 metals, especially in the Goiás Tin Province (GTP). Previous studies drew attention to the  
46 REE enrichment of A-type granites of the GTP, which was mainly due to the presence of  
47 REE-rich zircon and apatite (Marini et al., 1992; Botelho, 1992; Teixeira and Botelho, 1999,  
48 2002 and 2006). In this context, more recent studies have led to the characterization of an ion-  
49 adsorption deposit in the Serra Dourada Massif (Rocha et al., 2013; Santana et al., 2015) and  
50 important REE anomalies in the Serra do Mendes (Zapata and Botelho, 2018) and Mocambo  
51 (Vieira et al., 2019) massifs neighboring the Pedra Branca Massif, which is the subject of this  
52 study. This group of granites is also compared with the A-type granites of Pitinga in the  
53 Amazon region; known for their REEY enrichment (Lenharo et al., 2002).

54 The Faixa Placha is the main concentration area of tin ore in the Pedra Branca Massif, which  
55 is part of the Pedra Branca Suite in the GTP and located in the northern part of Goiás State.  
56 The Faixa Placha has relevant concentrations of REEs that could be used as byproducts of tin.  
57 These REEs are the focus of this work through studies carried out in granites and greisens and  
58 in the supergenic parts (soils and saprolites), where REE enrichment was observed, with  
59 greater enrichment of LREEs relative to HREEs.

## 60 2. Geological Context

61 The GTP consists of a succession of tin deposits housed in granite bodies of Paleo- to  
62 Neoproterozoic age, which are distributed across four subprovinces, of which the most  
63 relevant are the Paranã Subprovince (PSP) and the Tocantins Subprovince (TSP) (Marini and  
64 Botelho, 1986) (**Fig. 1**). These subprovinces consist predominantly of A-type granites, which  
65 are intrusive in paragneisses and mica schists of the Ticunzal Formation, and in granite  
66 mylonites, granites, and tin pegmatites of the peraluminous Aurumina Suite. Granites of both  
67 subprovinces have high contents of alkalis, Sn, Y, Nb, Th, Rb, Nb, and REE, which define  
68 them as A-type granites (Botelho, 1992; Lenharo et al. 2002).

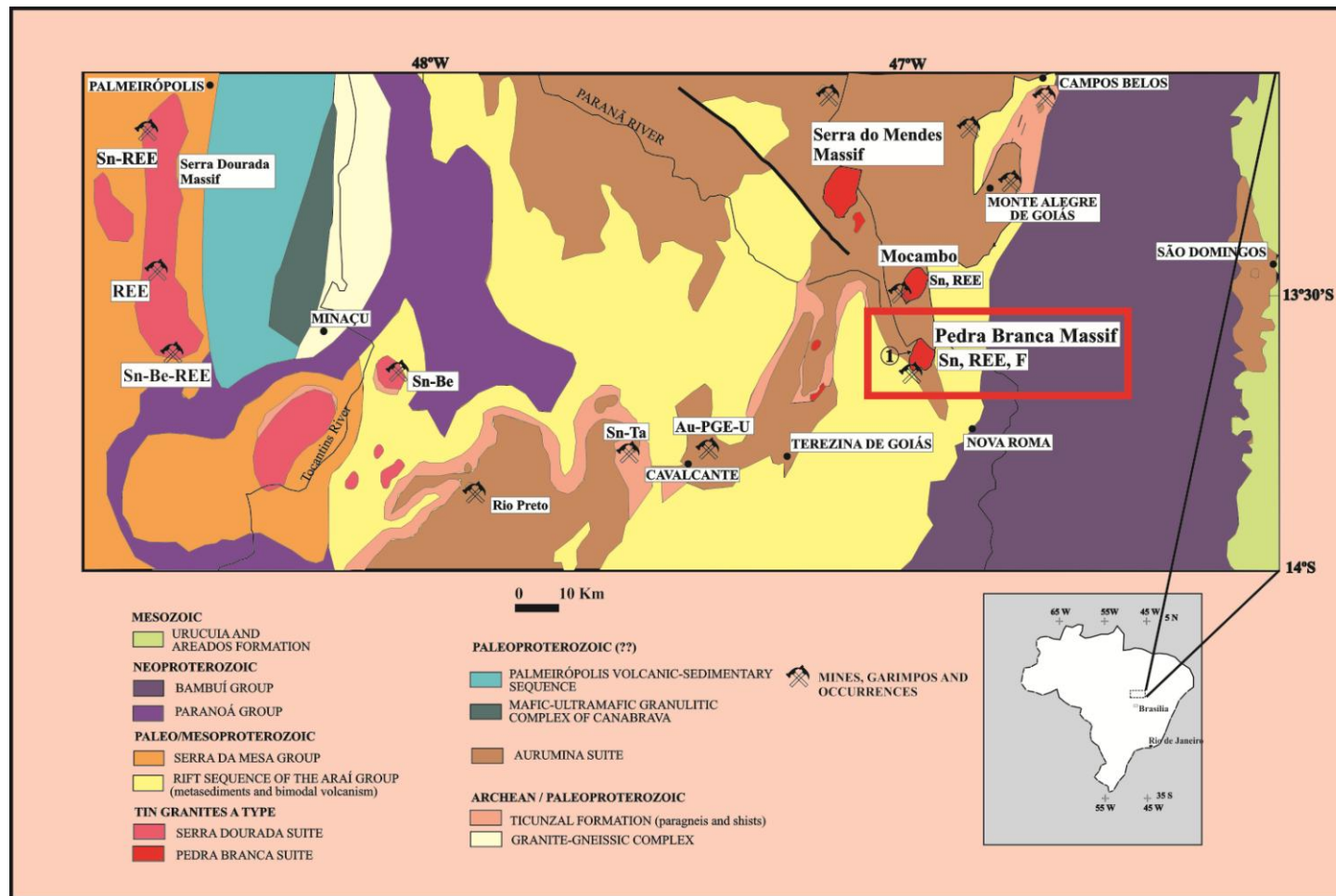
69 The A-type granites of the Paranã Subprovince are grouped in the Pedra Branca Suite (PBS)  
70 and subdivided into two groups, Pb1 (1.77 Ga., U/Pb zircon; Pimentel *et al.*, 1991) and Pb2  
71 (1.72 Ga, monazite dating, Teixeira, 2002). The Pb1 granites exhibit alkaline to subalkaline  
72 trends; high levels of Zr, Y and REE; and incompatibility of Nb and Th during their magmatic  
73 evolution. These granites are subdivided into facies Pb1a, Pb1b and Pb1c in increasing order  
74 of evolution, whereas Pb2 granites are represented by facies Pb1a, Pb2a, Pb2b, Pb2c, Pb2d,  
75 and Pb2e, which range from metaluminous to peraluminous and are responsible for Sn  
76 deposits (Botelho, 1992). The Pedra Branca Suite consists of an extensive volcano-plutonic  
77 system related to the Araí Group, a volcano-sedimentary continental rift sequence. The  
78 plutonic part of the PBS is composed of granite intrusions that form topographic highs with a  
79 circular or elliptical shape. More detailed information on these granites can be found in  
80 Lenharo et al. (2002), where granites Pb1 and Pb2 are called g1 and g2, respectively. The  
81 study area is located in the Pedra Branca Massif, which is the type area of the Pedra Branca  
82 Suite. The Pedra Branca Massif consists of granites pb1 and pb2 (**Fig. 1**), whose  
83 mineralogical composition is summarized in **Table 1**. Pb1 granites are pink biotite granites,  
84 which are represented by facies pb1b and pb1c. Pb2 granites consist of biotite granites pb2a,  
85 pb2b and pb2c and Li-mica leucogranite pb2d. Leucogranite pb2d is the most evolved facies  
86 of the Pedra Branca Massif, which is responsible for the tin deposits. The Pedra Branca  
87 massif has the largest tin deposits in the GTP and central Brazil in areas called the Basin Zone  
88 and Faixa Placha. The Basin Zone is the cupola of the granite massif, which consists of Li-  
89 muscovite-topaz-quartz greisens hosted in a pb2d granite. The Faixa Placha is located in the  
90 fracture zone at the edge of this cupola.

91 **Table 1**

92 Mineralogy and petrography of the granites of the Pedra Branca Suite (adapted from Botelho, 1992; Teixeira and Botelho, 1999; Zapata and Botelho, 2018; Vieira et al., 2019)

pb1 granites alkaline to subalkaline				
Facies	pb1a	pb1b		pb1c
Rock	grey monzogranite	pink porphyritic monzogranite		pink sienogranite
Essential Minerals	quartz, oligoclase, microcline, biotite (5%MgO)	quartz, oligoclase, microcline and annite		quartz, microcline, albite and syderophyllite
Accessory minerals	ilmenite, allanite, apatite, zircon, and fluorite	ilmenite, zircon, allanite, monazite, apatite, xenotime and fluorite		ilmenite, zircon, monazite, thorite and fluorite
Alteration and secondary minerals	Hydrothermal alteration in fractures, giving rise to greisenized granites and gresisens. Replacement of magmatic biotite and neof ormation of Li-syde rophyllite, Li-muscovite, topaz, fluorite, cassiterite, Nb-Ta minerals, sulfides, chlorite, magnetite and carbonates. REE-bearing accessory minerals replaced by monazite, britholite, bastinaesite, fergusonite, fluocerite, REE-oxifluorides, xenotime, fergusonite, hingganite,.			
pb2 granites metaluminous to peraluminous				
Facies	pb2a	pb2b	pb2c	pb2d
Rock	dark grey monzogranite	pink porphyritic monzogranite with coarse groundmass	medium pink equigranular monzo- to sienogranite	medium to coarse leucosienogranite to albite granite
Essential Minerals	quartz, oligoclase, microcline, biotite (6% MgO)	quartz, oligoclase, microcline, syde rophyllite (4,5% MgO)	quartz, oligoclase, microcline, syde rophyllite (1,5% MgO)	quartz, albite, microcline, Li-syde rophyllite to zinnwaldite
Accessory minerals	ilmenite, allanite, apatite, zircon, monazite thorite and fluorite	ilmenite, allanite, apatite, zircon, xenotime and fluorite	apatite, zircon, monazite, xenotime and fluorite	zircon, fluorite, monazite, cassiterite, Nb-Ta minerals
Alteration and secondary minerals	Hydrothermal alteration in cupolas and fractures, giving rise to greisenized granites and gresisens. Replacement of magmatic biotite and neof ormation of Li-syde rophyllite, zinnwaldite, Li-muscovite, topaz, cassiterite, wolframite, sulfides, In-bearing minerals, chlorite, magnetite, fluorite and carbonates. REE-bearing accessory minerals replaced by monazite, britholite, bastinaesite, fluocerite, and REE-oxifluorides. Local albitization related to pb2d granites.			

93



94

95

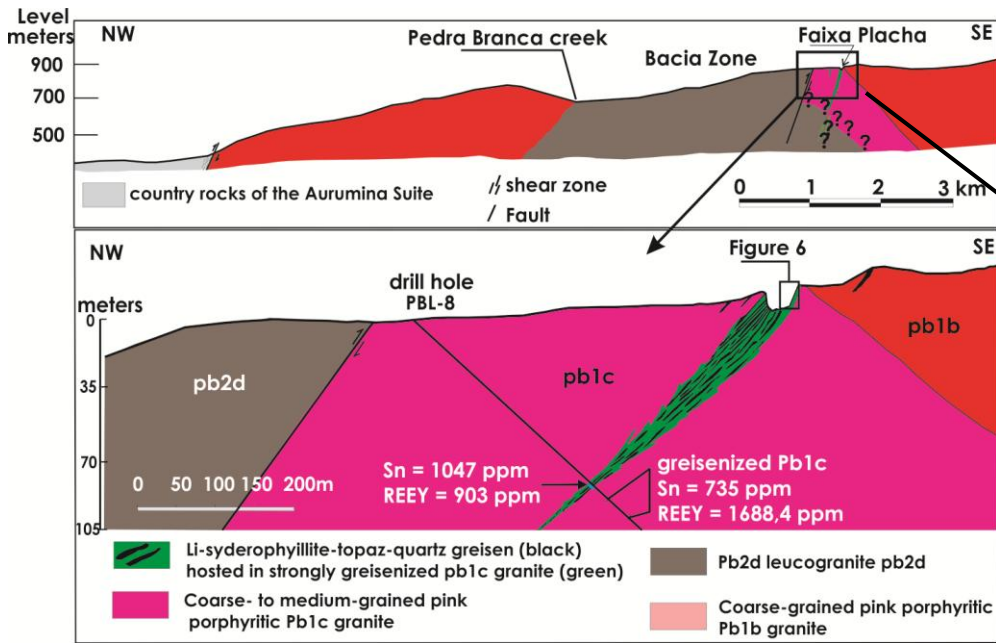
**Fig. 1.** Geological map of the northern part of the Goiás Tin Province, showing the location of the Pedra Branca Massif (Botelho, 2013).

96 **3. Faixa Placha Tin Deposit**

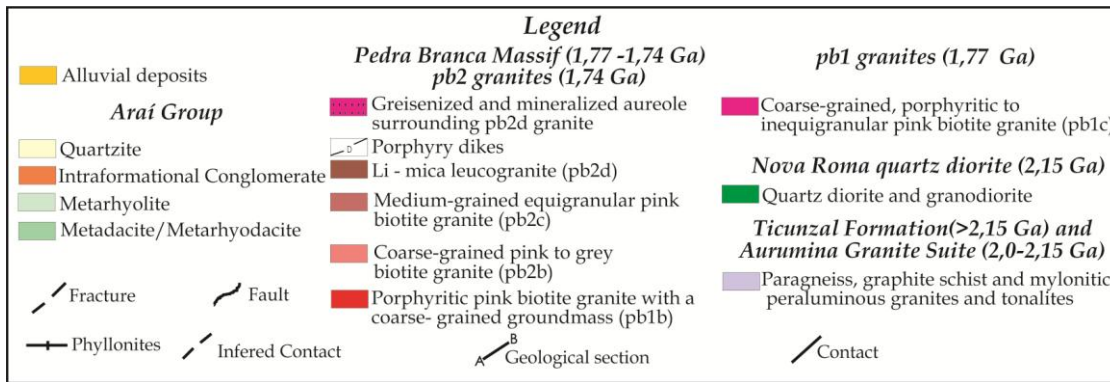
97 The Faixa Placha is the most important mineralized zone of the Pedra Branca Massif, with a  
98 length of 4 km and thickness between 20 and 150 meters. However, at 100 meters deep, this  
99 thickness is reduced to 10 meters (**Fig. 2**). The general orientation of the Faixa Placha is N30-  
100 40E, 70-80NW, which represents an intensively deformed and cataclased fracture zone. The  
101 mineralization is all pre-tectonic. The dominant mineralized rock is a Li-siderophyllite-topaz-  
102 quartz greisen called “black greisen” The central part of the Faixa Placha that represents  
103 approximately 1/4 of its extension, contain an indicated reserve of 15 kt of Sn (Botelho and  
104 Rossi, 1988). This prospect is now owned by EDEM Projetos  
105 (<http://edemprojetos.com.br/projetos/projeto-pedra-branca-sn-f-etr/>)

106 The highest concentration of cassiterite mining occurred in this central and richer part of the  
107 Faixa Placha. The greisens are composed of topaz, quartz, Li-siderophyllite and cassiterite.  
108 The cassiterite in this region contains 0.2% of In (Botelho and Moura, 1998). At a depth of  
109 approximately 120 meters, drilling works have intercepted a 10-meter sulfide-rich zone,  
110 below the main mineralized band, containing sphalerite with 1% In. (**Fig. 2**).

111

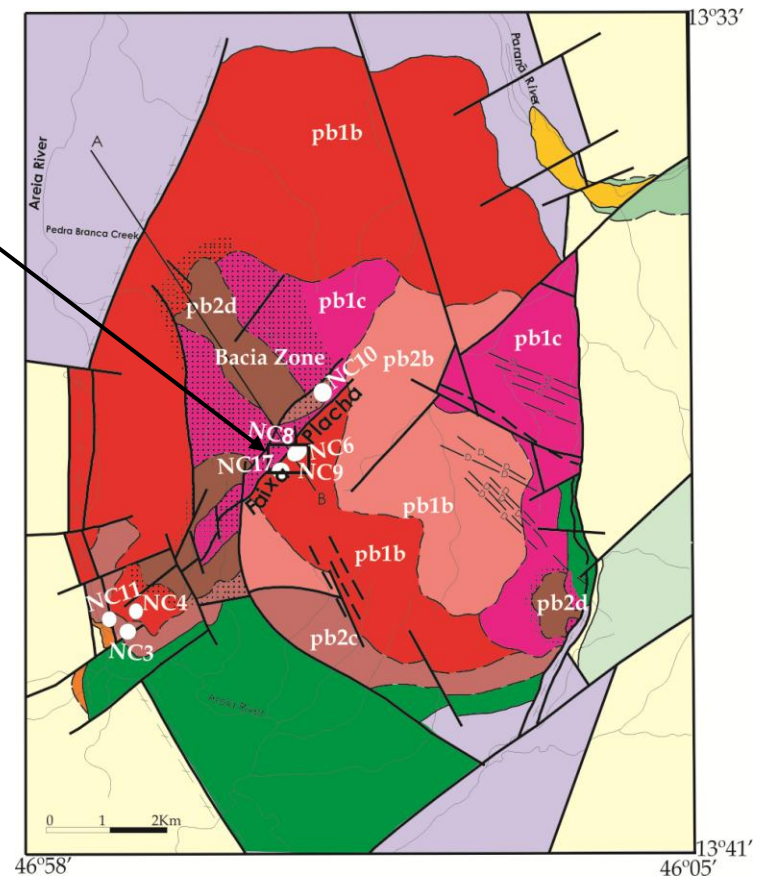


112



113

**Fig. 2.** Geological map of the Pedra Branca massif and schematic cross section (A-B) with detail of the central part of the Faixa Placha (modified from Botelho, 1992).



114 **4. Materials and Methods**

115 **4.1. Sampling of saprolites and soils of the Faixa Placha and nearby areas**

116 The first samples of saprolites were collected in weathering profiles of the Faixa Placha,  
117 located in the vicinity of an experimental tin ore mine (**Fig. 3A**). In this area, a large  
118 concentration of greisen veins was observed. Soils (**Fig. 3B and 3C**) were also sampled in  
119 several auger drilling holes located in the central-south portion of the Pedra Branca Massif to  
120 compare it with the Faixa Placha.



123 **Fig. 3.** Sampling of saprolite in the Faixa Placha (A) and auger soil sampling in planing surface near the Faixa  
124 Placha (B) and (C).

125 **4.2. Clay separation by the sieving method**

126 This work was carried out at the X-ray Diffraction Laboratory of the Institute of Geosciences,  
127 University of Brasilia (UnB). The samples were quartered and sieved into  $\geq 250$ ,  $\geq 125$ ,  $\geq 62$ ,  
128  $\geq 45$ ,  $\geq 20$  and  $< 20$   $\mu\text{m}$  fractions. The procedure used to extract the clay fraction ( $< 20$   $\mu\text{m}$ )  
129 for subsequent ion exchange analysis was washing the sample for clay disaggregation.

130 **4.3. Clay fraction separation for X-ray diffraction analysis**

131 The clay fraction was separated from the total sample. Three steps were completed; in the first  
132 step, 2 g of the sample and 50 ml of distilled water were placed into two separate tubes and  
133 then centrifuged at 750 rpm for 7 min. In the second step, the suspended clay fraction was  
134 recovered and placed into two tubes with 50 ml of distilled water for further centrifugation at  
135 3,000 rpm for 30 min. In both steps, the temperature was 30°C. The last step consisted of the  
136 recovery of the precipitated clay fraction at the bottom of the tubes and its preparation for X-  
137 ray diffraction (XRD) analysis.

138 **4.4. Powder XRD analysis**

139 This work was carried out in whole rock and clay fraction analyses were performed on a  
140 Rigaku Ultima IV diffractometer using the powder method. The samples were crushed in an  
141 agate mortar. The analyzed material consisted of 8 total samples, including 5 saprolites  
142 (NC17\_3 to NC17\_7, 2 soils (NC17\_1 and NC17\_2), and 1 laterite (NC17\_LC). Kaolinite was  
143 observed in all analyzed samples. The diffractograms were processed using Jade 9 software  
144 for Windows with the PC-PFC database run by the International Center for Diffraction Data  
145 (ICDD).

146 **4.5. Cation extractions and ion exchange analysis**

147 Before starting sample extractions, the tubes were rinsed in ultrapure water, cleaned by  
148 immersion in 1 M HNO<sub>3</sub> for 24 hours, and again rinsed repeatedly in ultrapure water.  
149 The extractions were carried out at the Geochemistry Laboratory, UnB, and analyzed at  
150 Actlabs Laboratory in Canada. The analyzed material comprised the 5 saprolite and 1 lateritic  
151 crust samples. The concentrations of the extracted elements were determined by high-  
152 resolution inductively coupled plasma mass spectrometry (HRICP-MS).

153 **4.5.1. Single-step extraction (clay fraction and total sample)**

154 The single-stage extraction was performed on 11 samples from the weathering profile of the  
155 Faixa Placha (NC17), from which 5 samples (NC17\_3, 4, 5, 6, and 7) were used for the  
156 extraction of the clay fraction and 6 samples were used for the extraction of the total sample  
157 (NC17\_3, 4, 5, 6, 7, and LC). The procedure was based on the studies of Sanematsu et al.  
158 (2015), and Sanematsu and Kon (2013).

159 One gram of the sample and 40 ml of a 0.5 M (6.6% weight) solution of ammonia sulfate  
160 [(NH<sub>4</sub>)SO<sub>4</sub>] with pH ~5.7 were added to a 50-ml centrifuge tube. The tube was mechanically  
161 stirred for 24 hours at room temperature and then centrifuged for 15 minutes at 4,500 rpm to  
162 separate the solids from the solution. The supernatant solution was then filtered with a  
163 cellulose acetate membrane filter ( $\phi = 0.22 \mu\text{m}$ ) and prewashed with ultrapure acidified water  
164 using 1% HNO<sub>3</sub> (**Table 2**).

165 **Table 2**

166 Experimental conditions of the single-step extraction using the ammonium sulfate solution.

Extraction Step	Reagent	pH	Reaction Time (hrs)	Dominantly reacting material
1	0.5M ammonium sulphate	5.7	24	Ion-exchangeable material

171 **4.5.2. Two-step extraction**

172 **4.5.2.1. Amorphous oxides of Fe and Mn - Step 1**

173 In this step and step 2, only the 6 whole samples (NC17\_3, 4, 5, 6, 7, LC) were processed  
174 (Table 2).

175 Based on the procedure of Rauret et al. (1999), 10 ml of a mixture of 0.2 M  $\text{NH}_4\text{C}_2\text{O}_4\text{H}_2\text{O}$   
176 (ammonium oxalate) with 0.2 M  $\text{C}_2\text{H}_2\text{O}_4$  (oxalic acid) were added to the solid that was  
177 retained in the tube used for the single-step extraction. The solution was mechanically stirred  
178 for 4 hours at 20° C. After this, the solution was centrifuged for 17 minutes and then filtered.

179 **4.5.2.2. Fe and Mn oxides - Step 2**

180 Step 2 consisted of the extraction performed with the solid residue retained in step 1 using 40  
181 ml of the reagent 1.24 M hydroxylamine ( $\text{NH}_2\text{OH}$ ) at pH = 1. The solution was stirred for 16  
182 hours at room temperature, then centrifuged for 20 minutes and filtered with a 0.22- $\mu\text{m}$   
183 membrane (Table 3).

184 **Table 3**

185 Experimental conditions of the two-step extraction.

Extraction step	Reagent	pH	Reaction Time (hrs)	Dominantly reacting materials
1	0,2M Ammonium oxalate and 0,2M oxialic acid	1	4	Amorphous Fe oxide and Mn oxide
2	1,24M hydroxylamine	1	16	Fe and Mn oxide

#### 186 **4.6. Whole-rock geochemistry**

187 The samples for geochemistry were crushed in an agate mortar and sent for analysis at the  
188 Acme Analytical Laboratories Ltd., Canada. Fifteen samples were obtained, the same 5  
189 samples of saprolite, 4 samples of soil (NC4E, NC10B, NC17\_1, NC17\_2), 2 samples of  
190 parental granite (NC3A, NC4C and NC10A), 7 samples of greisenized granite (NC3B, NC4B,  
191 NC6, NC7, NC8, NC9, NC11), 1 sample of greisens (NC4A) and the sample of lateritic crust.  
192 The adopted analytical routine involved the melting of the samples with lithium metaborate,  
193 multi-acid attack, inductively coupled plasma emission spectrometry (ICP-ES) for analysis of  
194 the major elements and ICP-MS for the minor and trace elements except for the base metals,  
195 which were extracted with HNO<sub>3</sub>.

#### 196 **4.7. Electron microprobe and scanning electron microscopy**

197 The analyses were carried out on a JEOL JXA-8230 electron microprobe at the Electron  
198 Microprobe Laboratory at the Institute of Geosciences of the UnB, and it was equipped with  
199 five wavelength-dispersive spectrometers (WDS) and one energy-dispersive spectrometer  
200 (EDS) for qualitative analyses. Two stages of analysis were conducted. In the first stage,  
201 secondary electron (SE) and backscattered electron (BSE) images were acquired and an EDS  
202 analysis was conducted to identify the minerals enriched in REEY. The second stage  
203 consisted of quantitative analyses performed using two analytical programs. In the first  
204 program, an accelerating voltage of 15 kV, beam current of 10 nA and beam diameter of 1 μm  
205 were used for the analysis of Si, Al, F, P, Sr, Mn, Ti, Y, Ca and Fe. In the second program,  
206 REE, Y, Na, Pb, K, Th, Zr, U, and Ba were analyzed with an accelerating voltage of 20 kV,  
207 beam current of 50 nA and beam diameter 1 μm. The count times for all elements was 10  
208 seconds at the peak and 5 seconds in the background. Interference corrections were performed  
209 in all necessary cases.

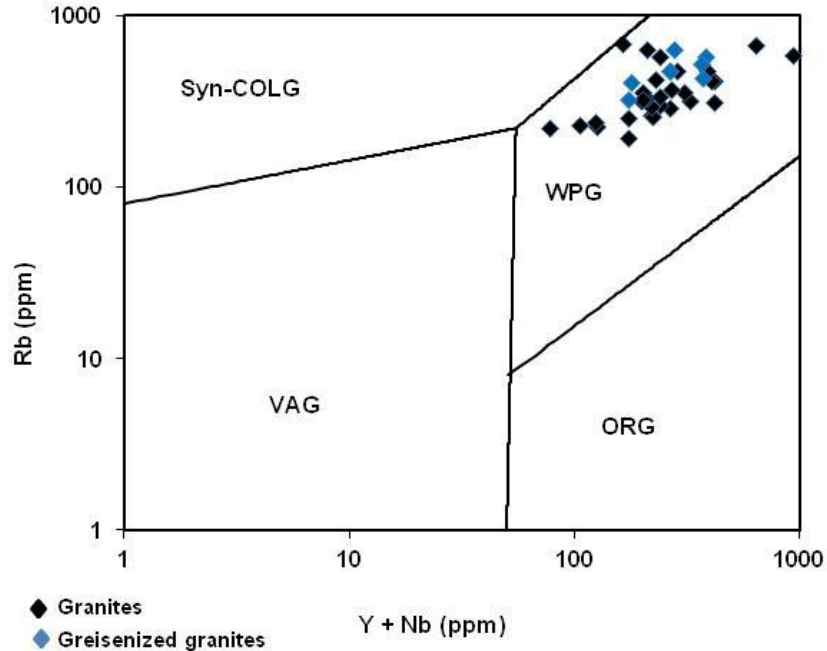
### 210 **5. Results**

211 This work addresses the supergene enrichment of REE, which was studied by sampling the  
212 soils and saprolites from the Faixa Placha and surroundings. The samples were geochemically  
213 analyzed based on information about the concentrations of REEs in these materials.

#### 214 **5.1. Comparisons between granites, greisens, saprolites and soils**

215 The Pedra Branca Massif consists of A-type granite or intraplate granite, which are associated  
216 with the evolution of a continental rift system (Marini and Botelho, 1986; Marini et al., 1992).

217 The granites and greisenized granites analyzed in this study plot in the field of intraplate  
 218 granites in the diagram of Pearce (1984) (**Fig. 4**).

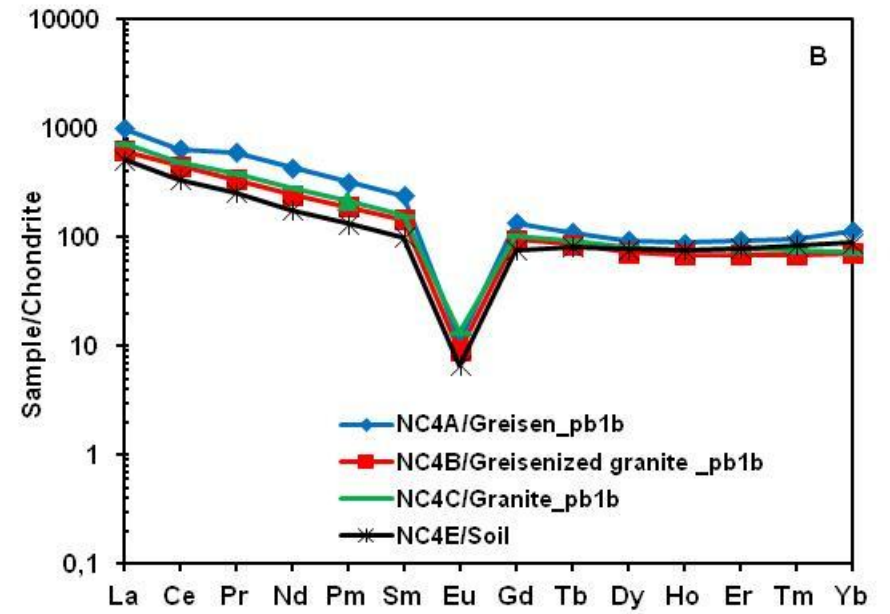
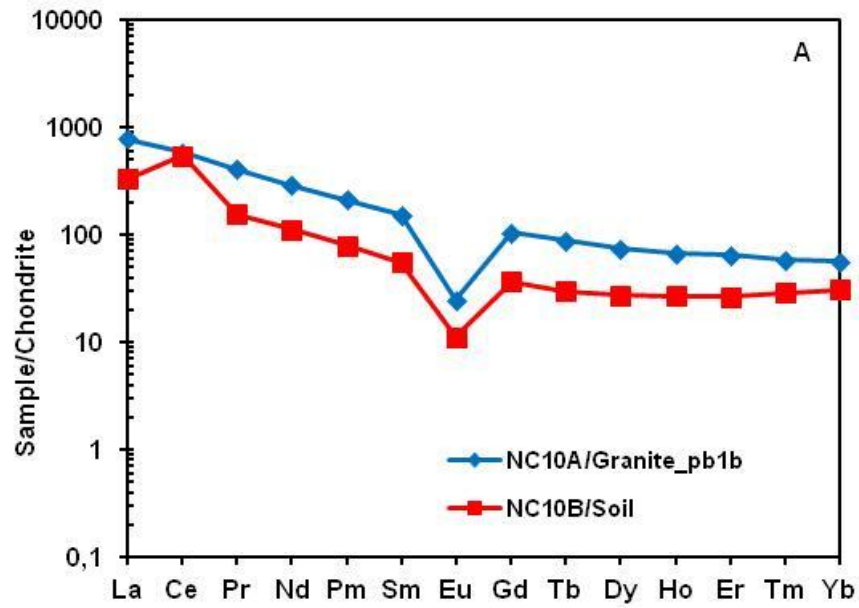


219  
 220 **Fig. 4.** Plot of granites of the Pedra Branca Massif in the Y + Nb versus Rb diagram (Pearce, 1984). VAG,  
 221 volcanic-arc granite; ORG, ocean ridge granite; WPG, within plate granite, Syn-COLG, syn-collisional granite.

222 The comparison between the parental granite (NC10A) and corresponding soil (NC10B)  
 223 indicates that both are enriched in REE relative to chondrite, with minimum values above 10  
 224 times (**Fig. 5A**). However, the granite is more enriched in REE than the soil at values of  
 225 approximately 1042.6 and 666 ppm, respectively, and the LREE values were approximately  
 226 1,000 times higher than chondrite, whereas in the soil, the LREE values were approximately  
 227 600 times higher. The HREE content in granite is above 100 ppm, while in the soil it is  
 228 approximately 37 ppm, and the HREEY values are 221.5 and 81.3 ppm, respectively (**Table**  
 229 **4**).

230 The comparison among granites (parental and greisenized), greisen and soil resulting from the  
 231 greisenized granite from the NC4 samples (**Fig. 5B**) shows that all of them are enriched in  
 232 REE and present minimum values that are 10 times higher than chondrite, thus confirming the  
 233 previous findings. When comparing the samples, the greisen presents a slight enrichment of  
 234 REEs relative to other elements at 1,324.6 ppm and enrichment in HREEY of 417.9 ppm. The  
 235 parental and greisenized granites have almost the same REE pattern at 961.5 and 857.5 ppm,  
 236 respectively. Compared to the granites, the soil has a slight enrichment in HREE from

237 dysprosium, although the granite is more enriched in total HREE at a value of 98.5 ppm,  
238 while the soil has a value of 93.5 ppm (**Table 4**).



239

240 **Fig. 5.** Chondrite-normalized REE patterns (Boynton, 1984) of pb1b parental and greisenized granites and their correspondig soils, in the Faixa Placha (B) and nearby areas  
 241 (A).

242 **Table 4**

243 Whole-rock chemical analysis of the biotite granite, greisenized granite, greisen and soil of the Faixa Placha and nearby areas.

Sample	Faixa Placha									Nearby areas				
	NC4A greisen	NC4B greisenized granite	NC4C biotite granite	NC4E soil	NC6 greisenized granite	NC7-A greisenized granite	NC8 greisenized granite	NC9A greisenized granite	NC9B Greisenized granite	NC10A biotite granite	NC10B soil	NC3A biotite granite	NC3B greisenized granite	NC11 greisenized granite
(%)														
SiO <sub>2</sub>	70,37	88,18	72,9	75,32	76,79	74,6	65,19	76,87	68,89	74,34	68,92	75,42	73,85	71,94
TiO <sub>2</sub>	0,18	0,19	0,22	0,27	0,04	0,04	0,04	0,05	0,08	0,33	0,57	0,05	0,03	0,23
Al <sub>2</sub> O <sub>3</sub>	11,63	3,91	12,57	11,73	11,35	12,44	10,38	11,83	15,99	11,77	15,08	12,51	13,67	12,62
Fe <sub>2</sub> O <sub>3</sub>	6,43	3,11	2,21	4,93	1,18	1,45	1,3	1,33	3,06	3,62	6,49	1,47	1,24	2,56
MnO	0,08	0,01	0,06	0,02	0,01	0,02	0,02	0,03	0,05	0,03	0,02	0,01	0,02	0,03
MgO	0,06	0,07	0,11	0,14	0,1	0,15	0,51	0,07	0,23	0,18	0,15	0,09	0,04	0,13
CaO	3,21	1,02	1,27	0,06	1,14	0,78	11,36	0,86	0,34	0,88	<0,01	0,88	0,15	1,61
Na <sub>2</sub> O	0,03	0,01	1,98	0,03	2,64	2,38	1,23	2,51	1,35	2,58	<0,01	3,11	3,51	1,87
K <sub>2</sub> O	3,51	1,19	6,2	2,26	4,64	5,2	4,71	5,03	6,78	4,83	0,97	4,98	5,21	6,25
P <sub>2</sub> O <sub>5</sub>	0,03	0,03	0,03	0,03	<0,01	<0,01	<0,01	<0,01	<0,01	0,08	0,03	<0,01	<0,01	0,03
P.F.	3,9	1,5	1,9	4,9	1,5	2,3	4,8	1	2,8	1	7,4	1,1	1,8	2,2
<b>TOTAL</b>	<b>99,43</b>	<b>99,22</b>	<b>99,45</b>	<b>99,69</b>	<b>99,39</b>	<b>99,36</b>	<b>99,54</b>	<b>99,58</b>	<b>99,57</b>	<b>99,64</b>	<b>99,63</b>	<b>99,62</b>	<b>99,52</b>	<b>99,47</b>
(ppm)														
Be	5	1	7	8	15	16	5	6	37	6	5	1	7	10
Rb	1131,6	409,7	635,7	503,9	430,5	574,7	527,9	472,2	871,1	253	101,9	0,1	628,2	323,5
Cs	12,2	5	4,9	6,2	5	3,7	3,4	2,5	5,1	5,8	3,3	0,1	5,5	3
Ba	56	45	434	122	202	166	185	179	301	896	266	1	40	557
Sr	23,5	24,1	35,3	14,7	13,5	10,8	15,2	22,3	15,6	96,7	13,4	0,5	8,5	44,3
Ga	46,7	22,6	30,2	42,8	34,9	39,8	32,4	33,2	58,9	25,2	28,9	0,5	46,5	28
V	<8	<8	<8	15	<8	<8	<8	<8	<8	<8	31	8	<8	12

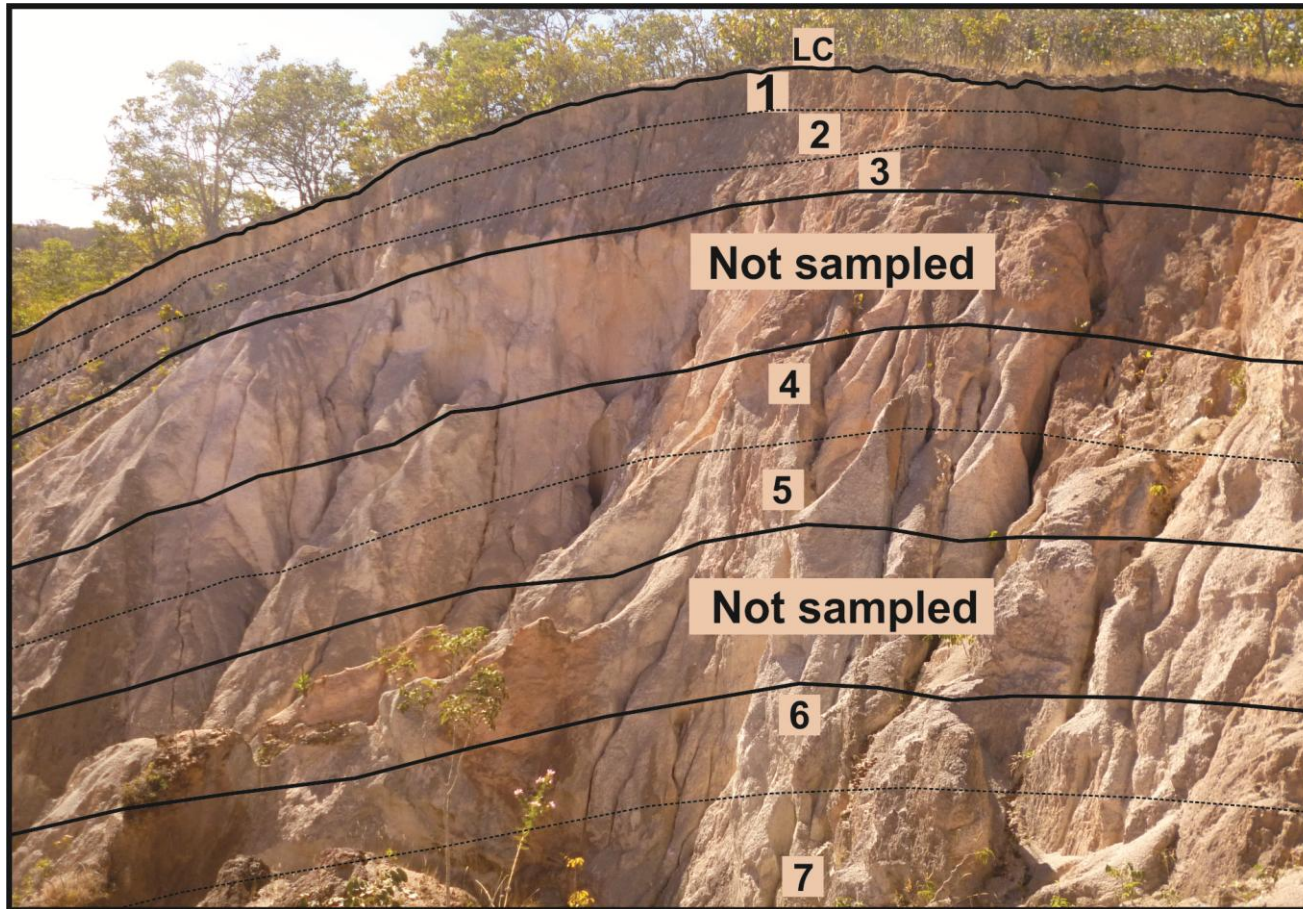
Sn	785	124	15	193	7	467	30	25	103	9	20	1	22	29
Ta	5	5,4	7,2	8,6	10,2	11,7	9,5	13,1	14,5	2,5	3,9	0,1	23,4	6,6
Nb	50,9	37,9	60,7	84,3	83,8	93	74,1	105,4	111,9	40,4	61,2	0,1	108,8	54,3
Th	58	58	61,9	61,3	59,3	45,9	46	66,9	75,3	35,3	36,7	0,2	49,9	65,2
U	7,7	5,9	3,8	6,4	8,5	19,6	10,5	16,9	32,7	5,3	16,9	0,1	6,5	11
Zr	345,3	364,5	388,5	410,9	120,4	95,2	99,4	156,9	178,7	496,1	1194,6	0,1	83,8	375,6
Hf	13,2	12,4	13	14,2	7	5,4	5,4	8,6	9,8	15,1	30,5	0,1	5,8	12,5
Y	291,9	140,7	149,1	161,4	285,1	291,2	289,3	160,9	295,9	133,2	46	0,1	168,9	119,1
Sc	8	7	6	7	7	7	6	6	15	6	9	1	6	6
Ni	0,8	1,5	1,3	0,2	1,7	2,7	1,5	1,3	1,2	2	0,9	0,1	2,3	1,7
Cu	71,6	100,7	46,6	17,7	74,1	101,6	135,9	151,8	133,2	152,1	35,3	0,1	20,9	24
Zn	403	2584	707	82	79	80	68	45	56	204	26	1	104	71
Pb	9,6	14,2	26,6	26,8	78	29,3	123,4	102,7	133,2	62,9	21,1	0,1	14,7	24
Mo	2,9	1,3	2,5	3,3	2,4	4,2	0,7	1,6	1,7	3	2,1	0,1	0,6	1,1
As	<0.1	1,7	0,9	3,3	0,6	<0,5	<0,5	9	6,3	0,6	2,4	0,5	0,6	<0,5
Bi	7,7	5,9	0,4	1	0,4	0,5	1	0,6	0,9	0,2	0,3	0,1	0,8	0,1
Tl	2,8	0,9	0,6	0,5	0,8	1,4	1,8	0,6	1,4	0,7	0,2	0,1	0,9	0,5
(ppm)														
La	305,7	192,6	221,9	159,5	102	72	310,1	84,2	30,4	240,4	102,3	0,1	176	229,3
Ce	514	357,9	391,6	267,8	192,3	156,4	491,1	189,4	88,7	460,6	431,2	0,1	215,2	466,2
Pr	72,37	41,26	47,18	31,14	25,87	19,01	74,62	20,38	8,53	49,07	18,89	0,02	40,53	49,5
Nd	259,4	146,9	170,5	106	99,7	71,6	279,4	73,5	35,9	172,8	66,7	0,3	141,5	172,8
Sm	46,37	28,12	30,86	19,52	27,98	24,79	66,37	19,59	16,34	29,67	10,78	0,05	34,31	30,76
Eu	0,8	0,66	0,98	0,49	0,6	0,4	1,77	0,32	0,3	1,8	0,82	0,02	0,24	1,1
Gd	34,65	24,28	26,69	19,55	34,83	33,86	56,03	19,77	25,88	26,86	9,46	0,05	30,51	25,56
Tb	5,23	4,06	4,39	3,85	7,72	8,56	8,85	4,31	6,99	4,12	1,4	0,01	5,76	3,91
Dy	29,77	23,27	26,01	24,78	53,1	59,12	46,9	29,3	51,82	23,74	8,71	0,05	34,3	21,48

Ho	6,14	4,79	5,29	5,33	11,28	12,6	7,96	6,85	12,25	4,64	1,89	0,02	6,63	4,23
Er	19,55	14,44	16,16	16,47	36,53	39,3	23,49	23,66	42,9	13,59	5,5	0,03	19,99	12,3
Tm	3,12	2,21	2,41	2,7	6	6,45	3,57	4,23	7,41	1,89	0,93	0,01	3,37	1,86
Yb	23,82	14,86	15,26	18,44	41,99	44,15	25,24	30,75	53,36	11,8	6,43	0,05	23,57	12,24
Lu	3,7	2,13	2,27	2,69	6,02	5,95	3,73	4,44	7,87	1,67	1	0,01	3,43	1,81
REE	1324,62	857,5	961,5	678,26	645,92	554,2	1399,1	510,7	388,65	1042,65	666,01	0,82	735,34	1033,05
REEY	1616,52	998,18	1110,6	839,66	931,02	845,4	1688,4	671,6	684,55	1175,85	712,01	0,92	904,24	1152,15
LREE	1198,64	767,44	863,02	584,45	448,45	344,2	1223,4	387,89	180,17	954,34	630,69	0,59	607,78	949,66
HREE	125,98	90,04	98,48	93,81	197,47	210	175,77	123,31	208,48	88,31	35,32	0,23	127,56	83,39
HREEY	417,88	230,74	247,58	255,21	487,57	501,2	465,7	284,21	504,38	221,51	81,32	0,33	296,46	202,49

244

245 **5.2. Faixa Placha weathering profile**

246 In a pit of the Faixa Placha (Point 17), the laterite zone, soils, and saprolites were sampled in a  
247 weathering profile with a thickness of approximately 20 meters (**Fig. 6**). Except in the laterite,  
248 all the samples were taken in channels. The top of the profile consists of a 20 cm thick laterite  
249 crust (NC17\_LC). The A horizon consists of a poorly developed soil, sampled at a thickness  
250 of 50 cm (NC17\_1). The transition of soil to saprolite occurs at a depth of 90 cm. and a  
251 soil/saprolite sample was collected at a thickness of 60 cm (NC17\_2). Below this level, a  
252 mottled clay-rich saprolite was sampled at a thickness of 50 cm (NC17\_3). An interval of 6.4  
253 meters below this point could not be sampled. The sampling proceeded from the base of the  
254 profile, with an 80 cm sample collection (NC17\_7) in grayish saprolite, followed by another  
255 80 cm sampled in yellowish gray saprolite (NC17\_6). A new interval of 8.4 meters was not  
256 sampled. Two more samples of 80 cm each were collected, consisted of a whitish gray  
257 saprolite at 10.8 meters from the base (NC17\_5) and a whitish to pink saprolite between 10.8  
258 meters and 11.6 meters (NC17\_4).



259

260 **Fig. 6.** Photography of the weathering profile sampled at the center of the Faixa Placha (NC 17).

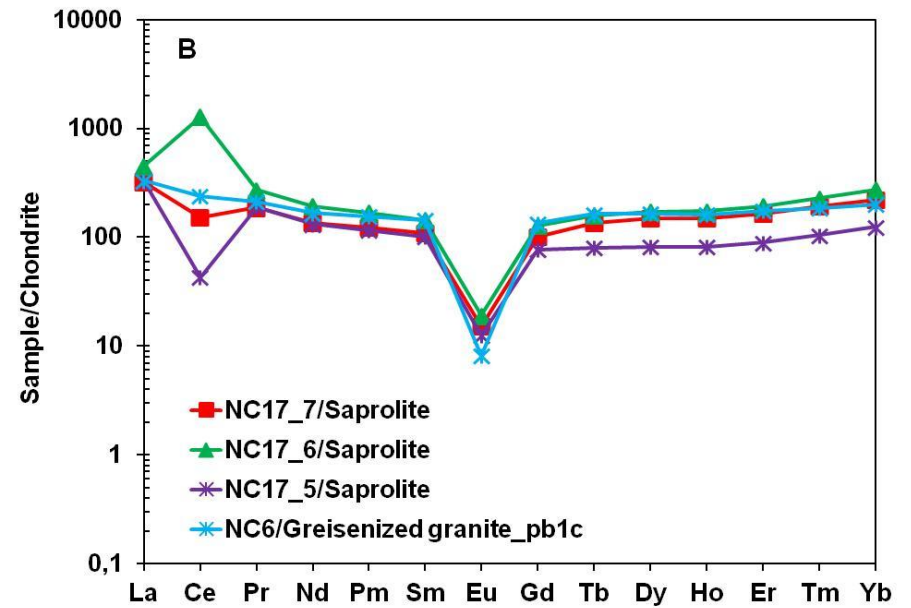
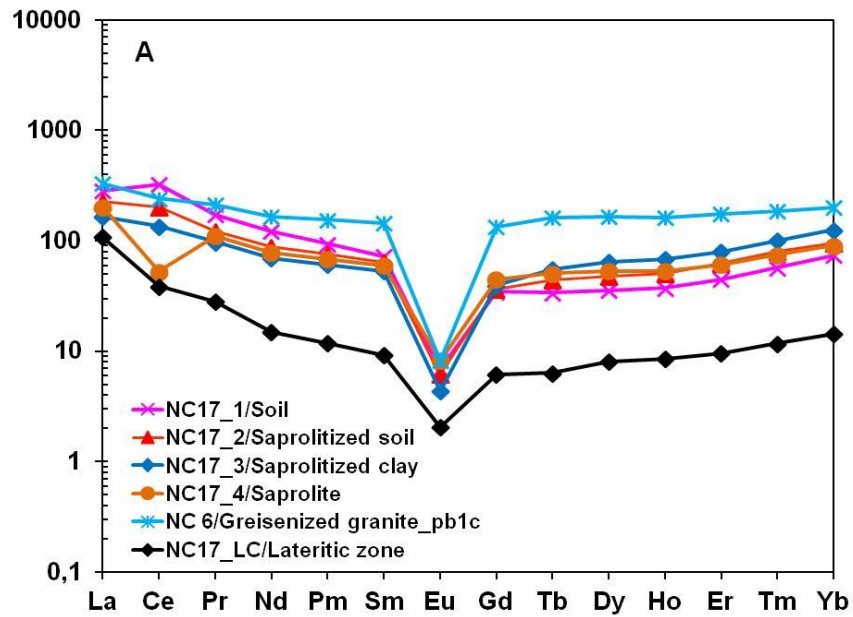
261 **5.3. Geochemical results**

262 In the weathering profile of the Faixa Placha (point 17), samples of lateritic crust (NC17\_LC),  
263 soil (NC17\_1), saprolite soil (NC17\_2) and saprolites (NC17\_3 and NC17\_4) were compared  
264 with the greisenized granite pb1c, which was sampled in a gallery just below the profile  
265 (NC17) (**Fig. 7**). The granite is more enriched in REEs than the laterite zone, soils (NC17\_1  
266 and NC17\_2) and saprolites (NC17\_3 and NC17\_4), and the REE values are 645.92; 89.74;  
267 509.49; 382.25; 312.79 and 248.79 ppm, respectively. However, the slight enrichment of Ce  
268 in the soil sample (NC17\_1) relative to granite stands out. The Ce value is 258 ppm in soil but  
269 192.3 ppm in granite. Regarding the HREE, the clayey saprolite (NC17\_3) is the most  
270 enriched in these elements compared to the other saprolites and soils that are at the top of the  
271 weathering profile, which had values above 100 times the chondrite (**Fig. 8A**). The HREE  
272 value is 197.47 ppm in the greisenized granite and 89.17 ppm in the clayey saprolite,  
273 revealing higher enrichment in the greisenized granite compared to the clayey saprolite  
274 (**Table 5**).

275 In the base (NC17\_7) and (NC17\_6) and intermediate (NC17\_5) portions of the profile,  
276 compared to greisenized granite pb1c (**Fig. 8B**), the NC17\_6 sample, which is a saprolite of  
277 the base, is more enriched in the REEs in relation to the granite, presenting values of 1569.94  
278 and 645.92 ppm, respectively (**Table 5**). This sample has a positive Ce anomaly that is 1,000-  
279 times higher than chondrite, while in granite, it is approximately 200-times higher. Regarding  
280 the saprolites, the base ones (NC17\_7 and NC17\_6) are more enriched in REEs than the  
281 saprolites in the intermediate part of the profile (NC17\_5), and the values are 532.55,  
282 1569.94, 365.73 ppm, respectively.

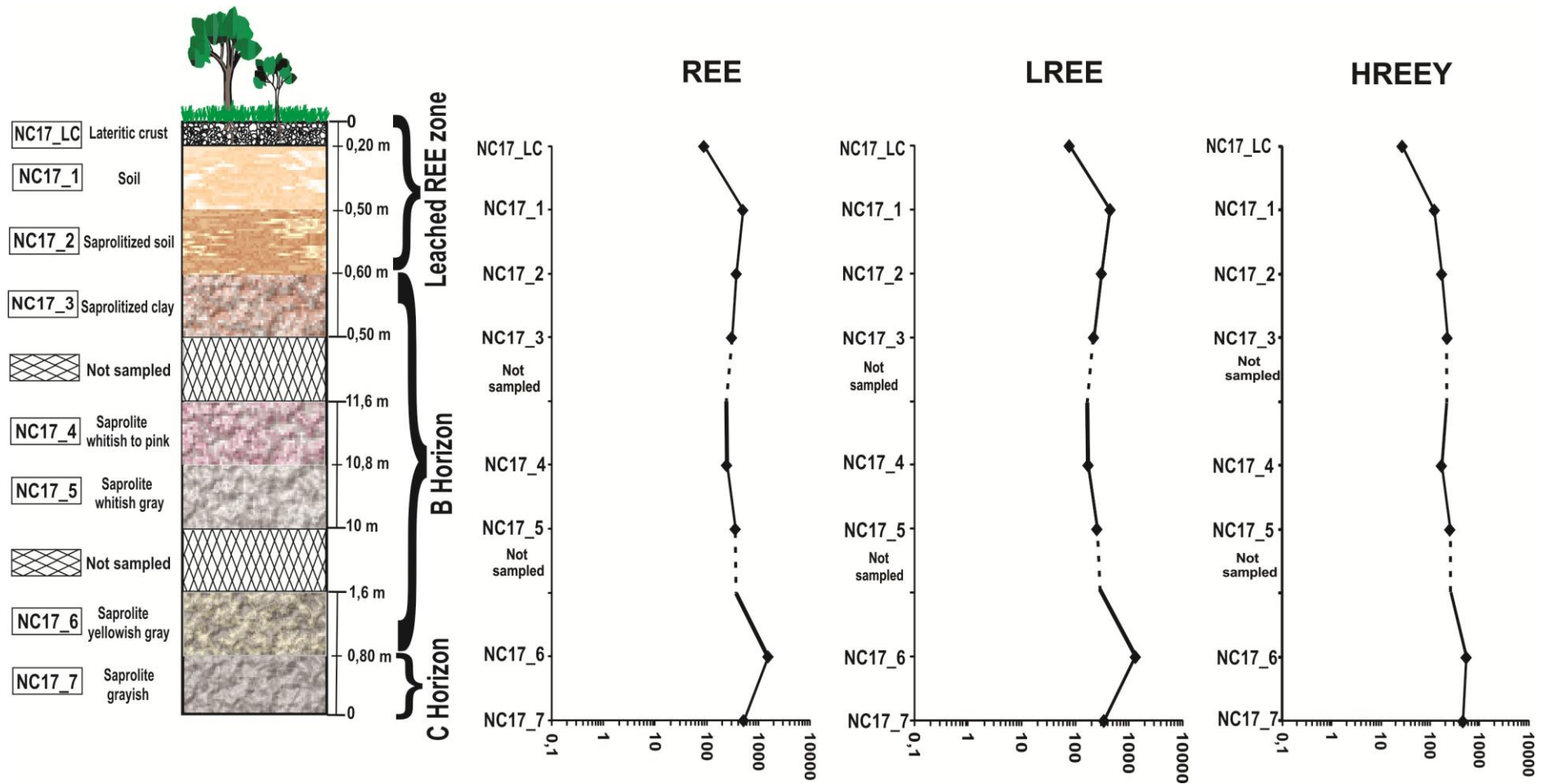
283 The NC17\_6 saprolite, which is the most basal part of the B horizon, is the most enriched in  
284 REEs in the entire profile. This horizon is the zone of greatest accumulation of REEs, which  
285 are adsorbed in kaolinite. This sample has a LREE value of 1348.5 ppm and HREEY value of  
286 559.44 ppm (**Table 5**).

287 The NC17\_7 sample has a chemical composition close to that of the greisenized granite below  
288 the weathering profile.



289

290 **Fig. 7.** Diagrams showing the variation of the relative REEY concentration in the whole-rock samples from the weathering profile of the Faixa Placha.



291

292 **Fig. 8.** Chondrite-normalized REE patterns (Boynton, 1984) of the saprolite, soil and laterite in samples from the upper zone (A) and lower zone (B) of the Faixa Placha  
 293 weathering profile. Comparison with the greisenized granite (N6C) below the weathering profile.

294

Chemical analysis of the laterite crust, soil, saprolites and greisenized granite of the Faixa Placha.

Samples	NC17_LC Laterit. crust	NC17_1 Soil	NC17_2 Soil	NC17_3 Saprolite	NC17_4 Saprolite	NC17_5 Saprolite	NC17_6 Saprolite	NC17_7 Saprolite	NC6 Greisenized granite
(ppm)									
V	433	9	< 5	< 5	< 5	< 5	< 5	< 5	<8
Cu	110	50	25	30	70	60	90	70	74,1
Zn	< 30	50	40	50	50	60	90	70	79
Ga	30	52	46	61	47	55	58	60	34,9
Ge	2	2	< 1	2	2	2	3	2	-
As	62	7	<5	< 5	6	15	10	18	0,6
Rb	4	230	247	314	235	460	725	803	430,5
Sr	8	3	2,5	4	< 2	< 2	3	5	13,5
Y	17	73	105	141	104	152	338	294	285,1
Zr	363	227	208	216	134	126	253	276	120,4
Nb	33	99	87	144	102	119	189	168	83,8
Ag	1,2	0,7	< 0,5	0,6	< 0,5	< 0,5	0,8	0,8	0,4
In	2,3	3	< 0,2	0,9	0,5	1	0,6	2	-
Sn	29	289	261	322	22	49	17	118	7
Ba	20	38	31	61	34	55	178	137	202
Cs	< 0,5	6,5	3,7	4,8	3,5	12	12	9,8	5
Hf	10,4	9,6	8,4	10,9	6,8	7	13,4	13,4	7
Ta	3,1	13,5	11	18,9	13,4	14,7	22,2	18,5	10,2
W	3	13	7	9	6	7	18	14	2664,2
Tl	0,2	0,6	0,5	0,9	1,1	2,2	3,8	3,1	0,8
Pb	61	82	74	97	63	54	231	64	78
Bi	0,6	< 0,4	< 0,4	0,4	< 0,4	0,9	0,4	0,9	0,4
Th	99,9	77,1	72	84,6	51,9	57,5	158	82,6	59,3
U	16,9	4,9	4,1	5,5	4,8	5,3	13,4	8,6	8,5
La	33,5	88,4	70,4	51,4	62,6	101	140	99,2	102
Ce	30,9	258	162	108	42	34,3	1030	122	192,3
Pr	3,41	20,9	14,8	11,9	13,5	22,9	33	22,8	25,87
Nd	9	73,4	52,6	41,6	46,6	79	116	81,4	99,7
Sm	1,8	14	12,5	10,4	11,7	19,7	28,1	21,4	27,98
Eu	0,15	0,51	0,45	0,32	0,6	0,92	1,4	1,12	0,6
Gd	1,6	8,9	9,4	10,2	11,5	20	33,3	26,1	34,83
Tb	0,3	1,6	2,1	2,6	2,4	3,8	7,5	6,4	7,72
Dy	2,6	11,4	15,2	20,7	17,2	26,3	55	48	53,1
Ho	0,6	2,6	3,5	4,8	3,7	5,7	12,1	10,4	11,28
Er	2	9,4	13,1	16,7	12,8	18,7	40,3	34,4	36,53
Tm	0,38	1,84	2,59	3,26	2,41	3,38	7,36	6,23	6
Yb	3	15,5	20,1	26,3	18,9	26	57,1	46,1	41,99
Lu	0,5	3,04	3,51	4,61	2,88	4,03	8,78	7	6,02

REE	89,74	509,49	382,25	312,79	248,79	365,73	1569,94	532,55	645,92
REEY	106,74	582,49	487,25	453,79	352,79	517,73	1907,94	826,55	931,02
LREE	78,76	455,21	312,75	223,62	177	257,82	1348,5	347,92	448,45
HREE	10,98	54,28	69,5	89,17	71,79	107,91	221,44	184,63	197,47
HREEY	27,98	127,28	174,5	230,17	175,79	259,91	559,44	478,63	482,57

#### 297 **5.4. Single-step ion exchange extraction**

298 The concentration of REE in extraction by ammonia sulfate  $[(\text{NH}_4)\text{SO}_4]$  in the clay fraction  
 299 reached values of 3425,93 to 36762,45 ppm of REEY, 3124,14 to 16178,22 ppm of LREE,  
 300 149,09 to 7188,19 ppm of HREE, 1.44 to 4.95 ppm of Th and 2.04 to 26.91 ppm of U. The  
 301 highest REEY concentrations are in the NC17\_6 sample, which is in the basal part of the  
 302 weathering profile, on horizon B, and the lowest concentrations of REEs occur in the NC17\_3  
 303 sample, which is at the top of the profile in the leaching zone of REEs. Although it has lower  
 304 REEY concentrations compared to the other samples and is located in the leaching zone, the  
 305 concentrations of REEY, especially of LREEs, can be considered high in the NC17\_3 sample  
 306 **(Fig.9)**.

307 In the whole-rock extraction, the REEY concentrations are between 2,804 and 21,689 ppm,  
 308 the LREE concentrations range from 2412 to 10376 ppm, HREE ranges from 21.78 to 3,992  
 309 ppm, Th ranges from 3.66 to 11.23 ppm and U ranges from 8.06 to 24.61 ppm. However,  
 310 comparing the REE concentrations from the whole-rock extraction with samples of the same  
 311 name of the clay fraction, higher concentrations are observed in the NC17\_6 sample and  
 312 lower concentrations are observed in the NC17\_3 sample. The NC17\_LC sample (lateritic  
 313 crust) was added to the whole-rock extraction, which revealed lower concentrations of REE at  
 314 a value of 179.72 ppm and the highest concentration of U in the analyzed weathering profile  
 315 at 31.48 ppm.

316 The results obtained in this study show values with significant Ce depletion, which is  
 317 represented by Ce/Ce\* ratios between 0.02 and 0.12 in the clay fraction extraction and  
 318 between 0.05 and 0.58 in the total sample extraction. A significant depletion of Ce in the ion  
 319 exchange extraction represented by a negative anomaly is commonly observed in the  
 320 literature, such as in the work of Sanematsu and Kon, (2013). The  $\text{La}_N/\text{Yb}_N$  ratio indicates the  
 321 fractionation between LREEs and HREEs. In the ion exchange of the clay fraction, the  
 322  $\text{La}_N/\text{Yb}_N$  ratio is between 4.32 and 111.69, while in whole rock, it ranges from 4.34 to 25.11.  
 323 In the comparison between LREE and HREE from the ion exchange extraction in the clay  
 324 fraction and whole rock, the concentrations of light and heavy REEs are more enriched in the  
 325 clay fraction. The exception is the sample NC17\_3 (clayey saprolite) in whole rock, where the

326 HREE concentration of 211.78 ppm is higher compared with that of the clay fraction at  
327 149.09 ppm. Th and U have contrasting behavior in the sampled material, with Th more  
328 enriched in whole rock as opposed to U, which is more enriched in the clay fraction. Despite  
329 the alternation of enrichment of U and Th throughout the weathering profile, these elements  
330 are more concentrated in the middle and basal part of the profile (**Table 6**).

331 The normalization of the extraction products to the parental granite give evidence of the  
332 supergene mobility and fractionation of the REEY with important enrichments towards the  
333 products of alteration (Fig. 9C and D). The extractions in the whole-rock display 40 to 50-fold  
334 enrichment in the LREE and HREE, respectively, whereas in the clay fraction this enrichment  
335 reaches 70 to 100-fold.

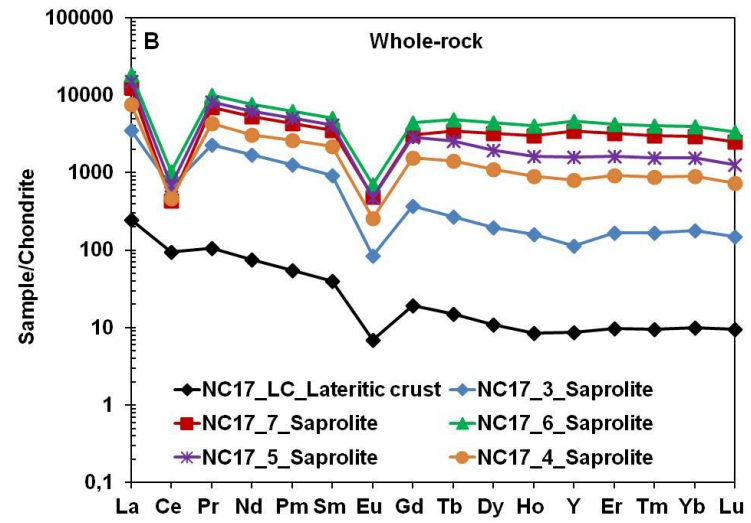
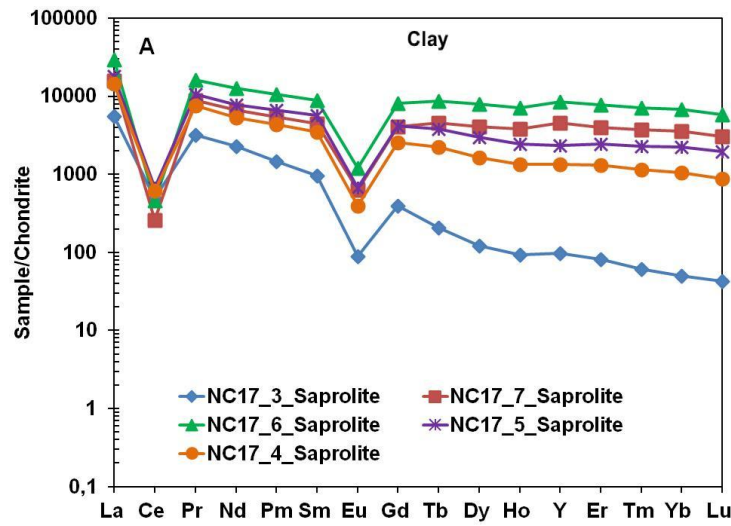
336  
337

**Table 6**  
Results of the single step extraction showing extracted elements concentrations (ppm) in the clay fraction and in the Total sample .

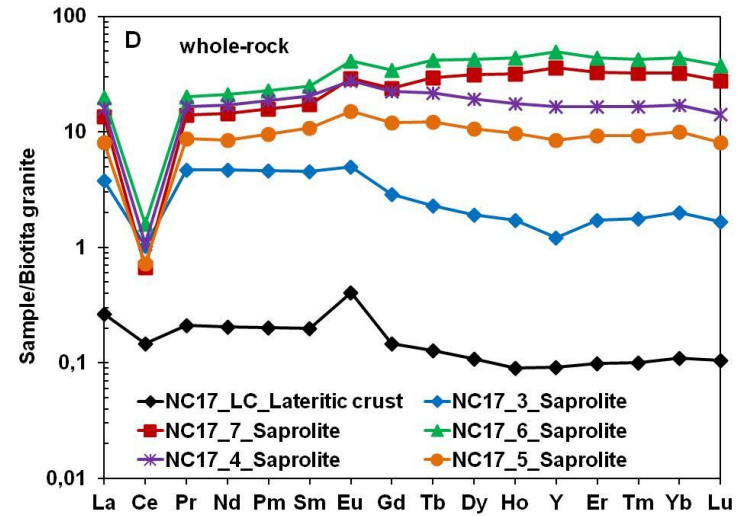
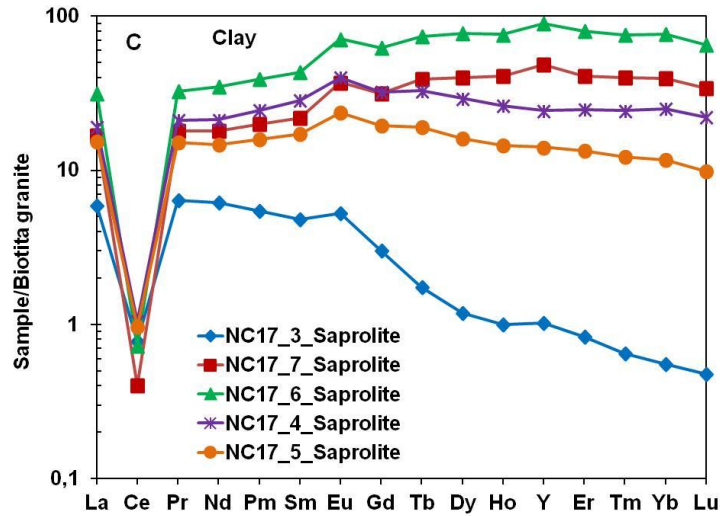
Sample	Fraction	LREE (ppm)	HREE (ppm)	REE (ppm)	Y (ppm)	REEY (ppm)	Th (ppm)	U (ppm)	Ce/Ce*	Eu/Eu*	La <sub>N</sub> /Yb <sub>N</sub>
NC17_3	Saprolite argilized	3124.14	149.09	3273.23	152.70	3425.93	1.92	2.04	0.12	0.14	111.69
NC17_4	Saprolite	7544.76	1544.41	9089.18	2100.04	11189.22	1.92	3.62	0.06	0.13	13.72
NC17_5	Saprolite	10177.27	2790.78	12968.05	3626.16	16594.21	1.44	26.91	0.05	0.14	7.97
NC17_6	Saprolite	16178.22	7188.19	23366.41	13396.03	36762.45	2.97	13.93	0.02	0.14	4.32
NC17_7	Saprolite	8529.00	3697.64	12226.64	7188.39	19415.03	4.95	26.31	0.02	0.15	4.45
NC17_LC	Lateritic crust	168.19	11.53	179.73	13.70	193.42	3.28	31.48	0.58	0.25	25.11
NC17_3	Saprolite argilized	2412.05	211.78	2623.82	180.38	2804.20	6.06	8.06	0.23	0.14	19.87
NC17_4	Saprolite	4286.74	1049.54	5336.28	1260.03	6596.31	11.23	14.73	0.08	0.14	8.5
NC17_5	Saprolite	8340.80	1883.77	10224.57	2475.25	12699.82	7.42	22.49	0.06	0.14	9.83
NC17_6	Saprolite	10375.97	3992.22	14368.19	7320.66	21688.86	7.30	24.61	0.07	0.15	4.76
NC17_7	Saprolite	6937.22	2903.65	9840.87	5383.18	15224.05	3.66	20.46	0.05	0.15	4.34

338  $Ce/Ce^* = Ce_N / (La_N \times Pr_N)^{1/2}$ ,  $Eu/Eu^* = Eu_N / (Sm_N \times Gd_N)^{1/2}$ , where subscript N represents normalization by C1-chondrite (Sun and McDonough, 1989).

339



340



341 **Fig. 9.** Chondrite-normalized REE patterns (Sun and McDonough, 1989) (A and B) and parental granite  
 342 normalized REE (C and D) of ion-exchangeable from the single extraction in the clay fraction and in the whole-rock samples from the Faixa Placha saprolites and lateritic crust.

### 343 **5.5. Two-step sequential extraction**

344 A two-step sequential extraction was performed to determine the concentrations of the ion  
345 exchange elements, such as REEs, Y, Th, and U, in saprolites and laterite crust, and they are  
346 associated with the amorphous Fe and Mn oxides in step 1 and Fe and Mn oxides in step 2.

347 Step 1 shows that the REEY concentrations are between 44.03 and 430.76 ppm and the LREE  
348 and HREE concentrations range from 127.40 to 320.07 ppm and from 6.61 to 153.92 ppm,  
349 respectively. The Th concentration ranges from 127.40 to 320.07 ppm, and the U  
350 concentration ranges from 4.58 to 39.94 ppm. The Ce/Ce\* ratio shows values between 0.36  
351 and 2.26, thus showing a positive anomaly in samples NC17\_3, 6 and 4 and negative Ce  
352 anomalies in samples NC17\_LC, 7, and 5. The Eu/Eu\* ratio ranges from 0.15 to 0.21,  
353 indicating a negative Eu anomaly, and the  $La_N/Yb_N$  ratio ranges from 0.18 to 3.16.

354 The laterite crust (NC17\_LC) and saprolite (NC17\_3), which are at the top or close to the top  
355 of the weathering profile of the Faixa Placha, present lower REEY concentrations in  
356 amorphous Fe-Mn oxides compared to the other samples, while the highest REEY  
357 concentration is in the NC17\_6 sample, which is located in the most basal part of the profile.  
358 The highest concentration of Th is found in sample NC17\_6 and the lowest in sample  
359 NC17\_4, while the highest concentration of U is in the laterite crust (NC17\_LC) and the  
360 lowest concentration is in the NC17\_3 sample.

361 In step 2, the concentration of REEY in the Fe and Mn oxides ranges from 162.68 to 9,727.48  
362 ppm, with concentrations of LREEs between 143.94 and 8,853.57 ppm and HREEs between  
363 1.46 and 531.30 ppm. The concentrations of Th and U range between 207.59 and 1,625.72  
364 ppm and 13.98 and 94.83 ppm, respectively. The Ce/Ce\* ratio ranges from 1.04 to 22.46, thus  
365 showing a positive Ce anomaly, with an emphasis on sample NC17\_6, where this anomaly is  
366 very strong. The Eu/Eu\* ratio is between 0.12 and 0.21, indicating a negative Eu anomaly,  
367 and the  $La_N/Yb_N$  ratio ranges from 1.18 to 7.82.

368 In saprolites, the highest and lowest concentrations of REEY, Th and U in the Fe-Mn oxides  
369 are found in samples NC17\_6 and NC17\_3, respectively. In the comparison between  
370 amorphous Fe-Mn oxides and Fe-Mn oxides, the ion exchange shows that there is a high  
371 enrichment of REEY, Th and U in the Fe-Mn oxides. The Ce anomalies are always positive  
372 and stronger in the Fe-Mn oxides but negative to weakly positive anomalies in the amorphous  
373 Fe-Mn oxides. The Eu exhibits a greater negative anomaly in the Fe-Mn oxides relative to the  
374 amorphous Fe-Mn oxides (**Fig. 10**).

375

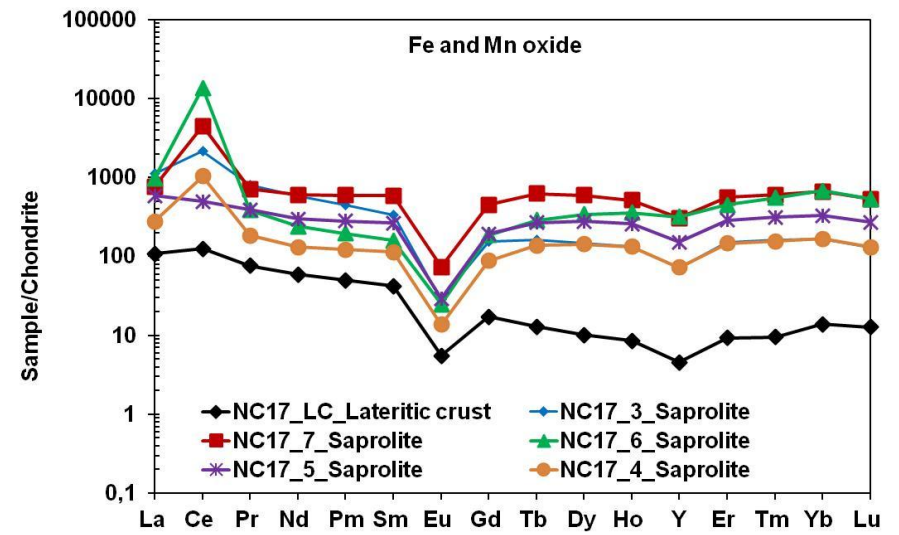
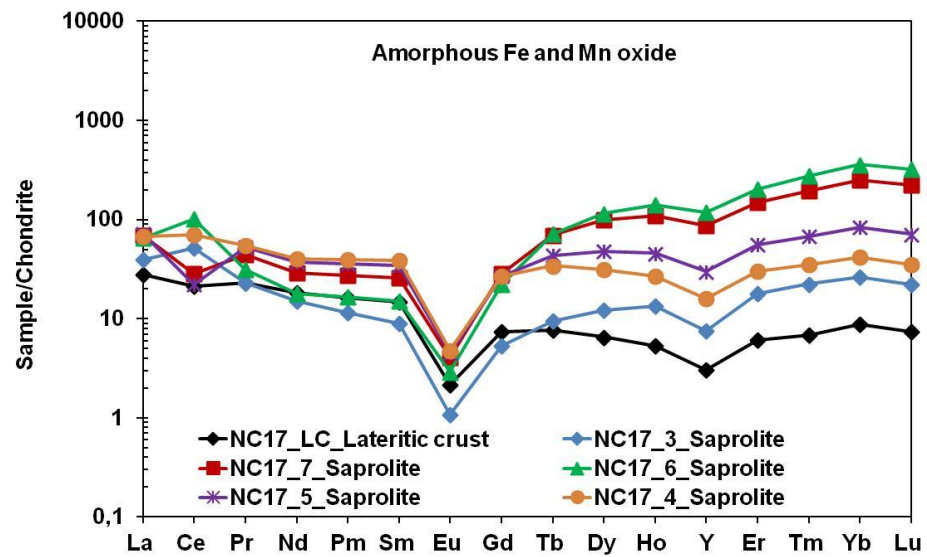
**Table: 7**

376

Results of the two - step extraction showing extracted elements concentrations (ppm) in amorphous Fe-Mn oxides and in Fe-Mn oxides.

Sample		Fraction	LREE (ppm)	HREE (ppm)	REE (ppm)	Y (ppm)	REY (ppm)	Th (ppm)	U (ppm)	Ce/Ce*	Eu/Eu*	La <sub>N</sub> /Yb <sub>N</sub>	
NC17_LC	Lateritic crust	Amorphous Fe and Mn oxide	Ion-exchangeable	32.66	6.61	39.27	4.76	44.03	155.18	39.94	0.85	0.21	3.46
NC17_3	Saprolite argilized		Ion-exchangeable	51.31	13.87	65.18	11.87	77.05	154.87	4.58	1.71	0.16	1.51
NC17_4	Saprolite		Ion-exchangeable	89.46	30.15	119.61	25.14	144.75	127.40	6.81	1.16	0.15	1.38
NC17_5	Saprolite		Ion-exchangeable	58.38	48.59	106.98	46.81	153.78	176.96	9.69	0.36	0.15	0.86
NC17_6	Saprolite		Ion-exchangeable	91.34	153.92	245.26	185.50	430.76	320.07	17.94	2.26	0.16	0.18
NC17_7	Saprolite		Ion-exchangeable	55.59	117.83	173.42	135.48	308.91	210.91	13.92	0.52	0.15	0.38
NC17_LC	Lateritic crust		Fe and Mn oxides	Ion-exchangeable	143.94	1.46	155.49	7.19	162.68	207.59	40.06	1.38	0.21
NC17_3	Saprolite argilized	Ion-exchangeable		1999.28	144.59	2143.87	111.00	2254.87	582.39	13.98	2.28	0.12	6.77
NC17_4	Saprolite	Ion-exchangeable		801.45	133.24	928.58	114.06	1042.65	432.49	14.65	4.60	0.14	1.98
NC17_5	Saprolite	Ion-exchangeable		663.95	254.55	918.50	237.31	1155.81	567.48	18.94	1.04	0.13	1.78
NC17_6	Saprolite	Ion-exchangeable		8853.57	375.03	9228.61	498.87	9727.48	1625.72	94.83	22.46	0.14	1.44
NC17_7	Saprolite	Ion-exchangeable		3360.16	531.30	3891.46	485.50	4376.96	801.53	35.27	5.99	0.14	1.38

387 Ce/Ce\* =  $Ce_N / (La_N \times Pr_N)^{1/2}$ , Eu/Eu\* =  $Eu_N / (Sm_N \times Gd_N)^{1/2}$ , where subscript N represents normalization by the chondrite of (Sun and McDonough, 1989).



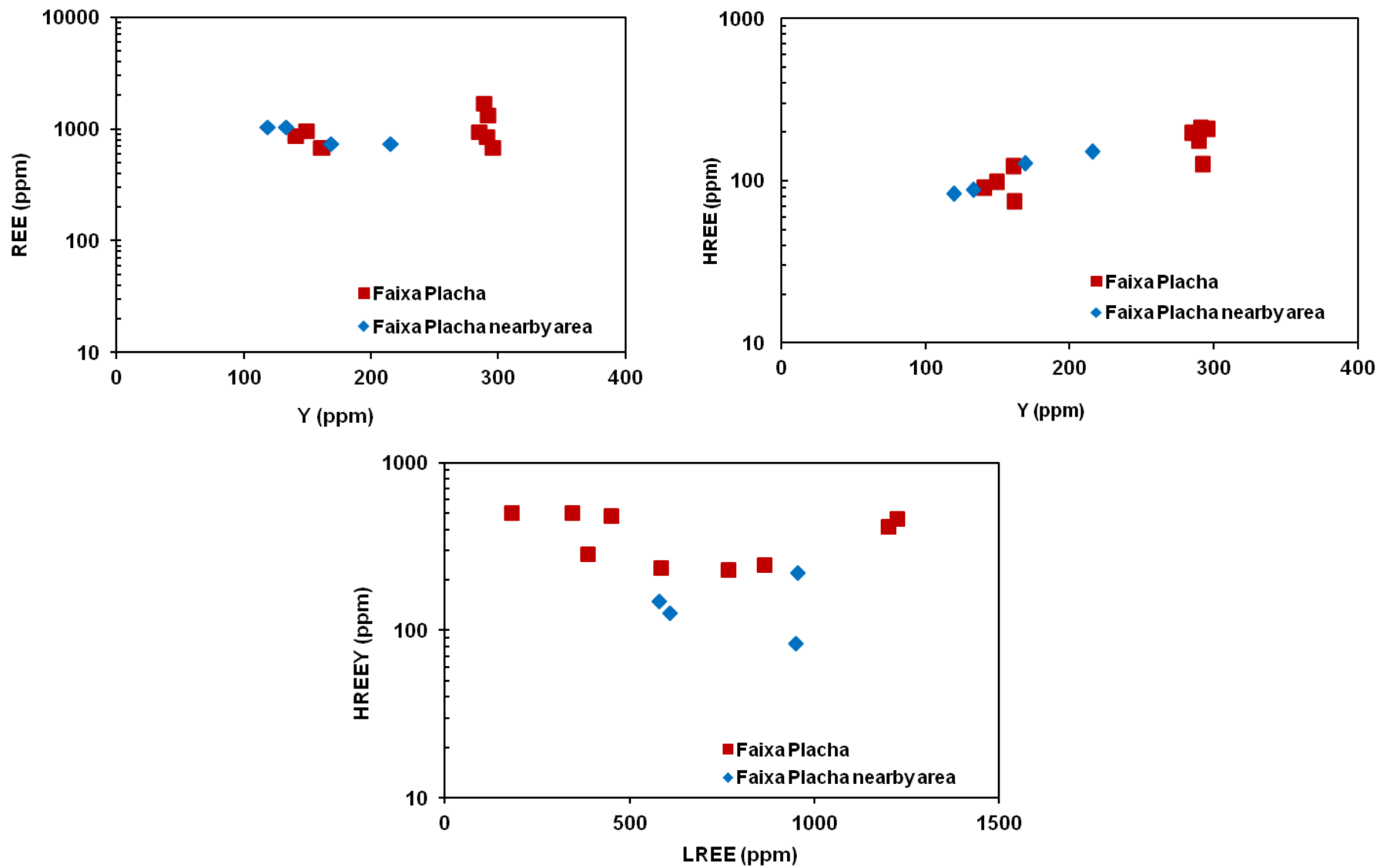
388

389 **Fig. 10.** Chondrite-normalized REE patterns of the sequential extraction in amorphous Fe and Mn oxides and in Fe and Mn oxides from the Faixa Placha saprolites and  
 390 lateritic crust (profile NC17).

## 391 6. Discussion and Conclusions

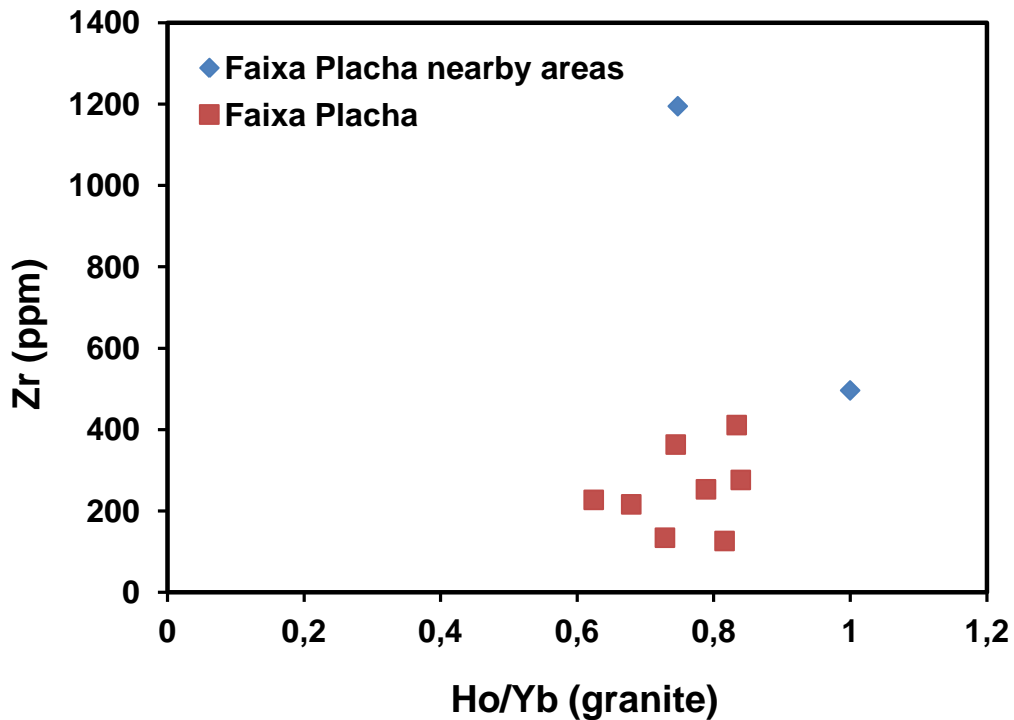
### 392 *6.1. Comparison of REE enrichment between the Faixa Placha and nearby areas*

393 The areas close to the Faixa Placha were sampled near the north boundary (NC10) and the  
394 south boundary (NC4), including granites and soils (**Fig. 2A**). The REEY concentrations in  
395 the biotite granite and soil of sample NC10 are 1,175 and 712 ppm, respectively. For the  
396 biotite granite and soil of sample NC4, the values are 1,110 and 839 ppm, respectively (**Table**  
397 **4**). The comparison between the concentrations of REEY in the Faixa Placha and in the  
398 nearby areas did not identify large variations, and similar values were observed for both  
399 LREE and HREE, indicating that the enrichment in REE is a characteristic of these granites  
400 without the effective influence of hydrothermal changes due to the presence of REE-bearing  
401 primary minerals (**Fig. 11**). These relationships have already been pointed out in previous  
402 studies on the Pedra Branca Massif and other A-type granites of the GTP (Marini and  
403 Botelho, 1986; Botelho, 1992; Marini et al., 1992; Teixeira and Botelho, 1999). The positive  
404 Ce anomaly in the soil (NC10B) is due to the fixation of the element because  $Ce^{4+}$  is located  
405 at the most oxidized surface levels due to the dissolution of REE-bearing phosphates, such as  
406 monazite and apatite, which control the mobilization of REE and Th from the surface and  
407 their content in the soil (Aubert et al., 2001). The main difference between the Faixa Placha  
408 and the nearby areas is its Y enrichment, which is approximately twice as high and mainly  
409 observed in the greisens (**Fig. 5B**). The Faixa Placha greisenized granites and greisens have a  
410 high concentration of metamict zircons that are rich in HREEs, with  $HREE_2O_3$  contents of up  
411 to 4.86%. (Costa and Botelho, 2019). According to Aubert et al. (2001), the positive  
412 correlation between the  $(Yb/Ho)_N$  ratio and the concentration of Zr in soil is indicative of the  
413 enrichment of HREE; that is, a high  $(Yb/Ho)_N$  ratio accompanied by the high concentration of  
414 Zr indicates that the HREE must be controlled by a mineral phase heavily enriched in HREE,  
415 such as in the case of zircon of the Faixa Placha (**Fig. 12**).



416

417 **Fig. 11.** Comparison of the REEY enrichment between the Faixa Placha and nearby areas.



418

419 **Fig. 12.** Correlation between Zr and  $(Yb / Ho)_{Gran}$  ratio in granites of the Faixa Placha and nearby areas.

420 **6.2. Ion exchange extractions in the Faixa Placha weathering profile**

421 According to Duddy (1980), Nesbitt and Markovics (1997) and Sanematsu et al. (2015), in  
 422 the weathering process, the mobile elements, including REEs, are removed from the top and  
 423 accumulated at the bottom of the weathering profile. Generally, the upper part is enriched in  
 424 Ce, thus showing a positive Ce anomaly. This phenomenon can be explained by the oxidation  
 425 of  $Ce^{3+}$  to  $Ce^{4+}$  and the retention of Ce in the profile and incorporation into cerianite ( $CeO_2$ ),  
 426 Mn oxides and hydroxides under oxidizing conditions close to the surface (Braun et al., 1990;  
 427 Mongelli, 1993; Laveuf and Cornu, 2009; Sanematsu et al., 2013; Sanematsu et al., 2015;  
 428 Janots et al., 2015).

429 According to Laveuf and Cornu (2009), the acid water in the soil dissolves and moves the  
 430  $REE^{3+}$  to the lower levels of the weathered profile, where they are immobilized because of  
 431 their incorporation into secondary minerals or by adsorption to the surfaces of weathering  
 432 products, such as clays. Since the immobilized REEs are depleted in Ce, the lower part of the  
 433 profile tends to display a negative Ce anomaly (Braun et al., 1990; Wu et al., 1990; Mongelli,  
 434 1993; Ohta and Kawabe 2001; Bao and Zhao, 2008; Sanematsu et al., 2013; Yusoff et al.,  
 435 2013; Sanematsu et al., 2015).

436 According to the above-cited studies, which analyzed a profile of the Faixa Placha, we  
 437 suggest that the negative Ce anomalies observed in clay and whole rock extractions are due to

438 the retention of the element at the top and adsorption of the immobilized REEs in the clays,  
439 whole rock and secondary minerals at the bottom of the weathering profile.

440 The concentration of REEY in the clay fraction shows a slight enrichment relative to the  
441 whole rock, but both are enriched in REEY, which is explained by the adsorption of the REEs  
442 immobilized in kaolinite throughout the profile.

443 In the whole rock extraction, a slight enrichment in HREE was observed in the upper part of  
444 the weathering profile (NC17\_3) compared to the clay fraction of the same sample,  
445 suggesting that the zircon was not fully degraded by the acid of the solution and was retained  
446 in the residual fraction. This finding is confirmed in Sanematsu and Kon (2013), who relate  
447 the enrichment in LREE and/or HREE to the presence of REE-bearing minerals and their  
448 resistance to chemical weathering. These minerals are abundant in the greisenized rock that  
449 occurs in the Faixa Placha. The same similarity in ion-adsorption type REE mineralization is  
450 observed in Sanematsu et al. (2013) in granites in Phuket, Thailand.

451 The Th concentration of the Faixa Placha weathering profile is higher in the whole rock  
452 compared to the clay fraction extraction, suggesting that Th is more moderate in the clay  
453 fraction and more concentrated in the residual fraction, indicating the occurrence of insoluble  
454 Th silicates, probably thorite, preserved in granite as suggested by Sanematsu and Kon (2013)  
455 in granites of Jiangxi Province, China.

456 According to Sanematsu and Kon (2013), U is significantly present in the residual fraction, in  
457 the clay fraction and rarely in the Fe-Mn oxide fraction. However, the Fe-Mn oxide fraction  
458 of the Faixa Placha has a high U concentration, suggesting that in all fractions, the abundance  
459 of U may be derived from zircon and other minerals, such as uraninite ( $\text{UO}_2$ ), fergusonite  
460 ( $\text{YNbO}_4$ ) and coffinite  $[(\text{U}, \text{Th})\text{SiO}_4 \cdot n\text{H}_2\text{O}]$ , which have U and are relatively common in  
461 granites as indicated by Sanematsu and Kon (2013), although they have not been identified in  
462 scanning electron microscopy (SEM)-EDS analyses.

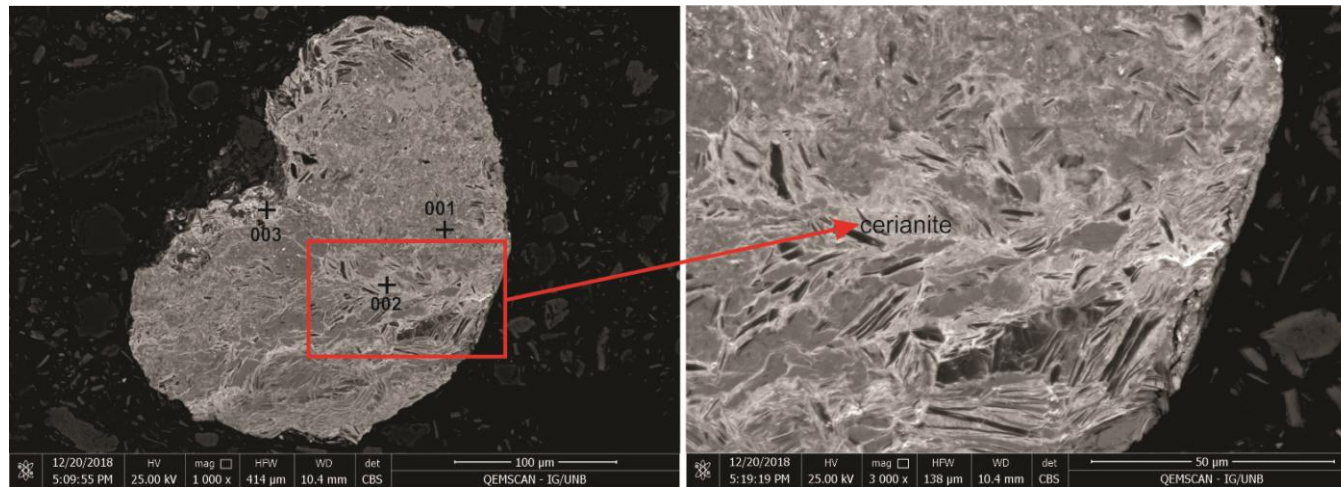
463 The extraction in amorphous Fe-Mn oxides and Fe-Mn oxides from the Faixa Placha  
464 weathering profile samples shows a strong positive Ce anomaly in Fe-Mn oxides, likely due  
465 to oxidizing conditions that favor the incorporation of Ce into Fe-Mn oxides and cerianite as  
466 shown in **Fig. 13**, in addition to the kaolinite that occurs throughout the profile. In the Fe-Mn  
467 oxides, the concentration of REEY is higher and presents a maximum value of 9,727.48 ppm,  
468 and the concentration of LREE and HREE reach maximum values of 8,853.57 ppm and  
469 531.30 ppm, respectively. In the amorphous Fe-Mn oxides, the REEY, LREE, and HREE  
470 contents reach values of 430.76 ppm, 91.34 ppm and 153.92 ppm, respectively, suggesting

471 that the greater incorporation of REEY in the Fe-Mn oxides, mainly in the basal part of the B  
472 horizon of the weathering profile. This enrichment is related to ionic adsorption, which is  
473 responsible for the incorporation of REEY in these oxides as noted by Bau and Koschinsky  
474 (2009) for ferromanganesiferous crusts.

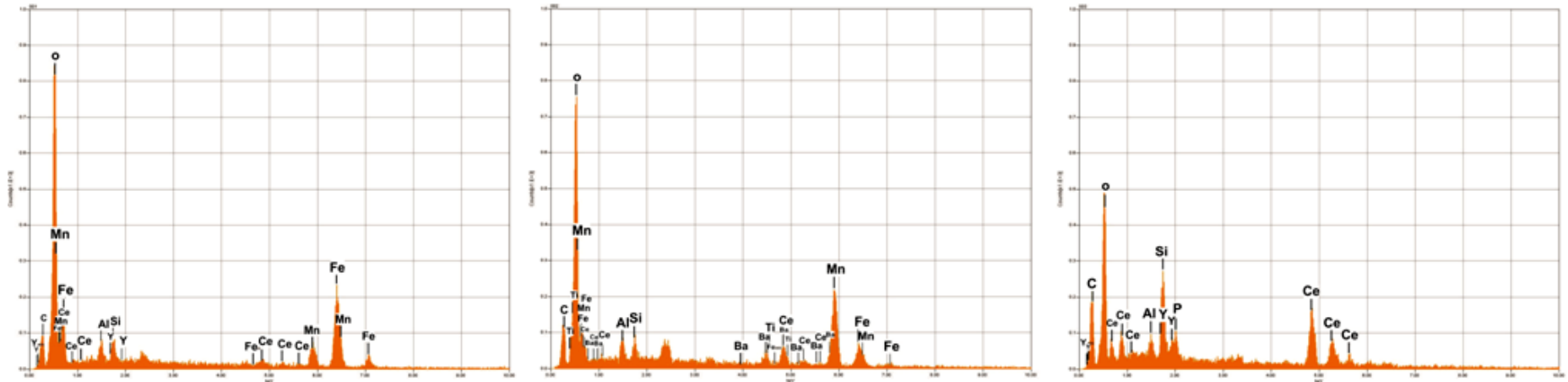
475 The slight Y anomaly in the amorphous Fe-Mn oxides and Fe-Mn oxides observed in these  
476 extractions indicates that the removal of this element is preferentially related to the Mn oxides  
477 relative to the Fe oxides as stated by Bau and Koschinsky (2009). The concentrations of Th  
478 and U are influenced by the reagents and the pH of the solution. Solutions using  $\text{NH}_4$  favor  
479 the ionic exchange of REEY, and these extractions are more efficient with decreased pH  
480 (Moldoveanu and Papangelakis, 2012). However, in the Faixa Placha study, the opposite  
481 occurs, with a higher concentrations of REEY occurring at a pH of approximately 5.7, which  
482 was observed in the ion exchange extraction of the clay and whole rock fractions, in which the  
483 reagent is ammonia sulfate  $[(\text{NH}_4)\text{SO}_4]$ , while in the extraction of the amorphous Fe-Mn  
484 oxide and Fe-Mn oxide fractions, the reagents are ammonia oxalate  $(\text{NH}_4\text{C}_2\text{O}_4\text{H}_2\text{O})$  + oxalic  
485 acid and hydroxylamine, respectively, the pH was equal to 1 and the REEY concentrations  
486 were lower.

487 In accordance with the REEY contents in the Faixa Placha tin deposit, mainly in the  
488 weathering profile, we suggest that this tin deposit has a potential for REEY economic  
489 concentrations of the ion-adsorption type, especially for HREE+Y. Additionally, there are  
490 extensive weathering surfaces in the Faixa Placha nearby areas and in other regions of the  
491 Pedra Branca Massif that need to be investigated in more detail.

492



493



494 Fig. 13. Concretion of Fe and Mn oxide containing cerianite (CeO<sub>2</sub>) in fissures.

495 **7. Referências**

- 496 Aubert, D., Stille, P., and Probst, A., 2001. REE fractionation during granite weathering and  
497 removal by waters and suspended loads: Sr and Nd isotopic evidence: *Geochimica et*  
498 *Cosmochimica Acta.* 65, 387–406.
- 499 Bao, Z., and Zhao, Z., 2008. Geochemistry of mineralization with exchangeable REY in the  
500 weathering crusts of granitic rocks in South China: *Ore Geology Review.* 33, 519–535.
- 501 Bau, M., and Koschinsky, A., 2009. Oxidative scavenging of cerium on hydrous Fe oxide:  
502 Evidence from the distribution of rare earth elements and yttrium between Fe oxides and  
503 Mn oxides in hydrogenetic ferromanganese crust. *Geochemical Journal.* 43, 37-47.
- 504 Boynton, W. V., 1984. Geochemistry of Rare Earth Elements: Meteorite Studies. In:  
505 Henderson, P., Ed., *Rare Earth Element Geochemistry*, Elsevier, New York, 63-114.
- 506 Braun, J. J., Pagel, M., Muller, J.P., Bilong, P., Michard, A., and Guillet, B., 1990. Cerium  
507 anomalies in lateritic profiles: *Geochimica et Cosmochimica Acta.* 54, 781–795.
- 508 Botelho, N. F., 1992. *Les ensembles granitiques subalcalins a peralumineux mineralisés en*  
509 *Sn et In de la sous-province Paranã, état de Goiás, Brésil.* Université de Paris VI, Paris,  
510 Thèse de Doctorat, 344p.
- 511 Botelho, N. F., and Moura, M. A., 1998. Granite-ore deposit relationships in Central Brazil.  
512 *Journal of South American Earth Sciences* 11 (5), 427-438.
- 513 Botelho, N.F., and Rossi, G., 1988. Depósito de estanho da Pedra Branca, Nova Roma, Goiás.  
514 Principais Depósitos Brasileiros - Metais Básicos Não Ferrosos, Ouro e Alumínio.  
515 DNPM, 3, 1431.
- 516 Braun, J.J., Pagel, M., Muller, J.P., Bilong, P., Michard, A., Guillet, B., 1990. Cerium  
517 anomalies in lateritic profiles. *Geochimica Cosmochimica Acta.* 54, 781-795.
- 518 Costa, N. O., and Botelho, N.F., 2019. Mineralogical and chemical characterization and  
519 economic potential of rare earth elements in granites and greisens from the A-type Pedra  
520 Branca Granite Massif Tin Deposit, Central Brazil. Submitted to the *Journal Geochemical*  
521 *Exploration.*
- 522 Duddy, L.R., 1980. Redistribution and fractionation of rare-earth and other elements in a  
523 weathering profile. *Chemical Geology.* 30, 363-381.
- 524 Garcia, M. D. M., 2013. O projeto ETR da mina Pitinga. Apresentação no Ministério da  
525 Ciência e Tecnologia. Brasília, julho de 2013.

526 Hoshino, M., Sanematsu, K., and Watanabe, Y., 2016. REE mineralogy and Resources. In:  
527 Bünzli Jean-Claude and Pecharsky Vitalij K (eds.) Handbook on the Physics and  
528 Chemistry of Rare Earths, vol. 49, p.129 -291.

529 Janots, E., Bernier, F., Brunet, F., Muñoz, M., Trcera, N., Berger, A., Lanson, M., 2015. Ce  
530 (III) and Ce (IV) (re)distribution and fractionation in a lateritic profile from Madagascar:  
531 insights from in situ XANES spectroscopy at the Ce L<sub>III</sub> edge. *Geochimica Cosmochimica*  
532 *Acta.* 153, 134-148.

533 Laveuf, C., Cornu, S., 2009. A review on the potentiality of rare earth elements to trace  
534 pedogenetic processes. *Geoderma.* 154, 1-12.

535 Lenharo, S. L. R., Moura, M. A., and Botelho, N.F., 2002. Petrogenetic and mineralization  
536 process in Paleo to Mesoproterozoic rapakivi granites: example from Pitinga and Goiás,  
537 Brazil. *Precambrian Research.* 119, 277-299.

538 Marini, O. J., Botelho, N. F., 1986. A província de granitos estanífero de Goiás. *Revista*  
539 *Brasileira de Geociências.* 16, 119-131.

540 Marini, O. J., Botelho, N. F., and Rossi, P. H., 1992. Elementos terras raras em granitóides da  
541 província estanífera de Goiás. *Revista Brasileira de Geociências.* 22, 61-72.

542 Mogelli, G., 1993. REE and other trace elements in a granitic weathering profile from Serre,  
543 southern Italy. *Chemical Geology.* 103, 17-25.

544 Moldoveanu, G. A., and Papangelakis, V. G., 2012. Recovery of rare earth elements adsorbed  
545 on clay minerals: II. Leaching with ammonium sulfate. *Hydrometallurgy.* 117-118, 71-  
546 78.

547 Nesbitt, H.W., and Markovics, G., 1997. Weathering of granodioritic crust, long-term storage  
548 of elements in weathering profiles, and petrogenesis of siliciclastic sediments.  
549 *Geochimica Cosmochimica Acta.* 61, 1653-1670.

550 Naumov, A.V., 2008. Review of the World Market of Rare-Earth Metals Russian. *Journal of*  
551 *Non-Ferrous Metals.* 49 (1), 18–27.

552 Ohta, A. and Kawabe, I., 2001. REE(III) adsorption onto Mn dioxide ( $\delta$ -MnO<sub>2</sub>) and Fe  
553 oxyhydroxide: Ce(III) oxidation by  $\delta$ -MnO<sub>2</sub>. *Geochimica et Cosmochimica Acta.* 65, 695-  
554 703.

555 Pearce, J., 1996. Sources and settings of granitic rocks. *Episodes.* 19(4), 120-125.

556 Pimentel, M.M., Botelho, N.F., 2001. Sr and Nd isotopic characteristics of 1.77-1.58 Ga rift-  
557 related granites and volcanics of the Goiás tin province, Central Brazil. *Anais da*  
558 *Academia Brasileira de Ciências* 73, 263-276

559 Rauret, G, López-Sanches, J.F., Sahuquillo, A., Rubio, R., Davidson, C., Ure, A., and  
560 Quevauviller, Ph., 1999. Improvement of the BCR three step sequential extraction  
561 procedure prior to the certification of new sediment and soil reference materials. *Journal*  
562 *Environmental Monitoring*. 1, 57-61.

563 Rocha, A., Schissel, D., Sprecher, A., Tarso, P. and J. Goode, J., 2013. Process Development  
564 for the Serra Verde Weathered Crust Elution-deposited Rare Earth Deposit in Brazil. In  
565 *Rare Earth Elements – Proceedings of the 52nd Conference of Metallurgists (COM*  
566 *2013)*, Edited by I. London, J. Goode G. Moldoveanu and M. Rayat. Metallurgical  
567 Society of the Canadian Institute of Mining, Metallurgy and Petroleum (MetSoc-CIM),  
568 Montreal, Canada, 2013.

569 Roskill, 2007. The economics of rare earths and yttrium, 13th edn. Roskill Information  
570 Services, Ltd., London, 275 pp.

571 Roskill, 2018. Rare Earths. Global Industry, Markets & Outlook 2018  
572 (<https://roskill.com/market-report/rare-earths/>).

573 Santana, I. V., Wall, F., and Botelho, N. F., 2015. Occurrence and behavior of monazite-(Ce)  
574 and xenotime-(Y) in detrital and saprolitic environments related to the Serra Dourada  
575 granite, Goiás/Tocantins State, Brazil: potential for ETR deposits. *Journal of*  
576 *Geochemical Exploration* 155, 1–13.

577 Sanematsu, K., Murakami, H., Watanabe, Y., Duangsurigna, S. and Vilayhack, S., 2009.  
578 Enrichment of rare earth elements (REE) in granitic rocks and their weathered crusts in  
579 central and southern Laos. *Bull. Geol. Surv. Japan*, 60, 527–558.

580 Sanematsu, K., Kon, Y., Imai, A., Watanabe, K., and Watanabe, Y., 2013. Geochemical and  
581 mineralogical characteristics of ion-adsorption type REE mineralization in Phunket,  
582 Thailand. *Mineralium Deposita*. 48, 437-451.

583 Sanematsu, K., and Kon, Y., 2013. Geochemical characteristic determined by multiple  
584 extraction from ion-adsorption type REE ores in Dingnan Country of Jiangxi Province,  
585 South China. *Bulletin of the Geological Survey of Japan*. 64, 313-330.

586 Sanematsu, K., Kon, and Y., Imai, A., 2015. Influence of phosphate on mobility and  
587 adsorption of REEs during weathering of granites in Thailand. *Journal of Asian Earth*  
588 *Sciences*. 111, 14-20.

589 Service, R. F., 2010. Nations move to head off shortages of rare earths. *Science*, 327 (5973),  
590 1596–1597.

591 Stone, R., 2009. As China's rare earth R&D becomes ever more rarefied, others tremble.  
592 *Science*, 325: 1336-1337.

593 Teixeira, L. M., and Botelho, N. F., 1999. Comportamento dos Elementos Terras Raras  
594 Pesadas em Zircão, Xenotima e Torita de Granitos e Greisens da Subprovíncia Estanífera  
595 Paranã, Goiás. *Revista Brasileira de Geologia*, 29 (4), 549-556.

596 Teixeira, L. M., and Botelho, N. F., 2002. Comportamento cristal químico de monazita  
597 primária e hidrotermal durante a evolução de granitos e greisens: Exemplos das  
598 subprovíncias Tocantins e Paranã, Goiás. *Revista Brasileira de Geociências*, 32 (3), 335-  
599 342.

600 Teixeira, L. M., and Botelho, N. F., 2006. Comportamento Geoquímico de ETR durante  
601 evolução magmática e alteração hidrotermal de granitos: Exemplos da Província  
602 Estanífera de Goiás. *Revista Brasileira de Geociências*, 36 (4), 679-691.

603 U.S.G.S., 2019. Mineral Commodity Summaries 2019. U.S. Geological Survey, Reston, 200  
604 p. <https://doi.org/10.3133/70202434>.

605 Vieira, C. C., Botelho, N. F., and Ganier, J., 2019. Geochemical and mineralogical  
606 characteristics of REEY occurrences in the Mocambo Granitic Massif tin-bearing A-type  
607 granite, central Brazil, and its potential for ion-adsorption-type REEY mineralization. *Ore  
608 Geology Reviews*. 105, 467-486.

609 Wu, C. Y., Huang, D. H., and Guo, Z. G., 1990. REE geochemistry in the weathered crust of  
610 granites, Longnam area, Jiangxi Province. *Acta Geol. Sin.* 3, 193-210.

611 Xu, C., Kynicky, J., Smith, M.P., Kopriva, A., Brtnicky, M., Urubek, T., Yang, Y., Zhao, Z.,  
612 He, C., and Song, W., 2017. Origin of heavy rare earth mineralization in South China.  
613 *Nature Communications*, Open Access, DOI: 10.1038/ncomms14598, p. 1-7.

614 Yusoff, Z.M., Ngwenya, B.T., and Parsons, I., 2013. Mobility and fractionation of REEs  
615 during deep weathering of geochemically contrasting granites in a tropical setting,  
616 Malaysia. *Chemical Geology*. 349, 71–86.

617 Zapata, A. M., and Botelho, N. F., 2018. Mineralogical and geochemical characterization of  
618 rare-earth occurrences in the Serra do Mendes massif, Goiás, Brazil. *Journal of  
619 Geochemical Exploration*. 188, 398-412.

620

621

## 5. CONCLUSÕES GERAIS

Todos os granitos do depósito de estanho Faixa Placha são ricos em ETR com valores mais altos que 1000 vezes o valor do condrito, e este enriquecimento deve-se principalmente à evolução magmática. Embora os ETRL sejam mais abundantes que os ETRP, foram encontrados teores de ETRP até 500 vezes a concentração em condritos. Granitos parentais, granitos greisenizados e greisens têm os mesmos padrões e conteúdo de ETR, indicando que não há mudança relevante na concentração e fracionamento do ETR de forma contemporânea com a evolução hidrotermal dos granitos no Maciço da Pedra Branca.

Os resultados obtidos até o momento sugerem que o Maciço da Pedra Branca possui um granito rico em ETR + Y dominante devido à presença de allanita, monazita, xenotima, torita, zircão e apatita. Nos granitos parentais, granitos greisenizados e greisens, zircões metamictizados e alterados favorecem a concentração de ETRP + Y, que alcança valores acima de 500 ppm em algumas amostras.

A comparação entre as concentrações de ETRY na Faixa Placha e nas áreas vizinhas mostra que não há grande variação, com valores semelhantes tanto para ETRL quanto para ETRP, indicando que isso é uma característica desses granitos que são ricos em ETR, sem influência efetiva das alterações hidrotermais, devido a presença de minerais primários portadores de ETR.

A anomalia positiva de Ce nos solos se deve à fixação do elemento como  $Ce^{4+}$  nos níveis mais superficiais oxidados, devido a dissolução dos fosfatos portadores de ETR como monazita e apatita, que controlam a mobilização da ETR e Th a partir da superfície e seu conteúdo no solo (Aubert et al. 2001). A principal diferença entre a Faixa Placha e as áreas vizinhas está na concentração em Y, cerca de duas vezes maior, principalmente nos greisens. Granitos greisenizados e greisens da Faixa Placha têm grande concentração de zircão metamictico rico em ETRP, a correlação positiva entre a razão  $(Yb/Ho)_{Gran}$  e a concentração de Zr no solo é indicadora de enriquecimento em ETR, indicando que os ETRP devem ser controlados por uma fase mineral fortemente enriquecida nesses elementos, como no caso do zircão da Faixa Placha.

As extrações na fração argila e no óxido de Fe-Mn no perfil de intemperismo da Faixa Placha mostraram maior enriquecimento dos ETR em comparação com a rocha total e óxido de Fe-Mn amorfo respectivamente. Esse enriquecimento ocorre na parte inferior do perfil, em

que os elementos ficam imobilizados, devido a sua adsorção na caulinita e nos óxidos de Fe-Mn.

As concentrações de ETRY e as composições minerais sugerem um potencial econômico no depósito de Faixa Placha, principal depósito de estanho no Brasil central, para a recuperação de ETR como subprodutos. Além disso, a área também é favorável para os depósitos de ETR do tipo de adsorção iônica, tanto nos depósitos de estanho como nas superfícies intemperizadas do maciço granítico.

## 6. REFERÊNCIAS

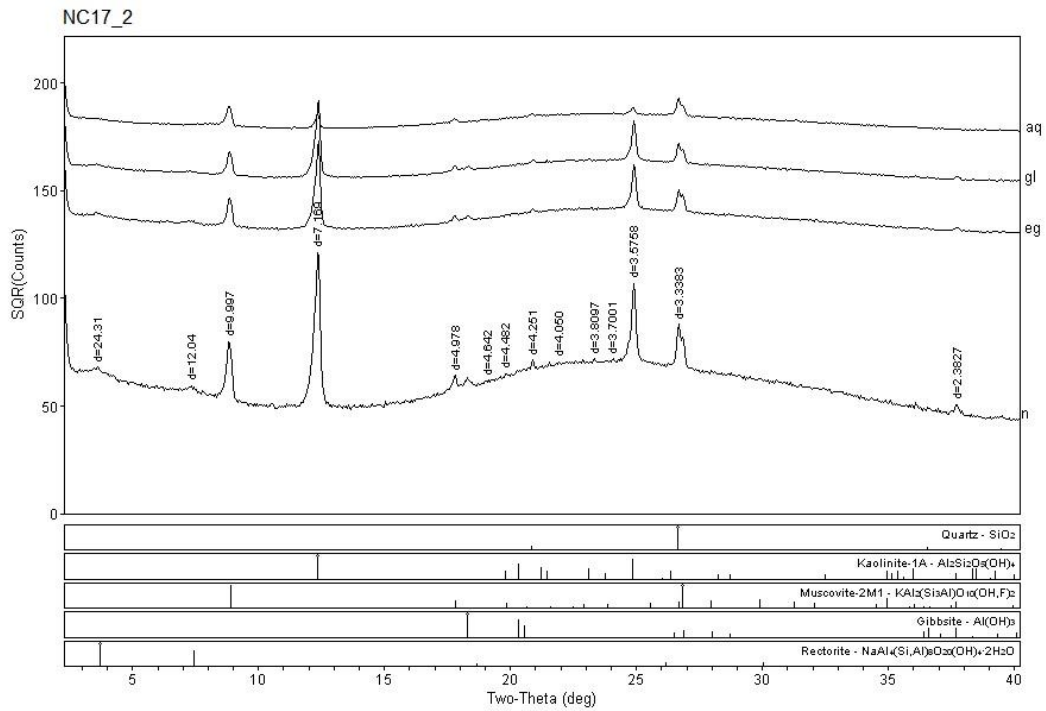
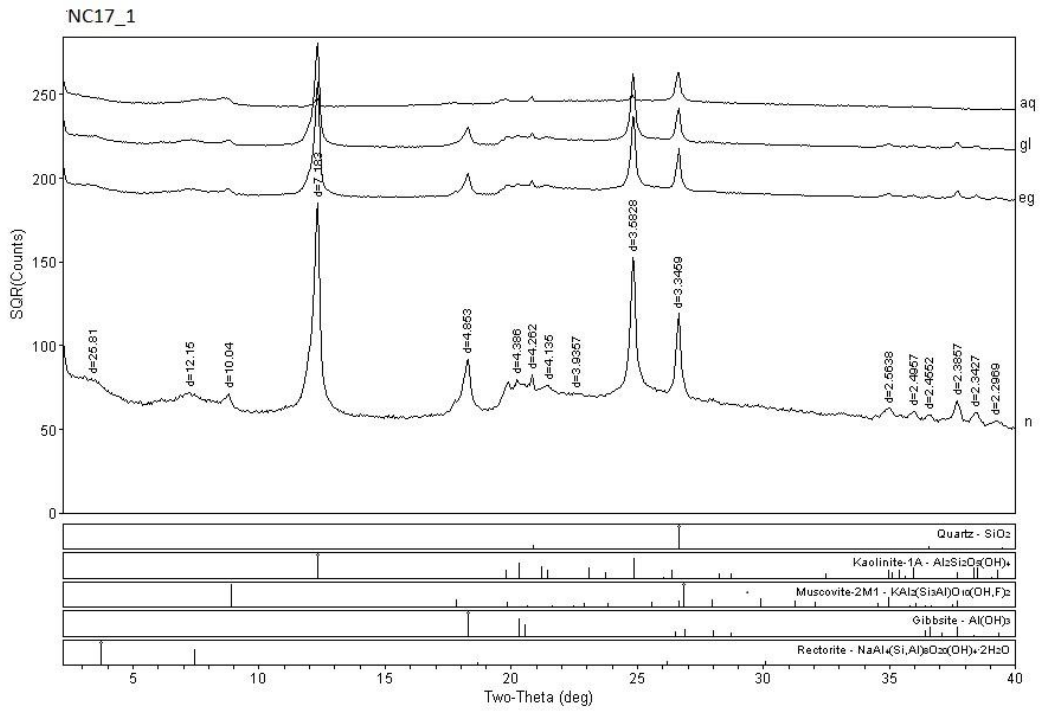
- Botelho, N.F., 1992. Les ensembles granitiques subalcalins a peralumineux mineralisés en Sn et In de la sous-province Paranã, état de Goiás, Brésil. Université de Paris VI, Paris, Thèse de Doctorat, 344p.
- Botelho N.F., Moura M.A. 1998. Granite-ore deposit relationships in Central Brazil. *Journal of South American Earth Sciences* 11 (5), 427-438.
- Botelho, N.F., Rossi, G., 1988. Depósito de estanho da Pedra Branca, Nova Roma, Goiás. *Principais Depósitos Brasileiros-Metais Básicos Não Ferrosos, Ouro e Alumínio. DNPM* 3, 1431.
- Botelho, N.F., Alvarenga, C.J.S., Menezes, P.R., D'el Rey, S. L. J. H., 1999. Suíte Aurumina: uma suíte de granitos paleoproterozóicos, peraluminosos e sintectônicos na Faixa Brasília. In: SBG/Núcleo Centro Oeste e Minas Gerais, *Simp.Geol. Centro Oeste*, 7, Brasília, *Boletim de Resumos*, v. 1. p. 49-49.
- Brasil. Plano Nacional de Mineração 2030 (PNM – 2030). Brasil, Ministério de Minas e Energia. Brasília, MME, 2010.
- Garcia, M.D.M., 2013. O projeto ETR da mina Pitinga. Apresentação no Ministério da Ciência e Tecnologia. Brasília, julho de 2013.
- Hoshino, M., Sanematsu, K., Watanabe, Y., 2016. REE mineralogy and Resources. In: Bünzli Jean-Claude and Pecharsky Vitalij K (eds.) *Handbook on the Physics and Chemistry of Rare Earths*, vol. 49, p.129 -291
- Lenharo, S.L.R., Moura, M.A., Botelho, N.F., 2002. Petrogenetic and mineralization processes in Paleo- to Mesoproterozoic rapakivi granites: example from Pitinga and Goiás, Brazil. *Precambrian Research* 119, 277-299.
- Marini, O. J., Botelho, N. F., Rossi, PH., 1992. Elementos terras raras em granitóides da província estanífera de Goiás. *Revista Brasileira de Geociências* 22, 61-72.
- Moura, M.A., Botelho, N.F., Olivo, G.R., Kyser, K., Pontes, R.M., 2014. Genesis of the Proterozoic Mangabeira tin-indium mineralization, Central Brazil: Evidence from geology, petrology, fluid inclusion and stable isotope data. *Ore Geology Reviews* 60, 36-49.
- Pimentel, M.M, Botelho, N.F., 2001. Sr and Nd isotopic characteristics of 1.77-1.58 Ga rift-related granites and volcanics of the Goiás tin province, Central Brazil. *Anais da Academia Brasileira de Ciências* 73, 263-276.
- Rauret, G, López-Sanches, J.F., Sahuquillo, A., Rubio, R., Davidson, C., Ure, A., Quevauviller, Ph., 1999. Improvement of the BCR three step sequential extraction

- procedure prior to the certification of new sediment and soil reference materials. *Journal Environmental Monitoring*. 1, 57-61.
- Rocha, A., Schissel, D., Sprecher, A., Tarso, P., Goode, J., 2013. Process Development for the Serra Verde Weathered Crust Elution-deposited Rare Earth Deposit in Brazil. In *Rare Earth Elements –Proceedings of the 52nd Conference of Metallurgists (COM 2013)*, Edited by I. London, J. Goode, G. Moldoveanu and M. Rayat. Metallurgical Society of the Canadian Institute of Mining, Metallurgy and Petroleum (MetSoc-CIM), Montreal, Canada, 2013.
- Roskill, 2007. The economics of rare earths and yttrium, 13th edn. Roskill Information Services, Ltd., London, 275 pp.
- Roskill, 2018. Rare Earths. Global Industry, Markets & Outlook 2018 (<https://roskill.com/market-report/rare-earths/>).
- Sanematsu, K., Murakami, H., Watanabe, Y., Duangsurigna, S., Vilayhack, S., 2009. Enrichment of rare earth elements (REE) in granitic rocks and their weathered crusts in central and southern Laos. *Bull. Geol. Surv. Japan*, 60, 527–558.
- Sanematsu, K., Kon, Y., 2013. Geochemical characteristic determined by multiple extraction from ion-adsorption type REE ores in Dingnan Country of Jiangxi Province, South China. *Bulletin of the Geological Survey of Japan*. 64, 313-330.
- Sanematsu, K., Kon, Y., Imai, A., 2015. Influence of phosphate on mobility and adsorption of REEs during weathering of granites in Thailand. *Journal of Asian Earth Sciences*. 111, 14-20.
- Santana I. V., Wall F., Botelho N. F., 2015. Occurrence and behaviour of monazite-(Ce) and xenotime-(Y) in detrital and saprolitic environments related to the Serra Dourada granite, Goiás/Tocantins State, Brazil: potential for ETR deposits. *Journal of Geochemical Exploration* 155, 1–13.
- Service, R. F., 2010. Nations move to head off shortages of rare earths. *Science* 327 (5973), 1596–1597.
- Stone, R., 2009. As China's rare earth R&D becomes ever more rarefied, others tremble. *Science* 325, 1336-1337.
- Teixeira, L.M., Botelho, N.F., 1999. Comportamento dos elementos terras raras pesadas em zircão, xenotima e torita de granitos e greisens da subprovincia estanífera Paranã, Goiás. *Revista Brasileira de Geociências* 29(4), 549-556.

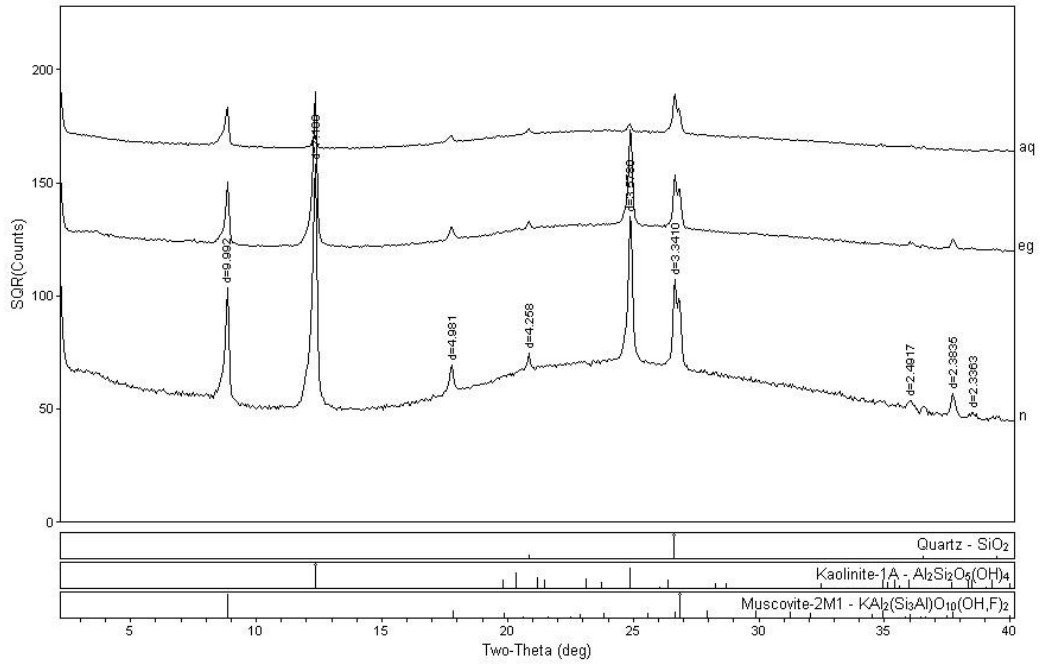
- Teixera, L.M., Botelho, N.F., 2002. Comportamento cristaloquímico de monazita primária e hidrotermal durante a evolução de granitos e greisens: Exemplos das subprovíncias Tocantins e Paranã, Goiás. *Revista Brasileira de Geociências* 32(3), 335-342.
- Teixeira, L.M., Botelho, N.F., 2006. Comportamento Geoquímico de ETR durante evolução magmática e alteração hidrotermal de granitos: Exemplos da Província Estanífera de Goiás. *Revista Brasileira de Geociências* 36(4), 679-691.
- U.S.G.S., 2019. Mineral Commodity Summaries 2019. U.S. Geological Survey, Reston, 200 p. <https://doi.org/10.3133/70202434>.
- Vieira, C. C., 2016. Caracterização Mineralógica, Geoquímica e Potencial Econômico de Ocorrências de Terras Raras do Maciço Granítico Mocambo, Goiás. Brasil. Universidade de Brasília. Dissertação de Mestrado, 74p.
- Xu, C., Kynicky, J., Smith, M.P., Kopriva, A., Brtnicky, M., Urubek, T., Yang, Y., Zhao, Z., He, C., Song, W., 2017. Origin of heavy rare earth mineralization in South China. *Nature Communications, Open Access*, DOI: 10.1038/ncomms14598, p. 1-7.
- Zapata, A. M. 2017. Caracterização Mineralógica, Geoquímica e Potencial Econômico de Ocorrências de Terras Raras do Maciço Granítico Serra Do Mendes, Goiás. Brasil. Universidade de Brasília. Dissertação de Mestrado, 66p.
- Zapata, A. M., Botelho, N. F., 2018. Mineralogical and geochemical characterization of rare-earth occurrences in the Serra do Mendes massif, Goiás, Brazil. *Journal of Geochemical Exploration*, 188, 398-412.

# ANEXOS – 1 (DRX)

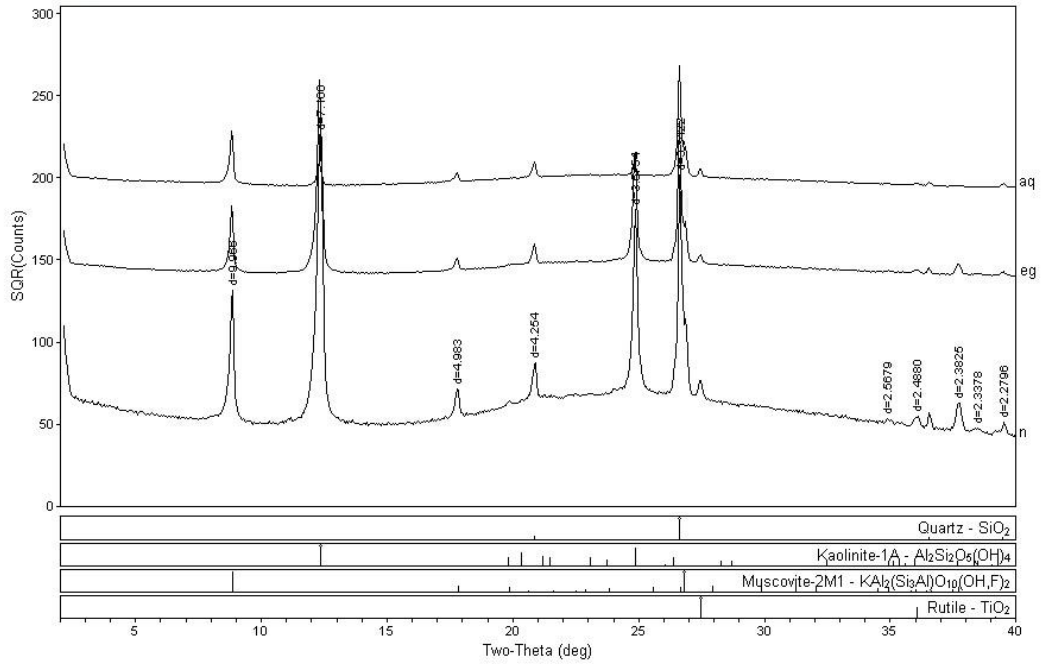
Difratogramas das análises de raios-X (rocha total e argila) do perfil de intemperismo (ponto 17) da Faixa Placha.

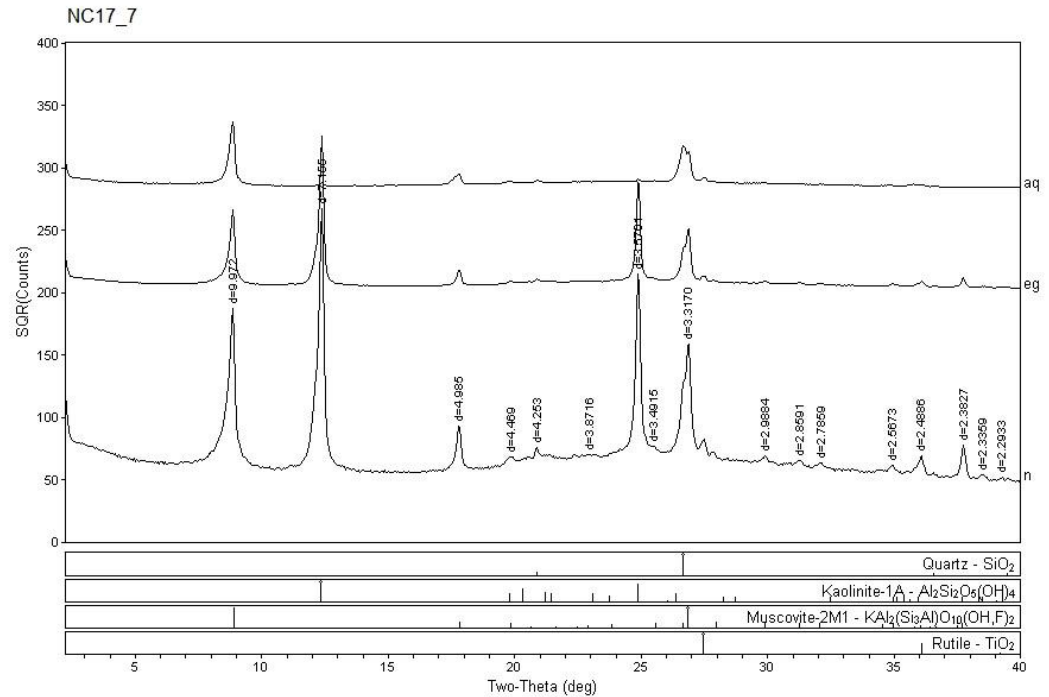
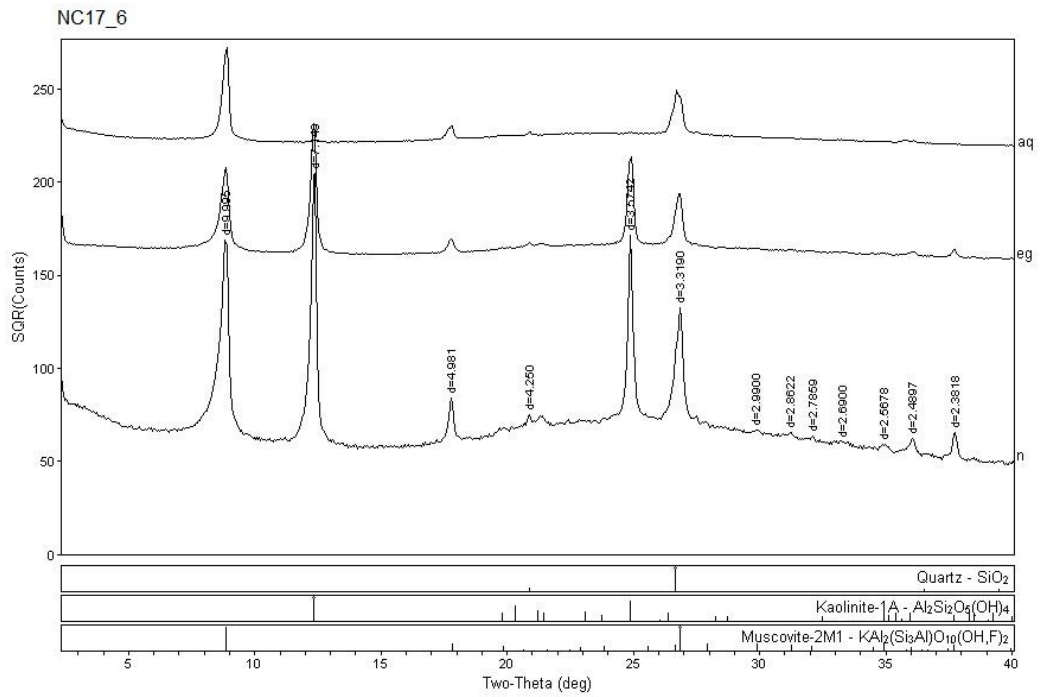


NC17\_3



NC17\_4





## **ANEXOS – 2**

### **Minerais na Faixa Placha**

## Zircao – Faixa Placha

### Biotita granito

(%)	NC4C 1	NC4C 2	NC4C 3	NC4C 4	NC4C 5	NC4C 6	NC4C 7	NC4C 8	NC4C 9	NC4C 10	NC4C 11	NC4C 12	NC4C 13	NC4C 14	NC4C 15	NC4C 16	NC4C 17
SiO <sub>2</sub>	33,397	30,472	33,396	32,736	33,009	30,242	33,086	27,605	32,464	31,052	33,047	32,733	32,807	33,064	26,049	33,003	32,845
Al <sub>2</sub> O <sub>3</sub>	0,016	0,28	0,014	0,009	0,011	0,646	0,003	0,735	0,027	0,208	0,024	0,015	0	0,038	0,909	0,017	0,03
FeO	0,427	0,503	0,064	0,688	0,556	0,663	0,234	0,577	0,726	0,982	0,304	0,254	0,363	0,677	0,356	0,855	0,575
CaO	0	0,675	0	0,194	0,032	0,52	0	0,917	0,163	0,569	0,116	0	0,178	0,284	2,205	0,161	0,251
Na <sub>2</sub> O	0	0	0	0,028	0	0	0,012	0	0	0,017	0	0	0	0,013	0	0,014	0
TiO <sub>2</sub>	0,012	0,242	0,133	0,067	0,115	0	0	0,042	0,042	0,048	0	0,109	0	0,055	0	0,115	0
MnO	0,008	0,313	0	0,027	0	0,498	0,053	0,653	0	0,213	0,022	0	0,022	0,099	0,773	0,044	0,047
K <sub>2</sub> O	0,002	0,014	0,001	0,021	0,016	0,028	0,011	0,023	0,038	0,012	0,002	0,019	0,007	0,001	0,025	0,026	0,072
P <sub>2</sub> O <sub>5</sub>	0,084	0,38	0,033	0	0,04	0,26	0,129	0,821	0,118	0,101	0,017	0	0,06	0,001	0,44	0	0,095
Nb <sub>2</sub> O <sub>5</sub>	0,504	0,593	0,432	0,137	0,231	0,376	0,604	0,16	0	0,54	0,183	0,233	0,048	0,558	0,37	0,659	0,702
HfO <sub>2</sub>	1,123	2,087	1,051	0,889	1,279	0,92	0,929	4,612	0,971	1,814	1,185	0,772	1,178	0,74	1,012	1,29	1,392
Y <sub>2</sub> O <sub>3</sub>	0,302	0,347	0,149	0,222	0,413	0,972	0,298	1,966	0,462	0,581	0,025	0,002	0,109	0,114	1,692	0,217	0,214
Ta <sub>2</sub> O <sub>5</sub>	0,036	0	0,201	0	0,227	0	0,047	0,145	0,057	0,156	0	0	0,238	0,129	0	0,214	0
UO <sub>2</sub>	0,274	0,359	0,25	0,251	0,195	0,425	0,228	0,699	0,196	0,418	0,203	0,221	0,26	0,248	0,576	0,275	0,389
BaO	0	0	0,03	0,031	0,013	0,041	0	0,032	0	0	0,019	0,014	0	0,032	0,058	0,029	0,045
F	0	0,047	0	0	0	0,559	0	0,613	0	0,283	0	0	0	0	0,363	0	0
PbO	0	0	0	0	0	0	0	0	0	0	0	0	0	0	0	0	0
ThO <sub>2</sub>	0,065	0,043	0	0,026	0,029	0,104	0,013	0,275	0,057	0,033	0,051	0,025	0,056	0,028	0,097	0,074	0,234
SrO	0,114	0,139	0,144	0,041	0,074	0,233	0,035	0,189	0,083	0,149	0,068	0,135	0,103	0,086	0,127	0,097	0,038
ZrO <sub>2</sub>	62,343	56,854	60,858	61,076	61,268	54,763	60,861	48,628	61,075	58,349	61,265	61,99	61,838	60,007	48,47	60,663	61,322
<b>Total</b>	<b>98,707</b>	<b>93,348</b>	<b>96,756</b>	<b>96,443</b>	<b>97,508</b>	<b>91,25</b>	<b>96,543</b>	<b>88,692</b>	<b>96,479</b>	<b>95,525</b>	<b>96,531</b>	<b>96,522</b>	<b>97,267</b>	<b>96,174</b>	<b>83,522</b>	<b>97,753</b>	<b>98,251</b>
La <sub>2</sub> O <sub>3</sub>	0	0,005	0,016	0,027	0	0,011	0,011	0	0,024	0	0,002	0	0	0	0	0,012	0,021
Ce <sub>2</sub> O <sub>3</sub>	0,076	0,143	0,016	0,065	0	0,276	0,019	0,3	0,099	0,125	0,075	0,003	0,044	0,062	0,3	0,037	0,21
Pr <sub>2</sub> O <sub>3</sub>	0	0,022	0	0,028	0,043	0,104	0	0	0,064	0,047	0,017	0,032	0	0,042	0,006	0	0,1
Nd <sub>2</sub> O <sub>3</sub>	0	0	0,024	0,022	0,004	0,023	0	0,04	0,02	0,036	0,029	0	0,008	0	0,049	0,012	0,083
Sm <sub>2</sub> O <sub>3</sub>	0,003	0,086	0,067	0	0	0,081	0,023	0	0	0	0,035	0,006	0	0	0,062	0,001	0
Eu <sub>2</sub> O <sub>3</sub>	0	0	0	0	0,011	0,006	0	0,01	0	0,039	0,014	0,024	0,075	0,023	0,081	0	0
Gd <sub>2</sub> O <sub>3</sub>	0	0	0,02	0,05	0,033	0,076	0,011	0,194	0,01	0,048	0	0	0	0	0,003	0,043	0,043
Tb <sub>2</sub> O <sub>3</sub>	0	0	0	0	0	0	0	0	0	0	0	0	0	0	0	0	0
Dy <sub>2</sub> O <sub>3</sub>	0	0,043	0,094	0	0	0,115	0	0,614	0	0,009	0	0	0	0	0,087	0	0,1
Ho <sub>2</sub> O <sub>3</sub>	0,155	0	0,111	0	0,021	0,235	0	0,079	0,03	0,038	0,032	0,053	0,048	0	0	0	0,056
Er <sub>2</sub> O <sub>3</sub>	0,061	0,051	0,024	0,083	0,021	0,12	0	0,526	0,064	0,151	0,062	0,102	0,039	0,002	0,247	0,046	0,211
Tm <sub>2</sub> O <sub>3</sub>	0	0	0	0	0	0	0	0,054	0	0	0	0	0	0	0	0	0,002
Yb <sub>2</sub> O <sub>3</sub>	0,077	0,019	0,061	0,014	0,06	0,251	0,009	0,621	0,021	0,223	0,056	0,008	0,016	0,027	0,234	0,069	0,263



<b>Nd<sub>2</sub>O<sub>3</sub></b>	0,024	0,005	0	0	0	0	0	0,026	0	0	0,036	0	0,008	0,045	0,042	0,024	0	0	0,032	0	0,013
<b>Sm<sub>2</sub>O<sub>3</sub></b>	0,029	0,017	0	0	0,028	0	0,011	0	0,033	0	0	0	0,064	0,04	0	0	0,023	0	0	0	0
<b>Eu<sub>2</sub>O<sub>3</sub></b>	0	0	0,032	0,029	0	0	0	0,005	0	0	0,016	0	0	0	0,027	0,025	0	0,022	0,005	0,021	0,006
<b>Gd<sub>2</sub>O<sub>3</sub></b>	0,036	0,026	0,048	0,029	0,043	0,012	0,01	0	0,025	0,024	0	0	0,02	0	0	0,065	0,041	0,027	0	0,042	0,015
<b>Tb<sub>2</sub>O<sub>3</sub></b>	0	0	0	0	0	0	0	0	0	0	0	0	0	0	0	0	0	0	0	0	0
<b>Dy<sub>2</sub>O<sub>3</sub></b>	0	0	0	0	0	0	0	0,007	0	0,156	0	0	0	0	0	0,089	0	0	0	0	0
<b>Ho<sub>2</sub>O<sub>3</sub></b>	0	0	0,072	0,013	0,028	0,008	0,087	0	0	0,092	0	0,05	0	0	0	0	0	0,075	0	0	0
<b>Er<sub>2</sub>O<sub>3</sub></b>	0,084	0,01	0,036	0,085	0,077	0,125	0,046	0,086	0	0,216	0,079	0,026	0	0,082	0	0,141	0,083	0,001	0,015	0,074	0,17
<b>Tm<sub>2</sub>O<sub>3</sub></b>	0	0,024	0	0,023	0,021	0	0	0	0	0,021	0	0,001	0,061	0	0	0	0,016	0	0	0,034	0
<b>Yb<sub>2</sub>O<sub>3</sub></b>	0,095	0,029	0,06	0,034	0,015	0,041	0,058	0,025	0,053	0,25	0,12	0,092	0	0,056	0,073	0,178	0	0,018	0	0,003	0,23
<b>Lu<sub>2</sub>O<sub>3</sub></b>	0,064	0	0,011	0	0,007	0,019	0	0	0	0,063	0,025	0,053	0,05	0,024	0,004	0	0	0,069	0,089	0	0,035
<b>REE</b>	0,487	0,134	0,26	0,322	0,258	0,308	0,212	0,328	0,189	1,008	0,342	0,379	0,334	0,284	0,228	0,701	0,212	0,356	0,183	0,26	0,538
<b>REEY</b>	0,559	0,412	0,481	0,643	0,544	0,526	0,565	0,442	0,189	2,602	0,633	0,661	0,479	0,336	0,317	1,899	0,704	1,665	0,717	0,26	3,646
<b>LREE</b>	0,208	0,045	0,033	0,138	0,067	0,103	0,011	0,21	0,111	0,186	0,118	0,157	0,203	0,122	0,151	0,228	0,072	0,166	0,079	0,107	0,088
<b>HREE</b>	0,279	0,089	0,227	0,184	0,191	0,205	0,201	0,118	0,078	0,822	0,224	0,222	0,131	0,162	0,077	0,473	0,14	0,19	0,104	0,153	0,45
<b>HREEY</b>	0,351	0,367	0,448	0,505	0,477	0,423	0,554	0,232	0,078	2,416	0,515	0,504	0,276	0,214	0,166	1,671	0,632	1,499	0,638	0,153	3,558

Continuação..

(%)	NC4C 39	NC4C 40	NC4C 41	NC4C 42	NC4C 43	NC4C 44	NC4C 45	NC4C 46	NC4C 47	NC4C 48	NC4C 49	NC4C 50	NC4C 51	NC4C 52
SiO <sub>2</sub>	32,904	32,71	32,53	33,421	6,193	32,894	29,072	31,753	32,405	31,22	27,657	29,585	24,603	31,609
Al <sub>2</sub> O <sub>3</sub>	0	0,002	0,004	0,001	1,12	0,027	0,6	0,14	0,006	0,062	0,46	0,069	0,073	0,046
FeO	0,218	0,274	0,163	0,136	11,678	0,426	0,795	0,784	0,308	0,055	0,59	0,766	0,372	1,192
CaO	0	0	0	0	0,407	0,44	1,015	0	0	0,088	0,743	0,098	0,249	0,322
Na <sub>2</sub> O	0	0,01	0,003	0,033	0	0,003	0,013	0,002	0	0,008	0,018	0,035	0,052	0,014
TiO <sub>2</sub>	0,006	0	0	0,206	0,048	0	0	0,127	0	0,097	0	0	0,169	0
MnO	0	0	0,086	0,017	0,078	0,119	0,319	0	0	0,104	0,525	0,045	0,071	0,178
K <sub>2</sub> O	0,014	0,05	0,009	0,008	0,029	0,011	0,779	0,015	0,007	0,008	0,01	0,003	0,008	0,025
P <sub>2</sub> O <sub>5</sub>	0,011	0,129	0,128	0,022	19,893	0,088	0,606	0,123	0,062	0,241	0,691	0,016	0,157	0,016
Nb <sub>2</sub> O <sub>5</sub>	0,383	0,419	0,601	0,625	0	0,596	0,365	0,528	0,361	0,225	0,484	0,319	0,172	0,357
HfO <sub>2</sub>	0,863	1,203	0,788	1,092	0,032	1,24	1,222	0,806	1,094	0,893	2,012	1,108	2,005	1,503
Y <sub>2</sub> O <sub>3</sub>	0,132	0,252	0,092	0,018	24,324	0,453	1,601	0,664	0,163	0,362	1,437	0,333	0,123	0,302

Ta <sub>2</sub> O <sub>5</sub>	0	0	0,073	0,047	0	0	0	0,18	0	0	0,036	0	0	0,012
UO <sub>2</sub>	0,231	0,225	0,231	0,367	0,364	0,239	0,245	0,231	0,263	0,232	0,257	0,241	0,289	0,335
BaO	0,001	0	0,003	0	0,019	0,014	0,053	0	0	0,015	0,015	0,02	0,045	0,024
F	0	0	0	0	1,216	0	0,362	0,111	0	0	0,383	0	0	0
PbO	0	0	0	0	0	0	0	0	0	0	0	0	0	0
ThO <sub>2</sub>	0,017	0,012	0,031	0,001	0,378	0,07	0,022	0	0,02	0	0,028	0,102	0,106	0,029
SrO	0,109	0,109	0,205	0,094	0,097	0,17	0,04	0,119	0,155	0,195	0,086	0,177	0,13	0,085
ZrO <sub>2</sub>	64,192	62,462	65,916	63,709	4,292	63,935	55,079	56,081	64,672	59,176	55,915	57,968	46,52	60,765
Total	99,081	97,857	100,863	99,797	70,168	100,725	92,188	91,664	99,516	92,981	91,347	90,885	75,144	96,814
La <sub>2</sub> O <sub>3</sub>	0,06	0	0,024	0	0	0	0	0,004	0,034	0,029	0,014	0	0,037	0
Ce <sub>2</sub> O <sub>3</sub>	0,049	0,105	0	0,132	0,189	0,097	0,049	0	0,076	0,067	0,043	0,074	0,135	0,046
Pr <sub>2</sub> O <sub>3</sub>	0	0	0,024	0	0	0,031	0,017	0,024	0	0,01	0,005	0,006	0,06	0,027
Nd <sub>2</sub> O <sub>3</sub>	0,019	0	0,01	0,027	0,05	0,041	0,024	0	0,025	0	0	0	0,006	0
Sm <sub>2</sub> O <sub>3</sub>	0	0	0,007	0	0	0	0	0	0,066	0	0,023	0	0,071	0
Eu <sub>2</sub> O <sub>3</sub>	0	0	0,068	0,032	0	0,037	0	0	0	0,037	0	0	0	0
Gd <sub>2</sub> O <sub>3</sub>	0	0	0	0	0,501	0	0,037	0,049	0	0,004	0,032	0,064	0,041	0,065
Tb <sub>2</sub> O <sub>3</sub>	0	0	0	0	0	0	0	0	0	0	0	0	0	0
Dy <sub>2</sub> O <sub>3</sub>	0	0	0	0	1,117	0	0,154	0	0	0,002	0	0	0	0,027
Ho <sub>2</sub> O <sub>3</sub>	0,046	0,09	0,065	0,024	0,296	0	0	0,122	0,047	0,033	0,007	0	0	0
Er <sub>2</sub> O <sub>3</sub>	0,013	0,04	0	0,154	0,831	0,002	0,023	0,107	0,101	0,06	0,169	0,069	0,094	0,053
Tm <sub>2</sub> O <sub>3</sub>	0,003	0,001	0	0	0,039	0	0	0	0	0,04	0	0	0,042	0
Yb <sub>2</sub> O <sub>3</sub>	0	0	0	0	0,825	0	0,042	0,01	0,093	0,016	0,056	0,13	0,077	0,045
Lu <sub>2</sub> O <sub>3</sub>	0,011	0,021	0	0	0,109	0	0	0,004	0,064	0,055	0	0	0	0,06
REE	0,201	0,257	0,198	0,369	3,957	0,208	0,346	0,32	0,506	0,353	0,349	0,343	0,563	0,323
REEY	0,333	0,509	0,29	0,387	28,281	0,661	1,947	0,984	0,669	0,715	1,786	0,676	0,686	0,625
LREE	0,128	0,105	0,133	0,191	0,239	0,206	0,09	0,028	0,201	0,143	0,085	0,08	0,309	0,073
HREE	0,073	0,152	0,065	0,178	3,718	0,002	0,256	0,292	0,305	0,21	0,264	0,263	0,254	0,25
HREEY	0,205	0,404	0,157	0,196	28,042	0,455	1,857	0,956	0,468	0,572	1,701	0,596	0,377	0,552

**Zircão**  
**Granito greisenizado**

(%)	NC9-1	NC9-2	NC9-3	NC9-4	NC9-5	NC9-6	NC9-7	NC9-8	NC9-9	NC9-10	NC9-11	NC9-12	NC9-13	NC9-14
SiO <sub>2</sub>	25,553	32,859	29,471	29,394	29,884	28,316	33,535	33,291	28,537	20,089	25,837	28,03	33,162	29,324
Al <sub>2</sub> O <sub>3</sub>	0,298	0,02	0,829	0,085	0,206	0,349	0	0,005	0,22	0,28	0,491	0,411	4,282	0,078
FeO	0,937	0,06	0,959	0,779	0,543	0,773	0,03	0,04	0,918	0,613	0,855	1,121	1,566	1,119
CaO	0,831	0	0,153	1,413	0,917	0,397	0	0	0,242	0,607	0,252	0,397	0,138	0,034
Na <sub>2</sub> O	0,006	0,014	0,028	0,04	0,037	0,014	0	0,001	0,05	0,029	0,068	0,038	0,046	0,116
TiO <sub>2</sub>	0,271	0	0,012	0	0,042	0	0,036	0	0,242	0	0,199	0,193	0,164	0,687
MnO	0,478	0,009	0,115	0,378	0,353	0,287	0,122	0,04	0,282	0,079	1,327	0,461	0,125	0,231
K <sub>2</sub> O	0,091	0,005	0,102	0,061	0,094	0,057	0	0	0,08	0,119	0,092	0,066	0,287	0,209
P <sub>2</sub> O <sub>5</sub>	3,469	0,056	0,743	0,144	0,199	1,385	0,032	0,044	0,635	8,89	0,176	0,325	0,615	0,198
Nb <sub>2</sub> O <sub>5</sub>	0,275	0,39	0,207	0,496	0,054	0,939	0,356	0,497	0,38	0,686	0,681	0,957	0,397	2,422
HfO <sub>2</sub>	2,971	0,838	2,203	3,003	2,333	2,45	1,291	1,213	2,131	2,545	2,258	2,001	2,308	0,115
Y <sub>2</sub> O <sub>3</sub>	5,444	0,211	1,414	0,011	0,709	4,072	0,296	0,074	2,245	13,542	3,11	3,609	1,904	0,047
Ta <sub>2</sub> O <sub>5</sub>	0,02	0,021	0,253	0,07	0,082	0,002	0	0	0,048	0,155	0,16	0,243	0	0,474
UO <sub>2</sub>	0,661	0,207	0,595	0,653	0,701	0,534	0,243	0,249	0,636	0,732	0,774	0,908	0,593	0,755
BaO	0,006	0	0,035	0,01	0	0,002	0,039	0	0,015	0,037	0,213	0,015	0	0
F	0,218	0	0,136	0,246	0,495	0,093	0	0	0,02	0,489	0,722	0,187	0,277	0
PbO	0,648	0	0,461	0,421	0,796	0,236	0	0	0,604	0,523	0,367	0,846	0,174	0,671
ThO <sub>2</sub>	0,119	0,021	0,198	0,023	0,236	0,71	0,015	0	0,369	1,126	2,533	2,046	0,171	0,035
SrO	0,09	0,11	0,018	0,05	0,06	0,053	0,083	0,165	0,145	0,001	0,043	0,059	0,075	0,026
ZrO <sub>2</sub>	47,663	64,122	53,176	54,291	53,688	48,306	62,661	63,103	54,477	35,646	50,006	46,924	45,562	53,004
Total	90,049	98,943	91,108	91,568	91,429	88,975	98,739	98,722	92,276	86,188	90,164	88,837	91,846	89,545
La <sub>2</sub> O <sub>3</sub>	0	0	0	0	0	0	0	0	0,018	0	0,023	0	0	0
Ce <sub>2</sub> O <sub>3</sub>	0,12	0,058	0,034	0,041	0,054	0,108	0,014	0,069	0,127	0,249	1,288	0,169	0,106	0,061
Pr <sub>2</sub> O <sub>3</sub>	0	0,027	0	0,026	0	0	0	0	0,031	0	0,018	0,046	0	0
Nd <sub>2</sub> O <sub>3</sub>	0,014	0	0,025	0,011	0,045	0,006	0,011	0,004	0,021	0,021	0,056	0,034	0,056	0,011
Sm <sub>2</sub> O <sub>3</sub>	0	0	0	0,009	0	0,074	0,063	0,076	0	0	0,008	0,006	0,046	0
Eu <sub>2</sub> O <sub>3</sub>	0	0,006	0	0	0,049	0	0	0	0,073	0,005	0,036	0	0,023	0,067
Gd <sub>2</sub> O <sub>3</sub>	0,03	0,067	0,067	0,002	0	0,151	0	0,072	0,046	0,167	0,118	0,172	0,066	0
Tb <sub>2</sub> O <sub>3</sub>	0	0	0	0	0	0	0,034	0	0	0	0	0	0	0
Dy <sub>2</sub> O <sub>3</sub>	0,15	0	0,222	0	0	0,287	0	0	0,088	0,514	0,377	0,387	0	0
Ho <sub>2</sub> O <sub>3</sub>	0	0	0	0	0	0,093	0,163	0,098	0	0	0,121	0,207	0	0
Er <sub>2</sub> O <sub>3</sub>	0,311	0,052	0,4	0,16	0,274	0,699	0	0,046	0,41	1,059	0,72	0,935	0,138	0,106
Tm <sub>2</sub> O <sub>3</sub>	0,014	0	0	0	0	0,07	0	0,011	0,064	0,117	0,2	0,138	0	0
Yb <sub>2</sub> O <sub>3</sub>	0,829	0	0,998	0,194	0,462	1,362	0	0,089	0,951	2,468	2,019	2,453	0,706	0,197

Lu <sub>2</sub> O <sub>3</sub>	0,169	0	0,254	0,042	0	0,234	0	0	0,158	0,535	0,276	0,438	0,159	0
REE	1,637	0,21	2	0,485	0,884	3,084	0,285	0,465	1,987	5,135	5,26	4,985	1,3	0,442
REY	7,081	0,421	3,414	0,496	1,593	7,156	0,581	0,539	4,232	18,677	8,37	8,594	3,204	0,489
LREE	0,134	0,091	0,059	0,087	0,148	0,188	0,088	0,149	0,27	0,275	1,429	0,255	0,231	0,139
HREE	1,503	0,119	1,941	0,398	0,736	2,896	0,197	0,316	1,717	4,86	3,831	4,73	1,069	0,303
HREY	6,947	0,33	3,355	0,409	1,445	6,968	0,493	0,39	3,962	18,402	6,941	8,339	2,973	0,35

---

<b>Zircão - Biotita granito</b>					<b>Zircão - Granito greisenizado</b>							
(%)	1A 1	1A 2	1A 3	1A 4	NC4B 1	NC4B 2	NC4B 3	NC4B 4	NC7A 1	NC7A 2	NC7A 3	NC7A 4
<b>SiO<sub>2</sub></b>	32,424	33,07	32,237	32,379	32,515	33,09	27,277	33,361	32,766	28,254	25,454	30,812
<b>Al<sub>2</sub>O<sub>3</sub></b>	0,027	0,003	0,036	0,056	0,003	0,009	0,687	0,002	0	0,884	0,689	0,008
<b>FeO</b>	0,578	0,397	0,312	0,969	1,025	0,307	0,895	0,11	0	0,587	0,861	0,726
<b>CaO</b>	0,295	0,122	0,155	0	0,082	0,079	0,529	0,221	0	0,947	1,401	0,039
<b>Na<sub>2</sub>O</b>	0,016	0,007	0,003	0,036	0,056	0	0	0	0,002	0	0,035	0,061
<b>TiO<sub>2</sub></b>	0	0,123	0,012	0	0	0,053	0,023	0,164	0	0,196	0,146	0
<b>MnO</b>	0,118	0,039	0,21	0,047	0,03	0	0,934	0,125	0,042	0	0,265	0,059
<b>K<sub>2</sub>O</b>	0,015	0,008	0,002	0,004	0,009	0,003	0,009	0,017	0	0,005	0,089	0,007
<b>P<sub>2</sub>O<sub>5</sub></b>	0,176	0,16	0,14	0,091	0,124	0,065	0,437	0,027	0,071	0,472	0,49	0,22
<b>Nb<sub>2</sub>O<sub>5</sub></b>	0,124	0,441	0,263	0,117	0,3	0,032	0,005	0,535	0,279	0,335	0,662	0,227
<b>HfO<sub>2</sub></b>	1,484	0,962	1,541	1,154	1,26	1,336	2,769	1,427	1,178	1,794	1,133	2
<b>Y<sub>2</sub>O<sub>3</sub></b>	0,14	0,197	0,607	0,407	0,191	0,223	1,926	0,154	0,346	5,554	9,578	0,066
<b>Ta<sub>2</sub>O<sub>5</sub></b>	0,116	0,117	0	0	0,046	0,021	0,154	0	0,054	0,18	0	0,279
<b>UO<sub>2</sub></b>	0	0	0,062	0	0	0	0,278	0	0	0	0,442	0,108
<b>BaO</b>	0,022	0	0,035	0,013	0	0	0,055	0	0,007	0,031	0,025	0
<b>F</b>	0	0	0	0	0	0	0,421	0	0	0,318	0,907	0
<b>PbO</b>	0	0	0	0	0	0	0	0	0	0	0	0
<b>ThO<sub>2</sub></b>	0,071	0,03	0,079	0,103	0,07	0	0,022	0	0	0,033	0,438	0,03
<b>SrO</b>	0,037	0,142	0,124	0,07	0,152	0,122	0,152	0,177	0,122	0,178	0,204	0,073
<b>ZrO<sub>2</sub></b>	64,047	63,106	63,264	62,806	64,902	67,099	55,415	65,974	64,453	48,066	40,734	60
<b>Total</b>	99,69	98,924	99,082	98,252	100,765	102,439	91,988	102,294	99,32	87,834	83,553	94,715
<b>La<sub>2</sub>O<sub>3</sub></b>	0	0	0	0,043	0,011	0,012	0	0,002	0,008	0,041	0	0
<b>Ce<sub>2</sub>O<sub>3</sub></b>	0,062	0,035	0,046	0,064	0,006	0,041	0,108	0	0,036	0,015	0,108	0,025
<b>Pr<sub>2</sub>O<sub>3</sub></b>	0	0,075	0,012	0,048	0,012	0,055	0,048	0	0,009	0,003	0,052	0,044
<b>Nd<sub>2</sub>O<sub>3</sub></b>	0	0,017	0,023	0	0	0,001	0,009	0	0,008	0,011	0,029	0

<b>Sm<sub>2</sub>O<sub>3</sub></b>	0,034	0	0,053	0,042	0	0	0,023	0	0	0	0,035	0,031
<b>Eu<sub>2</sub>O<sub>3</sub></b>	0,055	0	0,084	0,021	0,025	0	0,029	0	0,027	0,028	0,084	0,01
<b>Gd<sub>2</sub>O<sub>3</sub></b>	0,039	0,011	0,081	0,006	0,014	0	0,101	0	0,019	0,045	0,011	0,002
<b>Tb<sub>2</sub>O<sub>3</sub></b>	0	0	0	0	0	0	0	0	0,007	0	0	0
<b>Dy<sub>2</sub>O<sub>3</sub></b>	0	0	0,105	0	0	0	0,182	0,063	0	0	0,172	0
<b>Ho<sub>2</sub>O<sub>3</sub></b>	0	0	0	0	0,041	0,02	0	0,183	0,002	0,061	0,09	0,021
<b>Er<sub>2</sub>O<sub>3</sub></b>	0,093	0,066	0,05	0,085	0,045	0	0,086	0,038	0,036	0,074	0,504	0,135
<b>Tm<sub>2</sub>O<sub>3</sub></b>	0	0	0	0,086	0	0	0	0	0,005	0	0,107	0
<b>Yb<sub>2</sub>O<sub>3</sub></b>	0,071	0	0,134	0,17	0,152	0,012	0,217	0,049	0,111	0	1,285	0,049
<b>Lu<sub>2</sub>O<sub>3</sub></b>	0	0	0,093	0,012	0	0,039	0	0	0	0	0,207	0
<b>REE</b>	0,354	0,204	0,681	0,577	0,306	0,18	0,803	0,335	0,268	0,278	2,684	0,317
<b>REEY</b>	0,494	0,401	1,288	0,984	0,497	0,403	2,729	0,489	0,614	5,832	12,262	0,383
<b>LREE</b>	0,151	0,127	0,218	0,218	0,054	0,109	0,217	0,002	0,088	0,098	0,308	0,11
<b>HREE</b>	0,203	0,077	0,463	0,359	0,252	0,071	0,586	0,333	0,18	0,18	2,376	0,207
<b>HREEY</b>	0,343	0,274	1,07	0,766	0,443	0,294	2,512	0,487	0,526	5,734	11,954	0,273

## Monazita

<b>Monazita – Biotita granito</b>											
(%)	NC4C 1	NC4C 2	NC4C 3	NC4C 4	NC4C 5	NC4C 6	NC4C 7	NC4C 8	NC4C 9	NC4C 10	NC4C 11
<b>SiO<sub>2</sub></b>	1,51	0,623	0,667	0,642	0,258	0,399	0,222	0,469	0,193	0,663	0,331
<b>Al<sub>2</sub>O<sub>3</sub></b>	0,343	0,085	0	0	0,006	0,023	0,012	0	0,03	0,076	0,033
<b>FeO</b>	11,284	1,585	0,155	0,197	0,406	0,005	0,106	0,086	0	0,394	0,061
<b>CaO</b>	0,053	0,444	0,165	0,445	0	0	0,172	0,764	0	0,319	0,267
<b>Na<sub>2</sub>O</b>	0	0	0	0	0	0	0	0	0,012	0	0
<b>TiO<sub>2</sub></b>	0,083	0,081	0,094	0	0,05	0	0	0	0,056	0,069	0,063
<b>MnO</b>	0,05	0	0,045	0	0,052	0,111	0,007	0,083	0,043	0	0,131
<b>K<sub>2</sub>O</b>	0,023	0,088	0,021	0,04	0,084	0,047	0,06	0,066	0,051	0,475	0,045
<b>P<sub>2</sub>O<sub>5</sub></b>	21,559	24,277	23,647	22,727	25,125	23,902	24,128	24,119	25,659	24,43	24,471
<b>Nb<sub>2</sub>O<sub>5</sub></b>	0	0,38	0	0	0	0	0	0,291	0	0,135	0
<b>HfO<sub>2</sub></b>	0	0	0	0	0,051	0	0,007	0,119	0,162	0	0
<b>Y<sub>2</sub>O<sub>3</sub></b>	0,255	0,399	0,468	0,546	0,355	0,738	0,222	0,601	0,323	1,008	0,868
<b>Ta<sub>2</sub>O<sub>5</sub></b>	0	0,136	0,013	0	0,088	0,022	0	0,308	0	0	0
<b>UO<sub>2</sub></b>	0,356	0,234	0,419	0,436	0,29	0,463	0,406	0,416	0,271	0,368	0,386
<b>BaO</b>	0,062	0	0,038	0	0,013	0,068	0,049	0,054	0,029	0,044	0,02
<b>F</b>	0,835	1,258	1,216	0,924	1,302	1,297	1,397	1,208	1,279	1,079	1,472
<b>PbO</b>	0	0,025	0,172	0,045	0	0,13	0,039	0,16	0	0,115	0,233
<b>ThO<sub>2</sub></b>	2,143	1,402	3,063	3,354	2,667	2,548	3,227	2,488	0,377	1,461	2,057
<b>SrO</b>	0	0	0,022	0	0,265	0,047	0,101	0	0,328	0	0,018
<b>ZrO<sub>2</sub></b>	0,558	0,611	0,682	0,514	0,546	0,661	0,648	0,674	0,728	0,692	0,661
<b>La<sub>2</sub>O<sub>3</sub></b>	13,615	6,165	15,401	15,115	11,473	13,968	12,303	13,88	24,919	14,068	13,949
<b>Ce<sub>2</sub>O<sub>3</sub></b>	41,502	22,572	44,052	44,292	42,417	42,402	40,289	42,353	41,191	41,549	42,501
<b>Pr<sub>2</sub>O<sub>3</sub></b>	3,129	1,557	2,724	2,738	3,167	2,877	3,011	3,043	1,754	2,758	2,945
<b>Nd<sub>2</sub>O<sub>3</sub></b>	11,501	5,807	10,058	10,486	11,69	10,66	12,834	11,015	4,682	10,421	10,697
<b>Sm<sub>2</sub>O<sub>3</sub></b>	2,091	1,149	1,583	1,505	2,184	2,013	2,532	2,224	0,386	1,748	2,013
<b>Eu<sub>2</sub>O<sub>3</sub></b>	0,474	0,245	0,471	0,385	0,604	0,394	0,55	0,525	0,232	0,476	0,536
<b>Gd<sub>2</sub>O<sub>3</sub></b>	0,403	0,208	0	0	0,299	0,603	0,876	0,644	0	0,55	0,212
<b>Tb<sub>2</sub>O<sub>3</sub></b>	0	0	0	0	0	0,143	0	0,101	0	0	0,104
<b>Dy<sub>2</sub>O<sub>3</sub></b>	0	0	0,078	0,175	0	0,546	0,529	0,624	0	0,386	0,473
<b>Ho<sub>2</sub>O<sub>3</sub></b>	0,065	0,039	0,116	0	0	0,182	0,146	0,138	0	0,219	0,42
<b>Er<sub>2</sub>O<sub>3</sub></b>	0,057	0,166	0,022	0,168	0,041	0,169	0,122	0,222	0,088	0,205	0,167
<b>Tm<sub>2</sub>O<sub>3</sub></b>	0,068	0	0,035	0,078	0	0,059	0,115	0,042	0,007	0,124	0,06
<b>Yb<sub>2</sub>O<sub>3</sub></b>	0,012	0	0	0,002	0	0	0,01	0,08	0	0,061	0,089
<b>Lu<sub>2</sub>O<sub>3</sub></b>	0	0	0,139	0,025	0	0,069	0	0	0	0,024	0,029

<b>Total</b>	112,031	69,536	105,566	104,839	103,433	104,546	104,12	106,797	102,8	103,917	105,312
<b>O=F</b>	<b>-0,352</b>	<b>-0,530</b>	<b>-0,512</b>	<b>-0,389</b>	<b>-0,548</b>	<b>-0,546</b>	<b>-0,588</b>	<b>-0,509</b>	<b>-0,539</b>	<b>-0,454</b>	<b>-0,620</b>
<b>Total</b>	111,679	69,006	105,054	104,450	102,885	104,000	103,532	106,288	102,261	103,463	104,692
<b>REE</b>	72,917	37,908	74,679	74,969	71,875	74,085	73,317	74,891	73,259	72,589	74,195
<b>REEY</b>	73,172	38,307	75,147	75,515	72,23	74,823	73,539	75,492	73,582	73,597	75,063
<b>LREE</b>	72,312	37,495	74,289	74,521	71,535	72,314	71,519	73,04	73,164	71,02	72,641
<b>HREE</b>	0,605	0,413	0,39	0,448	0,34	1,771	1,798	1,851	0,095	1,569	1,554
<b>HREEY</b>	0,86	0,812	0,858	0,994	0,695	2,509	2,02	2,452	0,418	2,577	2,422

Monazita- Greisen							Monazita – Granito greisenizado			
(%)	1A 1	1A 2	1A 3	1A 4	1A 5	1A 6	NC4B 1	NC4B 2	NC4B 3	NC7A 1
SiO <sub>2</sub>	0,392	0,495	0,875	0,228	0,592	0,183	0,284	0,243	0,728	1,903
Al <sub>2</sub> O <sub>3</sub>	0	0,013	0,002	0	0,034	0,003	0,056	0	0,086	1,048
FeO	0,147	0,093	0,193	0,255	0,454	0,596	0,801	0,122	0,196	0,911
CaO	0,633	0,128	0	0,218	0	0,275	0	0	0,253	0,117
Na <sub>2</sub> O	0	0	0	0	0	0	0	0	0	0,101
TiO <sub>2</sub>	0,06	0,03	0,151	0	0,603	0	0,054	0,175	0,182	0,078
MnO	0,046	0,082	0	0,095	0,053	0,066	0,082	0	0	0
K <sub>2</sub> O	0,008	0,009	0,012	0,026	0,06	0,014	0,085	0,004	0	0,965
P <sub>2</sub> O <sub>5</sub>	24,725	24,36	26,331	24,539	25,509	25,373	25,249	25,914	25,878	27,124
Nb <sub>2</sub> O <sub>5</sub>	0,019	0,233	0,073	0	0	0	0	0	0	0
HfO <sub>2</sub>	0	0	0,092	0,167	0,321	0,005	0,094	0,122	0	0,196
Y <sub>2</sub> O <sub>3</sub>	1,493	0,195	0,376	0,23	1,176	0,924	0,084	0,214	0,728	40,447
Ta <sub>2</sub> O <sub>5</sub>	0,235	0	0	0,086	0,358	0,05	0,15	0,037	0,131	0,088
UO <sub>2</sub>	0,219	0	0	0,019	0,175	0,159	0,011	0,041	0	0,553
BaO	0	0,063	0	0	0,025	0,057	0	0,051	0,064	0,007
F	1,19	1,289	1,658	1,344	1,135	1,044	1,711	1,32	0,948	1,534
PbO	0,13	0,178	0,139	0,005	0,029	0,109	0,102	0	0,133	0,026
ThO <sub>2</sub>	1,989	2,176	1,775	1,064	0,984	1,387	2,698	1,727	2,311	16,767
SrO	0	0	0	0,058	0	0,077	0,213	0,084	0,089	0
ZrO <sub>2</sub>	0,597	0,826	0,67	0,541	0,795	0,546	0,695	0,775	0,604	1,502
La <sub>2</sub> O <sub>3</sub>	13,34	8,346	11,809	12,345	12,688	12,035	11,867	13,687	11,771	0,06
Ce <sub>2</sub> O <sub>3</sub>	35,287	34,22	36,162	35,544	33,711	33,166	39,028	34,296	36,944	0,672
Pr <sub>2</sub> O <sub>3</sub>	2,437	3,553	2,834	2,677	2,585	2,466	3,379	3,212	3,229	0,009
Nd <sub>2</sub> O <sub>3</sub>	8,938	15,261	9,657	9,543	8,326	8,854	11,988	11,399	11,444	0,304
Sm <sub>2</sub> O <sub>3</sub>	1,698	2,683	1,136	1,759	1,663	1,901	1,818	1,6	1,714	0,125
Eu <sub>2</sub> O <sub>3</sub>	0,49	0,598	0,632	0,504	0,355	0,332	0,57	0,48	0,531	0,015
Gd <sub>2</sub> O <sub>3</sub>	1,128	1,149	0,542	1,034	1,001	1,139	0,482	0,731	0,92	0,396
Tb <sub>2</sub> O <sub>3</sub>	0,158	0	0	0	0	0	0	0	0	0
Dy <sub>2</sub> O <sub>3</sub>	0,458	0,195	0	0,163	0,779	0,669	0	0,321	0,084	1,398
Ho <sub>2</sub> O <sub>3</sub>	0,09	0,047	0	0	0,11	0,117	0,072	0,263	0,13	0,393
Er <sub>2</sub> O <sub>3</sub>	0,233	0,085	0,021	0,083	0,215	0,218	0,101	0,249	0,089	1,876
Tm <sub>2</sub> O <sub>3</sub>	0,093	0,077	0,02	0,192	0,001	0,066	0,118	0,096	0,071	0,347
Yb <sub>2</sub> O <sub>3</sub>	0,072	0,014	0	0	0,062	0	0	0,025	0,035	3,437
Lu <sub>2</sub> O <sub>3</sub>	0,057	0	0	0	0	0,06	0	0,014	0	0,614
REE	64,479	66,228	62,813	63,844	61,496	61,023	69,423	66,373	66,962	9,646
<b>Total</b>	<b>96,362</b>	<b>96,398</b>	<b>95,16</b>	<b>92,719</b>	<b>93,799</b>	<b>91,891</b>	<b>101,792</b>	<b>97,202</b>	<b>99,293</b>	<b>103,013</b>
<b>O=F</b>	<b>-0,501</b>	<b>-0,543</b>	<b>-0,698</b>	<b>-0,566</b>	<b>-0,478</b>	<b>-0,440</b>	<b>-0,721</b>	<b>-0,556</b>	<b>-0,399</b>	<b>-0,646</b>
<b>Total</b>	<b>95,861</b>	<b>95,855</b>	<b>94,462</b>	<b>92,153</b>	<b>93,321</b>	<b>91,451</b>	<b>101,071</b>	<b>96,646</b>	<b>98,894</b>	<b>102,367</b>
REEY	65,972	66,423	63,189	64,074	62,672	61,947	69,507	66,587	67,69	50,093
LREE	62,19	64,661	62,23	62,372	59,328	58,754	68,65	64,674	65,633	1,185
HREE	2,289	1,567	0,583	1,472	2,168	2,269	0,773	1,699	1,329	8,461
HREEY	3,782	1,762	0,959	1,702	3,344	3,193	0,857	1,913	2,057	48,908

## Xenotima

<b>Xenotima – Granito greisenizado</b>												
(%)	NC4B 4	NC7A 1	NC9 1	NC9 2	NC9 3	NC9 4	NC9 5	NC9 6	NC9 7	NC9 8	NC9 9	NC9 10
SiO <sub>2</sub>	0	1,903	0	0,034	0,037	0	0	0,005	0,058	1,869	0,05	1,12
Al <sub>2</sub> O <sub>3</sub>	0,005	1,048	0	0	0	0	0	0	0,789	6,693	0	6,193
FeO	0,859	0,911	0,118	0,585	1,441	0,042	0,166	0,269	0,189	2,638	0,482	11,678
CaO	0	0,117	0,06	0,142	0,018	0,312	0,4	0,505	0,22	0,58	0	0,407
Na <sub>2</sub> O	0	0,101	0	0,015	0	0	0	0	0	0	0	0
TiO <sub>2</sub>	0,123	0,078	0	0,012	0	0	0,121	0	0,2	0,097	0,024	0,048
MnO	0	0	0	0,174	0,042	0,018	0,074	0,074	0	0,011	0,104	0,078
K <sub>2</sub> O	0,007	0,965	0	0,06	0,036	0	0	0,036	0	0,028	0,038	0,029
P <sub>2</sub> O <sub>5</sub>	30,395	27,124	31,673	27,938	32,121	29,985	28,256	28,329	23,038	23,53	31,523	19,893
Nb <sub>2</sub> O <sub>5</sub>	0	0	0,063	0	0	0,107	0	0	0	0	0	0
HfO <sub>2</sub>	0	0,196	0,012	0,181	0,109	0	0,084	0	0	0	0,162	0,032
Y <sub>2</sub> O <sub>3</sub>	33,362	40,447	38,856	32,161	40,352	34,745	31,605	31,919	26,336	28,754	38,872	24,324
Ta <sub>2</sub> O <sub>5</sub>	0	0,088	0	0,128	0	0	0,048	0	0,166	0,173	0,025	0
UO <sub>2</sub>	0	0,553	0,431	0,592	0,282	0,33	0,315	0,288	0,343	0,56	0,312	0,364
BaO	0	0,007	0	0,055	0	0,034	0	0	0	0	0,004	0,019
F	0,219	1,534	0	0,287	0	0	0,127	0	0,379	0,676	0	1,216
PbO	0	0,026	0	0,203	0	0	0	0	0	0,031	0	0
ThO <sub>2</sub>	0,062	16,767	0,373	3,228	0,536	0,145	0,68	0,2	0,992	0,172	0,192	0,378
SrO	0	0	0	0	0,003	0,012	0,14	0,006	0	0	0,037	0,097
ZrO <sub>2</sub>	0,681	1,502	0,828	1,274	0,913	0,908	0,779	0,88	2,093	0,873	0,8	4,292
<b>Total</b>	<b>65,713</b>	<b>93,367</b>	<b>72,414</b>	<b>67,069</b>	<b>75,89</b>	<b>66,638</b>	<b>62,795</b>	<b>62,511</b>	<b>54,803</b>	<b>66,685</b>	<b>72,625</b>	<b>70,168</b>
La <sub>2</sub> O <sub>3</sub>	0	0,06	0,018	0	0,037	0	13,232	0,085	0	0	0,001	0
Ce <sub>2</sub> O <sub>3</sub>	0,056	0,672	0,051	0,304	0,056	0,121	37,869	0,184	0,055	0,184	0,12	0,189
Pr <sub>2</sub> O <sub>3</sub>	0,056	0,009	0	0,035	0,013	0,003	2,947	0,025	0	0,04	0	0
Nd <sub>2</sub> O <sub>3</sub>	0,016	0,304	0,081	0,013	0,169	0,133	11,721	0,14	0,063	0,446	0,016	0,05
Sm <sub>2</sub> O <sub>3</sub>	0,367	0,125	0	0	0,167	0,394	2,282	0,433	0,353	0,842	0,105	0
Eu <sub>2</sub> O <sub>3</sub>	0,019	0,015	0	0	0	0,003	0,512	0	0,07	0,004	0	0
Gd <sub>2</sub> O <sub>3</sub>	2,697	0,396	1,01	0,142	1,29	2,218	1,452	3,113	2,718	3,104	0,584	0,501
Tb <sub>2</sub> O <sub>3</sub>	0	0	0,238	0	0	0,523	0,029	0,4	0,2	0,243	0	0
Dy <sub>2</sub> O <sub>3</sub>	8,385	1,398	2,833	1,061	2,667	4,862	0,325	5,386	5,287	6,683	1,731	1,117
Ho <sub>2</sub> O <sub>3</sub>	1,593	0,393	0,883	0,657	0,755	1,388	0,061	1,066	1,228	1,606	0,423	0,296
Er <sub>2</sub> O <sub>3</sub>	4,486	1,876	3,508	2,9	3,067	4,213	0,284	3,201	3,373	5,335	1,357	0,831
Tm <sub>2</sub> O <sub>3</sub>	0,601	0,347	0,748	0,725	0,51	0,636	0,233	0,472	0,517	0,799	0,141	0,039

<b>Yb<sub>2</sub>O<sub>3</sub></b>	3,491	3,437	6,349	7,831	5,055	4,696	0,253	3,534	3,324	4,782	1,245	0,825
<b>Lu<sub>2</sub>O<sub>3</sub></b>	0,878	0,614	1,327	1,618	1,069	1,049	0,125	0,794	0,638	1,025	0,199	0,109
<b>Total</b>	<b>88,358</b>	<b>103,013</b>	<b>89,46</b>	<b>82,355</b>	<b>90,745</b>	<b>86,877</b>	<b>134,12</b>	<b>81,344</b>	<b>72,629</b>	<b>91,778</b>	<b>78,547</b>	<b>74,125</b>
<b>O=F</b>	<b>-0,092</b>	<b>-0,646</b>	<b>0,000</b>	<b>-0,121</b>	<b>0,000</b>	<b>0,000</b>	<b>-0,053</b>	<b>0,000</b>	<b>-0,160</b>	<b>-0,285</b>	<b>0,000</b>	<b>-0,512</b>
<b>Total</b>	<b>88,266</b>	<b>102,367</b>	<b>89,460</b>	<b>82,234</b>	<b>90,745</b>	<b>86,877</b>	<b>134,067</b>	<b>81,344</b>	<b>72,469</b>	<b>91,493</b>	<b>78,547</b>	<b>73,613</b>
<b>REE</b>	22,645	9,646	17,046	15,286	14,855	20,239	71,325	18,833	17,826	25,093	5,922	3,957
<b>REEY</b>	56,007	50,093	55,902	47,447	55,207	54,984	102,93	50,752	44,162	53,847	44,794	28,281
<b>LREE</b>	0,514	1,185	0,15	0,352	0,442	0,654	68,563	0,867	0,541	1,516	0,242	0,239
<b>HREE</b>	22,131	8,461	16,896	14,934	14,413	19,585	2,762	17,966	17,285	23,577	5,68	3,718
<b>HREEY</b>	55,493	48,908	55,752	47,095	54,765	54,33	34,367	49,885	43,621	52,331	44,552	28,042

## Oxifluoretos

### Oxifluoretos – Granito greisenizados

(%)	NC4B 1	NC4B 2	NC4B 3	NC4B 4	NC4B 5	NC4B 6	NC4B 7	NC4B 8	NC4B 9	NC4B 10	NC4B 11	NC4B 12	NC4B 13	NC4B 14	NC4B 15	NC4B 16	NC4B 17	NC4B 18	NC4B 19
F	7,449	5,8	6,369	5,99	4,952	4,883	6,152	5,708	7,935	8,31	8,177	8,763	5,954	7,409	4,687	6,183	7,473	6,496	8,155
SiO <sub>2</sub>	0,094	0,328	0,063	0,485	0,299	0,282	1,069	0,015	0,148	0	0,012	3,496	0,019	0,2	0,146	0,136	0,037	0,098	1,39
Al <sub>2</sub> O <sub>3</sub>	0,012	0,041	0	0,004	0,021	0,003	0,068	0	0,038	0,043	0,002	0,314	0,05	0,072	0,043	0,013	0	0,031	0,161
FeO	0,047	0,381	0,524	1,363	0,072	0,137	1,409	0,572	2,094	0,582	0,079	0,237	0,869	0,159	0,07	0,887	0,266	0	0,084
CaO	0,902	1,253	0,184	0,149	0,106	0,05	1,902	0	1,148	2,13	1,403	1,93	0,275	0,204	0,293	0,227	0,532	0,664	1,49
Na <sub>2</sub> O	0	0	0	0	0,011	0	0	0,001	0	0	0	0	0,015	0	0	0	0	0	0
TiO <sub>2</sub>	0,29	0,105	0,148	0,056	0,006	0,091	0,034	0	0	0	0	0	0	0,086	0	0	0	0,07	0,077
MnO	0,132	0,083	0,035	0,121	0,108	0,131	0	0	0	0,21	0,112	0,06	0	0,027	0,009	0,019	0,064	0,05	0
K <sub>2</sub> O	0,005	0,016	0,03	0,088	0,018	0,006	0	0,025	0,013	0,013	0	0,019	0,071	0,013	0,013	0,014	0,042	0,001	0,037
P <sub>2</sub> O <sub>5</sub>	0,016	0,156	0	0,058	0,03	0	0,321	0	7,336	0	0,049	6,005	0,086	0	0,033	0	0,042	0,007	6,278
Nb <sub>2</sub> O <sub>5</sub>	0	0,092	0	0	0,069	0,072	0,048	0	0	0	0	0,182	0,027	0,112	0,061	0,061	0,055	0,016	0
HfO <sub>2</sub>	0	0	0	0	0	0	0	0	0,186	0,055	0	0,233	0,065	0	0,062	0,048	0	0,014	0
Y <sub>2</sub> O <sub>3</sub>	0,268	0,243	0,289	0,308	0	0,386	1,311	0,297	0,424	0,902	0,705	9,48	0,135	1,479	5,362	0,281	1,885	0,324	1,923
Ta <sub>2</sub> O <sub>5</sub>	0,119	0	0	0	0	0,055	0,315	0	0,174	0	0,04	0,062	0,129	0,053	0	0,098	0,161	0	0,166
UO <sub>2</sub>	0,07	0,024	0	0,044	0	0,042	0,192	0,129	0,079	0,07	0,014	0,157	0,1	0	0	0,008	0,073	0,052	0
BaO	0,033	0,002	0,008	0	0,062	0,021	0,024	0	0,023	0,011	0,007	0,066	0	0	0	0	0	0,057	0,031
PbO	0	0,056	0	0	0,006	0,01	0,033	0,23	0,162	0	0	0,01	0,072	0	0	0,021	0	0	0
ThO <sub>2</sub>	2,628	2,846	1,189	1,143	0,289	0,511	6,718	8,025	2,54	3,569	0,256	2,253	3,429	2,041	0,623	0,846	2,33	2,248	2,546
SrO	0,359	0,303	0,129	0,14	0	0	0,217	0,465	0,325	0,33	0,1	0,167	0,575	0,184	0,096	0,034	0,129	0,39	0,149
ZrO <sub>2</sub>	0	0	0	0,62	0	0	1,142	0	0,155	0	0	9,198	0	0	0	0	0	0	1,651
La <sub>2</sub> O <sub>3</sub>	18,529	18,165	19,743	17,972	17,471	16,041	16,25	13,366	12,429	12,79	15,856	12,545	16,78	11,241	10,102	17,223	13,972	15,726	18,866
Ce <sub>2</sub> O <sub>3</sub>	41,632	40,987	39,775	39,159	41,129	39,573	34,476	37,749	34,646	31,933	38,823	26,19	39,247	33,196	30,09	40,46	37,735	39,378	37,624
Pr <sub>2</sub> O <sub>3</sub>	3,5	3,048	2,862	3,179	3,145	3,655	2,728	3,155	3,308	3,053	3,469	3,428	3,275	3,436	2,944	3,26	3,206	3,044	2,598
Nd <sub>2</sub> O <sub>3</sub>	12,265	10,778	10,053	12,164	11,115	15,166	9,576	11,641	14,09	13,227	15,126	12,957	12,986	15,123	13,552	12,801	12,554	11,154	9,803
Sm <sub>2</sub> O <sub>3</sub>	1,461	1,48	1,051	1,928	1,395	2,641	1,081	2,128	2,899	2,689	2,542	2,467	1,946	3,564	3,826	1,973	2,552	1,657	1,436
Eu <sub>2</sub> O <sub>3</sub>	0,56	0,583	0,468	0,492	0,613	0,546	0,504	0,526	0,553	0,453	0,605	0,661	0,526	0,589	0,421	0,52	0,549	0,392	0,399
Gd <sub>2</sub> O <sub>3</sub>	0,429	0,032	0	0,36	0,109	1,618	0,262	0,768	1,409	1,519	1,596	1,233	0,737	3,81	4,444	0,578	1,641	0,493	0,52
Tb <sub>2</sub> O <sub>3</sub>	0,08	0	0	0	0	0,025	0	0	0	0	0,113	0	0	0,31	0,505	0	0	0,061	0
Dy <sub>2</sub> O <sub>3</sub>	0	0	0	0	0,099	0,238	0,125	0	0,094	0,137	0,293	0,737	0	1,373	3,033	0	0,488	0	0
Ho <sub>2</sub> O <sub>3</sub>	0,146	0,106	0,122	0	0,005	0,21	0,286	0	0	0,058	0,213	0,229	0,01	0,187	0,399	0,242	0,022	0	0,029
Er <sub>2</sub> O <sub>3</sub>	0,111	0,011	0,107	0	0,123	0,118	0,141	0,078	0,178	0,079	0,116	0,311	0,036	0,197	0,391	0,059	0,078	0,027	0,097
Tm <sub>2</sub> O <sub>3</sub>	0,052	0,05	0	0,058	0,116	0,034	0,03	0,044	0,051	0,137	0,112	0,063	0,07	0,224	0,129	0,081	0,092	0,106	0
Yb <sub>2</sub> O <sub>3</sub>	0,069	0	0,052	0	0	0	0	0	0	0	0,033	0,296	0	0	0,05	0	0,014	0	0,077

<b>Lu<sub>2</sub>O<sub>3</sub></b>	0,036	0	0	0	0	0	0,044	0	0	0,05	0,027	0,112	0,095	0,09	0,092	0	0,015	0,02	0
<b>Total</b>	91,294	86,969	83,201	85,881	81,369	86,545	86,458	84,922	92,437	82,35	89,88	103,861	87,579	85,379	81,476	86,073	86,007	82,576	95,587
<b>O=F</b>	<b>-3,137</b>	<b>-2,442</b>	<b>-2,682</b>	<b>-2,522</b>	<b>-2,085</b>	<b>-2,056</b>	<b>-2,591</b>	<b>-2,404</b>	<b>-3,341</b>	<b>-3,499</b>	<b>-3,443</b>	<b>-3,690</b>	<b>-2,507</b>	<b>-3,120</b>	<b>-1,974</b>	<b>-2,604</b>	<b>-3,147</b>	<b>-2,735</b>	<b>-3,434</b>
<b>Total</b>	88,157	84,527	80,519	83,359	79,284	84,489	83,867	82,518	89,096	78,851	86,437	100,171	85,072	82,259	79,502	83,469	82,860	79,841	92,153
<b>REE</b>	78,87	75,24	74,233	75,312	75,32	79,865	65,503	69,455	69,657	66,125	78,924	61,229	75,708	73,34	69,978	77,197	72,918	72,058	71,449
<b>REYY</b>	79,138	75,483	74,522	75,62	75,32	80,251	66,814	69,752	70,081	67,027	79,629	70,709	75,843	74,819	75,34	77,478	74,803	72,382	73,372
<b>LREE</b>	77,947	75,041	73,952	74,894	74,868	77,622	64,615	68,565	67,925	64,145	76,421	58,248	74,76	67,149	60,935	76,237	70,568	71,351	70,726
<b>HREE</b>	0,923	0,199	0,281	0,418	0,452	2,243	0,888	0,89	1,732	1,98	2,503	2,981	0,948	6,191	9,043	0,96	2,35	0,707	0,723
<b>HREYY</b>	1,191	0,442	0,57	0,726	0,452	2,629	2,199	1,187	2,156	2,882	3,208	12,461	1,083	7,67	14,405	1,241	4,235	1,031	2,646

### Oxifluoreto – Granito greisenizado

(%)	NC7A 1	NC7A 2	NC7A 3	NC7A 4	NC7A 5	NC7A 6	NC7A 7
F	4,765	5,713	8,52	9,215	5,98	6,702	8,534
SiO <sub>2</sub>	4,237	12,911	1,72	0	0,054	0,077	0
Al <sub>2</sub> O <sub>3</sub>	0,31	0,397	0,332	0,102	0	0	0,028
FeO	1,476	2,605	7,465	1,497	0,006	0,215	0,037
CaO	1,792	0,507	3,218	3,008	0,329	0,346	2,305
Na <sub>2</sub> O	0	0	0,07	0,107	0	0,029	0
TiO <sub>2</sub>	7,789	0	0,189	0	0,072	0	0,06
MnO	0	0,002	0,058	0,077	0	0	0,041
K <sub>2</sub> O	0,013	0,057	0,122	0,088	0,02	0,074	0,041
P <sub>2</sub> O <sub>5</sub>	0	3,029	0,087	0	0,036	0	0
Nb <sub>2</sub> O <sub>5</sub>	20,133	1,097	0,344	0	0	0	0
HfO <sub>2</sub>	0	0,121	0	0,045	0,04	0	0
Y <sub>2</sub> O <sub>3</sub>	18,325	15,194	15,27	27,626	0,3	1,024	11,301
Ta <sub>2</sub> O <sub>5</sub>	1,579	0,148	0,144	0	0	0,022	0,054
UO <sub>2</sub>	0,347	1,72	0,063	0,037	0	0	0,007
BaO	0,125	0,046	0,093	0	0,048	0,046	0,097
PbO	0,025	0	0,068	0	0	0	0
ThO <sub>2</sub>	2,602	25,2	3,311	3,103	0,83	0,659	1,315
SrO	0,072	0	0,094	0,149	0	0	0,129
ZrO <sub>2</sub>	0,329	5,968	0	0	0	0	0,026
La <sub>2</sub> O <sub>3</sub>	2,473	0,024	5,647	3,055	15,912	17,337	6,461
Ce <sub>2</sub> O <sub>3</sub>	6,724	0,332	12,524	7,349	25,855	26,23	15,937
Pr <sub>2</sub> O <sub>3</sub>	0,818	0,014	1,792	0,88	3,099	3,355	2,261
Nd <sub>2</sub> O <sub>3</sub>	3,184	0,174	6,747	3,885	10,582	11,207	10,153
Sm <sub>2</sub> O <sub>3</sub>	1,14	0,088	1,899	1,493	1,241	1,313	3,325
Eu <sub>2</sub> O <sub>3</sub>	0,109	0,049	0,286	0,054	0,442	0,425	0,291
Gd <sub>2</sub> O <sub>3</sub>	1,252	0,237	1,661	2,552	0	0	3,184
Tb <sub>2</sub> O <sub>3</sub>	0	0	0	0	0	0	0,927
Dy <sub>2</sub> O <sub>3</sub>	4,292	1,528	3,468	5,245	0,051	0	5,183
Ho <sub>2</sub> O <sub>3</sub>	0,639	0,538	0,486	0,845	0,134	0,073	0,767
Er <sub>2</sub> O <sub>3</sub>	2,629	2,274	1,453	2,536	0	0,056	1,568
Tm <sub>2</sub> O <sub>3</sub>	0,465	0,627	0,11	0,313	0,122	0,027	0,316
Yb <sub>2</sub> O <sub>3</sub>	2,519	4,632	0,987	1,386	0,043	0,05	0,879
Lu <sub>2</sub> O <sub>3</sub>	0,578	0,821	0,31	0,482	0,014	0,013	0,545
<b>Total</b>	<b>90,741</b>	<b>86,053</b>	<b>78,538</b>	<b>75,129</b>	<b>65,21</b>	<b>69,28</b>	<b>75,772</b>
<b>O≡F</b>	<b>-2,007</b>	<b>-2,406</b>	<b>-3,588</b>	<b>-3,880</b>	<b>-2,518</b>	<b>-2,822</b>	<b>-3,594</b>
<b>Total</b>	<b>88,734</b>	<b>83,647</b>	<b>74,950</b>	<b>71,249</b>	<b>62,692</b>	<b>66,458</b>	<b>72,178</b>
<b>REE</b>	<b>26,822</b>	<b>11,338</b>	<b>37,37</b>	<b>30,075</b>	<b>57,495</b>	<b>60,086</b>	<b>51,797</b>
<b>REEY</b>	<b>26,822</b>	<b>11,459</b>	<b>37,37</b>	<b>30,12</b>	<b>57,535</b>	<b>60,086</b>	<b>51,797</b>
<b>LREE</b>	<b>14,448</b>	<b>0,681</b>	<b>28,895</b>	<b>16,716</b>	<b>57,131</b>	<b>59,867</b>	<b>38,428</b>
<b>HREE</b>	<b>12,374</b>	<b>10,657</b>	<b>8,475</b>	<b>13,359</b>	<b>0,364</b>	<b>0,219</b>	<b>13,369</b>
<b>HREEY</b>	<b>12,374</b>	<b>10,778</b>	<b>8,475</b>	<b>13,404</b>	<b>0,404</b>	<b>0,219</b>	<b>13,369</b>

## Fluorita

<b>Fluorita – Granito greisenizado</b>		
(%)	N4B 1	NC7A 1
F	38,202	48,497
SiO <sub>2</sub>	0,189	0,106
Al <sub>2</sub> O <sub>3</sub>	0,008	0
FeO	0,049	0
CaO	38,206	71,342
Na <sub>2</sub> O	0	0,006
TiO <sub>2</sub>	0,037	0,132
MnO	0	0,116
K <sub>2</sub> O	0,008	0
P <sub>2</sub> O <sub>5</sub>	0	0,071
Nb <sub>2</sub> O <sub>5</sub>	0	0
HfO <sub>2</sub>	0	0,203
Y <sub>2</sub> O <sub>3</sub>	0,514	1,207
Ta <sub>2</sub> O <sub>5</sub>	0	0
UO <sub>2</sub>	0	0
BaO	0,014	0,012
PbO	0	0
ThO <sub>2</sub>	1,407	0
SrO	0,203	0,078
ZrO <sub>2</sub>	0	0
La <sub>2</sub> O <sub>3</sub>	8,824	0
Ce <sub>2</sub> O <sub>3</sub>	26,284	0,02
Pr <sub>2</sub> O <sub>3</sub>	2,666	0
Nd <sub>2</sub> O <sub>3</sub>	11,918	0,017
Sm <sub>2</sub> O <sub>3</sub>	3,165	0,039
Eu <sub>2</sub> O <sub>3</sub>	0,362	0
Gd <sub>2</sub> O <sub>3</sub>	3,132	0
Tb <sub>2</sub> O <sub>3</sub>	0,178	0,057
Dy <sub>2</sub> O <sub>3</sub>	1,037	0
Ho <sub>2</sub> O <sub>3</sub>	0,108	0
Er <sub>2</sub> O <sub>3</sub>	0,063	0,052
Tm <sub>2</sub> O <sub>3</sub>	0,151	0,022
Yb <sub>2</sub> O <sub>3</sub>	0	0,235
Lu <sub>2</sub> O <sub>3</sub>	0,179	0,117
<b>Total</b>	<b>120,819</b>	<b>101,905</b>
<b>O=F</b>	<b>-16,087</b>	<b>-20,422</b>
<b>Total</b>	<b>104,732</b>	<b>81,483</b>
REE	58,067	0,559
REEY	58,581	1,766
LREE	53,219	0,076
HREE	4,848	0,483
HREEY	5,362	1,69

## **ANEXOS -3**

### **Minerais em áreas próximo a Faixa Placha**

## Próximo a Faixa Placha

### Zircão – Biotita granito

(%)	NC10A 1	NC10A 2	NC10A 3	NC10A 4	NC10A 5	NC10A 6	NC10A 7	NC10A 8	NC10A 9	NC10A 10	NC10A 11	NC10A 12	NC10A 13	NC10A 14	NC10A 15	NC10A 16	NC10A 17	NC10A 18	NC10A 19
SiO <sub>2</sub>	24,557	25,4	26,52	24,553	24,105	28,674	28,599	29,473	30,476	29,706	29,868	29,907	29,941	30,147	25,96	29,395	30	30,18	24,522
Al <sub>2</sub> O <sub>3</sub>	0,433	0,029	0,027	0,291	2,631	0,018	0,223	0,016	0	0,172	0	0,016	0	0,028	0,335	0,052	0,035	0,009	1,593
FeO	0,349	0,605	0,406	5,55	1,359	0,38	1,032	0	0,069	0,841	0,035	0,033	0	0,038	0,313	0,46	0	0,04	1,988
CaO	0,324	0,073	0,024	0,885	1,022	0,567	0,332	0	0	0	0,251	0	0,451	0,137	0,268	0,177	0	0,117	0,848
Na <sub>2</sub> O	0,002	0	0,033	0,03	0,006	0,06	0,04	0,018	0,018	0,083	0,027	0,018	0	0,019	0,026	0,113	0,021	0,023	0,036
TiO <sub>2</sub>	0,029	0	0,25	0,029	0,088	0	0	0	0	0	0,128	0,111	0	0,064	0	0	0	0,064	0
MnO	0	0,027	0,04	0,109	0	0,073	0,099	0,011	0	0,022	0,042	0	0	0,112	0,038	0,014	0	0,098	0
K <sub>2</sub> O	0,005	0,018	0,011	0,052	0	0,014	0,085	0	0,006	0,023	0	0	0,002	0,004	0,009	0,008	0,149	0,002	0,009
P <sub>2</sub> O <sub>5</sub>	0,505	0,127	0,021	0,015	0,482	0,047	0,089	0,1	0,094	0,083	0	0,084	0,086	0	0,306	0,042	0,037	0,037	0,303
Nb <sub>2</sub> O <sub>5</sub>	0,293	0,736	0,28	0,094	0,77	0,3	0,093	0,529	0,102	0,814	0,585	0,053	0,43	0,479	0,373	0,342	0,391	0,573	0,03
HfO <sub>2</sub>	1,53	2,186	1,64	1,361	1,631	1,286	1,944	1,519	1,006	1,109	0,952	0,763	1,371	1,255	0,883	1,796	1,092	1,369	1,819
Y <sub>2</sub> O <sub>3</sub>	0,591	0,26	0,288	1,769	3,212	0,459	0,503	0,009	0,269	0,586	0,042	0,075	0,043	0,2	0,839	0,156	0,195	0,252	2,987
Ta <sub>2</sub> O <sub>5</sub>	0	0,275	0	0,123	0	0	0	0,07	0,033	0	0	0,174	0	0,273	0	0	0	0,392	0,083
UO <sub>2</sub>	0	0	0	0,216	0	0,025	0,354	0	0	0,024	0	0	0	0	0	0	0	0	0,012
BaO	0,04	0,014	0	0,021	0,113	0,014	0,064	0	0,005	0,004	0	0	0	0,03	0,033	0	0,04	0,012	0,058
F	0,088	0	0	0,196	0,646	0	0	0	0	0	0	0	0	0	0,001	0	0	0	0,603
PbO	0	0	0	0	0	0	0	0	0	0	0	0	0	0	0	0	0	0	0
ThO <sub>2</sub>	0,038	0,031	0	0,177	0,111	0,054	0,256	0,011	0,048	0,017	0	0	0	0,013	0	0,058	0,069	0	0,094
SrO	0,12	0,096	0,148	0,183	0,141	0,137	0,156	0,13	0,149	0,111	0,096	0,131	0,2	0,183	0,13	0,177	0,15	0,126	0,148
ZrO <sub>2</sub>	51,591	54,568	56,369	46,618	45,745	57,58	55,388	59,368	59,139	57,829	61,299	60,657	60,423	60,458	55,011	57,353	59,649	61,138	47,606
<b>Total</b>	<b>80,495</b>	<b>84,445</b>	<b>85,807</b>	<b>82,493</b>	<b>82,003</b>	<b>89,776</b>	<b>89,257</b>	<b>91,254</b>	<b>91,414</b>	<b>91,424</b>	<b>93,197</b>	<b>92,039</b>	<b>93,058</b>	<b>93,264</b>	<b>84,663</b>	<b>90,167</b>	<b>91,842</b>	<b>94,334</b>	<b>82,837</b>
La <sub>2</sub> O <sub>3</sub>	0	0,042	0,021	0,038	0,04	0,033	0,049	0,021	0,006	0,024	0,044	0	0,029	0,005	0	0,005	0,595	0,022	0,053
Ce <sub>2</sub> O <sub>3</sub>	0,085	0,119	0,047	0	0,338	0,021	0,059	0,047	0,071	0,06	0,036	0,05	0,051	0,035	0,049	0,098	1,655	0,053	0,249
Pr <sub>2</sub> O <sub>3</sub>	0	0,028	0,013	0,034	0,028	0	0,024	0	0,023	0	0	0	0	0	0	0	0,169	0	0
Nd <sub>2</sub> O <sub>3</sub>	0	0	0,005	0,056	0,16	0,006	0	0,021	0,014	0,025	0	0,001	0,013	0,014	0	0	0,59	0,026	0,126
Sm <sub>2</sub> O <sub>3</sub>	0	0,022	0,03	0	0,05	0	0	0,03	0	0	0,091	0,017	0,054	0	0	0,01	0,124	0	0,013
Eu <sub>2</sub> O <sub>3</sub>	0,014	0,051	0,049	0	0	0,003	0	0,003	0	0	0	0,039	0	0,107	0	0	0	0	0,099
Gd <sub>2</sub> O <sub>3</sub>	0	0,008	0	0,038	0,145	0,004	0,04	0	0	0,024	0	0	0,068	0,007	0	0	0,105	0	0,151
Tb <sub>2</sub> O <sub>3</sub>	0	0	0	0	0	0	0	0	0	0	0	0	0,055	0,008	0,021	0	0	0	0
Dy <sub>2</sub> O <sub>3</sub>	0	0	0	0	0,379	0,069	0	0	0	0,073	0	0,022	0,04	0	0	0	0	0	0,253

<b>Ho<sub>2</sub>O<sub>3</sub></b>	0,081	0	0,037	0,088	0,061	0,105	0,086	0	0,07	0,026	0	0,046	0,022	0	0,122	0	0,105	0	0
<b>Er<sub>2</sub>O<sub>3</sub></b>	0	0,048	0	0,2	0,421	0,01	0,119	0,036	0,04	0,037	0	0,05	0	0,054	0	0	0,039	0	0,36
<b>Tm<sub>2</sub>O<sub>3</sub></b>	0	0,02	0	0,006	0,087	0	0	0	0	0	0	0	0,035	0	0	0,036	0	0	0
<b>Yb<sub>2</sub>O<sub>3</sub></b>	0	0,044	0,07	0,135	0,643	0,091	0,167	0	0,044	0,037	0	0	0,01	0	0	0,031	0,039	0,041	0,617
<b>Lu<sub>2</sub>O<sub>3</sub></b>	0	0,066	0,011	0,023	0,07	0	0	0	0	0	0	0,013	0,008	0	0,016	0	0	0	0,128
<b>REE</b>	0,18	0,448	0,283	0,618	2,422	0,342	0,544	0,158	0,268	0,306	0,171	0,238	0,385	0,23	0,208	0,18	3,421	0,142	2,049
<b>REEY</b>	0,771	0,708	0,571	2,387	5,634	0,801	1,047	0,167	0,537	0,892	0,213	0,313	0,428	0,43	1,047	0,336	3,616	0,394	5,036
<b>LREE</b>	0,099	0,262	0,165	0,128	0,616	0,063	0,132	0,122	0,114	0,109	0,171	0,107	0,147	0,161	0,049	0,113	3,133	0,101	0,54
<b>HREE</b>	0,081	0,186	0,118	0,49	1,806	0,279	0,412	0,036	0,154	0,197	0	0,131	0,238	0,069	0,159	0,067	0,288	0,041	1,509
<b>HREEY</b>	0,672	0,446	0,406	2,259	5,018	0,738	0,915	0,045	0,423	0,783	0,042	0,206	0,281	0,269	0,998	0,223	0,483	0,293	4,496

Continuação...

(%)	NC10A 20	NC10A 21	NC10A 22	NC10A 23	NC10A 24	NC10A 25	NC10A 26	NC10A 27	NC10A 28	NC10A 29	NC10A 30	NC10A 31	NC10A 32	NC10A 33	NC10A 34
<b>SiO<sub>2</sub></b>	29,499	29,447	30,715	30,84	30,662	29,093	29,516	30,662	30,324	30,243	30,998	30,497	30,593	30,666	30,594
<b>Al<sub>2</sub>O<sub>3</sub></b>	0,049	0,34	0,013	0	0	0,027	0,03	0,03	0,036	0	0	0	0	0,003	0,015
<b>FeO</b>	0,858	0,38	0,018	0,035	0,088	0,077	0,308	0,025	0	0,002	0	0	0,012	0	0,155
<b>CaO</b>	0,122	0,049	0,026	0,113	0,029	0,264	0,188	0	0	0,023	0,01	0	0	0	0
<b>Na<sub>2</sub>O</b>	0,08	0,059	0	0,026	0,016	0,029	0,025	0	0,012	0,001	0,001	0,011	0,026	0	0,013
<b>TiO<sub>2</sub></b>	0	0,012	0,281	0	0,059	0,065	0,111	0	0	0,052	0,094	0,088	0	0	0,064
<b>MnO</b>	0	0,076	0	0,043	0	0	0,102	0	0	0	0	0,04	0	0,183	0,001
<b>K<sub>2</sub>O</b>	0	0,012	0	0,004	0,008	0,009	0,002	0,009	0	0	0,002	0,002	0,003	0	0,006
<b>P<sub>2</sub>O<sub>5</sub></b>	0,156	0,27	0,021	0	0,03	0,182	0,036	0	0,089	0	0,102	0,064	0,061	0,084	0,069
<b>Nb<sub>2</sub>O<sub>5</sub></b>	0,43	0,457	0,362	0,412	0,319	0,16	0,252	0,306	0,21	0,445	0,704	0,353	0,24	0,211	0
<b>HfO<sub>2</sub></b>	2,406	2,137	1,495	1,217	1,332	0,952	1,264	1,128	1,038	1,083	0,862	1,74	1,195	1,23	1,385
<b>Y<sub>2</sub>O<sub>3</sub></b>	0,188	0,61	0,188	0,085	0,117	0,654	0,405	0,034	0,027	0,098	0,065	0	0,048	0,233	0,259
<b>Ta<sub>2</sub>O<sub>5</sub></b>	0	0,022	0	0,06	0,012	0	0,046	0,024	0,391	0	0,094	0,121	0,152	0,132	0
<b>UO<sub>2</sub></b>	0,064	0,046	0	0	0	0	0	0	0	0	0	0	0	0	0
<b>BaO</b>	0,002	0	0	0	0	0,041	0	0	0,024	0	0,023	0	0	0,007	0
<b>F</b>	0	0	0	0	0	0	0	0	0	0	0	0	0	0	0
<b>PbO</b>	0	0	0	0	0	0	0	0	0	0	0	0	0	0	0
<b>ThO<sub>2</sub></b>	0,014	0,074	0	0	0,008	0,081	0	0	0	0,026	0,011	0,003	0	0,027	0,075
<b>SrO</b>	0,087	0,117	0,136	0,197	0,154	0,072	0,034	0,141	0,097	0,147	0,106	0,089	0,073	0,139	0,106
<b>ZrO<sub>2</sub></b>	56,778	56,71	60,531	61,318	60,386	56,487	57,308	59,667	60,874	61,089	61,454	61,247	62,857	61,874	59,545
<b>Total</b>	90,733	90,818	93,786	94,35	93,22	88,193	89,627	92,026	93,122	93,209	94,526	94,255	95,26	94,789	92,287
<b>La<sub>2</sub>O<sub>3</sub></b>	0,009	0,004	0	0,009	0	0	0	0	0,024	0,021	0	0	0	0	0,003
<b>Ce<sub>2</sub>O<sub>3</sub></b>	0	0,055	0,035	0,057	0	0,01	0	0	0	0,045	0,022	0,005	0,012	0,059	0,035
<b>Pr<sub>2</sub>O<sub>3</sub></b>	0,086	0,049	0,005	0,032	0	0	0	0,01	0	0,004	0	0	0	0,023	0,028

<b>Nd<sub>2</sub>O<sub>3</sub></b>	0	0,026	0,019	0	0,026	0,006	0,018	0	0	0,002	0	0,004	0	0	0
<b>Sm<sub>2</sub>O<sub>3</sub></b>	0,006	0	0,075	0,012	0	0	0	0	0,108	0	0,038	0,031	0	0,005	0
<b>Eu<sub>2</sub>O<sub>3</sub></b>	0,014	0,049	0,046	0,067	0,065	0	0	0,014	0,016	0	0,011	0	0,04	0,009	0
<b>Gd<sub>2</sub>O<sub>3</sub></b>	0	0,009	0,018	0,02	0,042	0,029	0	0	0	0	0,058	0,016	0,032	0	0,072
<b>Tb<sub>2</sub>O<sub>3</sub></b>	0	0	0,012	0	0,012	0	0	0	0	0,026	0	0,029	0,006	0	0
<b>Dy<sub>2</sub>O<sub>3</sub></b>	0	0	0	0	0	0,077	0	0	0,002	0,002	0	0	0	0	0
<b>Ho<sub>2</sub>O<sub>3</sub></b>	0	0,002	0,04	0,043	0	0,07	0	0,041	0,042	0,07	0	0	0	0,05	0
<b>Er<sub>2</sub>O<sub>3</sub></b>	0,028	0,117	0,122	0,071	0,063	0,115	0,089	0,072	0,029	0,038	0,031	0,027	0,011	0,003	0
<b>Tm<sub>2</sub>O<sub>3</sub></b>	0	0	0	0	0	0,027	0,006	0,024	0,026	0	0	0	0	0	0
<b>Yb<sub>2</sub>O<sub>3</sub></b>	0,028	0,148	0	0	0	0,051	0,053	0,045	0	0,019	0	0	0	0	0
<b>Lu<sub>2</sub>O<sub>3</sub></b>	0	0,081	0	0,015	0	0,004	0	0	0	0	0,046	0	0,033	0,016	0
<b>REE</b>	0,171	0,54	0,372	0,326	0,208	0,389	0,166	0,206	0,247	0,227	0,206	0,112	0,134	0,165	0,138
<b>REEY</b>	0,359	1,15	0,56	0,411	0,325	1,043	0,571	0,24	0,274	0,325	0,271	0,112	0,182	0,398	0,397
<b>LREE</b>	0,115	0,183	0,18	0,177	0,091	0,016	0,018	0,024	0,148	0,072	0,071	0,04	0,052	0,096	0,066
<b>HREE</b>	0,056	0,357	0,192	0,149	0,117	0,373	0,148	0,182	0,099	0,155	0,135	0,072	0,082	0,069	0,072
<b>HREEY</b>	0,244	0,967	0,38	0,234	0,234	1,027	0,553	0,216	0,126	0,253	0,2	0,072	0,13	0,302	0,331

**Zircão – Biotita granito**

(%)	NC3A 1	NC3A 2	NC3A 3	NC3A 4	NC3A 5	NC3A 6	NC3A 7	NC3A 8	NC3A 9	NC3A 10	NC3A 11	NC3A 12	NC3A 13	NC3A 14	NC3A 15	NC3A 16
<b>SiO<sub>2</sub></b>	29,013	29,552	23,361	24,186	29,335	26,052	27,03	27,227	26,113	29,927	22,437	24,652	29,885	26,606	27,907	26,169
<b>Al<sub>2</sub>O<sub>3</sub></b>	0,022	0	1,336	1,653	0	0,126	0,126	0,119	0,13	0,013	0,963	0,214	0,029	0,411	0,152	0,215
<b>FeO</b>	0,003	0	0,832	0,765	0,034	0,833	0,594	0,509	1,146	0	1,236	0,895	0,026	0,992	0,915	1,019
<b>CaO</b>	0,066	0	0,325	0,662	0,187	0,732	0,222	0,635	0,741	0	0,717	1,137	0,143	0,719	0	1,584
<b>Na<sub>2</sub>O</b>	0,017	0,002	0,023	0	0,013	0,092	0,117	0,092	0,053	0,001	0,002	0,061	0	0,023	0,095	0,013
<b>TiO<sub>2</sub></b>	0,006	0,117	0,216	0,006	0	0,023	0,064	0	0,117	0	0	0,123	0	0	0,076	0,14
<b>MnO</b>	0	0	0,243	0,334	0	0,266	0,153	0	0,376	0	0,17	0,512	0,009	0,278	0,176	0,654
<b>K<sub>2</sub>O</b>	0,01	0,002	0,036	0,028	0,007	0,014	0,047	0,009	0,031	0	0,003	0,038	0,002	0,082	0,004	0,013
<b>P<sub>2</sub>O<sub>5</sub></b>	0,081	0,094	0,638	0,406	0,073	0,4	0,116	0,258	0,178	0,116	0,65	0,662	0,052	0,973	0,133	0,188
<b>Nb<sub>2</sub>O<sub>5</sub></b>	0,426	0,313	0,076	0,982	0,411	0,421	0,083	0,365	0,334	0,473	1,351	0,304	0,486	0,452	0,541	0,208
<b>HfO<sub>2</sub></b>	0,948	1,053	1,118	1,008	0,998	2,462	1,494	3,282	1,064	1,1	1,415	1,537	0,849	2	1,924	3,195
<b>Y<sub>2</sub>O<sub>3</sub></b>	0,102	0,152	6,436	5,712	0,048	0,851	1,208	0,859	1,168	0,032	6,923	2,603	0,322	2,51	0,743	1,445
<b>Ta<sub>2</sub>O<sub>5</sub></b>	0	0	0	0,023	0,043	0,251	0,058	0	0	0,163	0,251	0	0	0,239	0,01	0,086
<b>UO<sub>2</sub></b>	0	0	0,382	0,355	0	0,233	0,252	0,12	0,327	0	0,305	0,253	0	0,282	0,182	0,746
<b>BaO</b>	0,005	0,019	0,011	0	0,006	0	0	0	0	0,027	0,025	0,031	0	0,013	0,001	0,027
<b>F</b>	0	0	1,353	1,773	0	0,14	0,045	0,148	0,204	0	2,415	0,655	0	0,086	0,09	0,436
<b>PbO</b>	0	0	0,308	0,24	0	0	0	0	0	0	0	0	0	0	0	0
<b>ThO<sub>2</sub></b>	0	0,004	0,358	0,353	0	0,075	0,258	0,061	0,273	0,044	0,581	0,233	0,038	0,159	0,059	0,129
<b>SrO</b>	0,078	0,068	0,154	0,015	0,116	0,191	0,042	0,081	0,152	0,09	0,105	0,175	0,169	0,18	0,144	0,14
<b>ZrO<sub>2</sub></b>	60,927	62,142	45,237	48,063	61,276	53,236	56,668	56,288	52,74	60,05	41,42	49,061	60,976	48,238	52,291	49,082
<b>Total</b>	91,704	93,518	82,443	86,564	92,547	86,398	88,577	90,053	85,147	92,036	80,969	83,146	92,986	84,243	85,443	85,489
<b>La<sub>2</sub>O<sub>3</sub></b>	0	0,007	0,003	0	0	0,048	0,012	0	0,049	0	0,028	0	0	0	0,005	0
<b>Ce<sub>2</sub>O<sub>3</sub></b>	0,038	0	0,057	0,084	0,013	0,021	0,029	0,057	0	0,055	0,221	0,017	0,05	0,067	0,031	0,057
<b>Pr<sub>2</sub>O<sub>3</sub></b>	0	0	0	0,042	0	0	0,021	0	0,026	0	0,095	0	0	0,019	0	0
<b>Nd<sub>2</sub>O<sub>3</sub></b>	0	0	0	0,017	0,004	0,017	0	0	0	0	0,09	0,014	0,019	0	0	0
<b>Sm<sub>2</sub>O<sub>3</sub></b>	0	0	0	0,026	0,007	0	0,003	0	0	0,123	0,03	0	0,055	0	0	0
<b>Eu<sub>2</sub>O<sub>3</sub></b>	0	0,036	0	0	0	0,005	0	0	0,008	0	0,01	0,01	0	0	0,044	0,074
<b>Gd<sub>2</sub>O<sub>3</sub></b>	0	0,015	0,053	0,081	0	0	0,109	0,007	0,005	0,024	0,137	0,034	0	0,074	0	0
<b>Tb<sub>2</sub>O<sub>3</sub></b>	0,017	0	0	0	0	0	0	0	0	0	0	0	0	0	0	0
<b>Dy<sub>2</sub>O<sub>3</sub></b>	0	0	0,278	0,162	0,025	0	0,149	0	0	0,017	0,593	0,061	0	0	0,115	0
<b>Ho<sub>2</sub>O<sub>3</sub></b>	0	0	0,117	0,369	0	0,009	0,088	0	0	0	0,111	0,046	0	0,057	0,132	0
<b>Er<sub>2</sub>O<sub>3</sub></b>	0,054	0,033	0,824	0,749	0,078	0,129	0,367	0,102	0,161	0,008	0,882	0,224	0,044	0,213	0,267	0,353

<b>Tm<sub>2</sub>O<sub>3</sub></b>	0,003	0	0,101	0,156	0	0	0,038	0	0	0	0,214	0,023	0	0	0,085	0,058
<b>Yb<sub>2</sub>O<sub>3</sub></b>	0	0	1,729	1,489	0	0,093	0,677	0,093	0,226	0,055	1,702	0,323	0,048	0,756	0,375	0,465
<b>Lu<sub>2</sub>O<sub>3</sub></b>	0	0,015	0,294	0,221	0,023	0,017	0,098	0,013	0	0	0,261	0,07	0,009	0,205	0	0,124
<b>REE</b>	0,112	0,106	3,456	3,396	0,15	0,339	1,591	0,272	0,475	0,282	4,374	0,822	0,225	1,391	1,054	1,131
<b>REEY</b>	0,214	0,258	9,892	9,108	0,198	1,19	2,799	1,131	1,643	0,314	11,297	3,425	0,547	3,901	1,797	2,576
<b>LREE</b>	0,038	0,043	0,06	0,169	0,024	0,091	0,065	0,057	0,083	0,178	0,474	0,041	0,124	0,086	0,08	0,131
<b>HREE</b>	0,074	0,063	3,396	3,227	0,126	0,248	1,526	0,215	0,392	0,104	3,9	0,781	0,101	1,305	0,974	1
<b>HREEY</b>	0,176	0,215	9,832	8,939	0,174	1,099	2,734	1,074	1,56	0,136	10,823	3,384	0,423	3,815	1,717	2,445

## Fluorita – Próxima a Faixa Placha

Fluorita – Biotita granito															
(%)	NC3A 1	NC3A 2	NC3A 3	NC3A 4	NC3A 5	NC3A 6	NC3A 7	NC3A 8	NC3A 9	NC3A 10	NC3A 11	NC3A 12	NC3A 13	NC3A 14	NC3A 15
F	43,138	45,022	36,071	48,845	45,395	20,827	31,628	46,573	45,257	45,407	40,3	44,525	50,907	49,411	45,727
SiO <sub>2</sub>	0,223	0,029	0,442	0,063	0,059	1,194	0,254	0,036	0,442	0,006	0,162	0,019	0,204	0,028	0,072
Al <sub>2</sub> O <sub>3</sub>	2,06	0,027	0,167	0,061	0,035	0,308	0,242	0,163	0,158	0,04	0,236	0,107	0,183	0,004	0,166
FeO	0,359	0,059	1,086	0,051	0,044	0,954	0,088	0,09	0,101	0,004	0,08	0,101	0,087	0	0,086
CaO	56,237	60,949	45,741	59,803	56,657	25,956	48,976	54,715	54,037	52,964	56,413	58,106	55,315	54,187	57,639
Na <sub>2</sub> O	0,042	0,026	0,024	0,035	0,028	0	0,025	0,021	0,026	0,049	0,063	0,069	0,063	0,037	0,091
TiO <sub>2</sub>	0	0	0	0,081	0,112	0,092	0,106	0	0,019	0,037	0,2	0,125	0,056	0,099	0
MnO	0,079	0	0,009	0	0	0,027	0	0	0	0,004	0,042	0,026	0	0	0
K <sub>2</sub> O	0,005	0	0,1	0,017	0	0,039	0	0,006	0	0,009	0,017	0,01	0,02	0	0,115
P <sub>2</sub> O <sub>5</sub>	0,016	0,07	0,116	0,032	0,07	0,043	0,038	0,034	0	0,006	0,015	0,021	0,052	0,061	0,05
Nb <sub>2</sub> O <sub>5</sub>	0	0,11	0	0,054	0	0,1	0	0,103	0,048	0	0	0,179	0	0	0
HfO <sub>2</sub>	0	0,15	0	0,217	0,068	0	0	0	0	0,095	0,033	0	0	0	0
Y <sub>2</sub> O <sub>3</sub>	0,862	0,539	1,63	0,696	0,453	2,354	0,205	0,555	1,021	1,752	0,276	0,618	0,851	1,223	0,181
Ta <sub>2</sub> O <sub>5</sub>	0	0,197	0	0,094	0	0,081	0,159	0	0	0,028	0,002	0	0,187	0	0
UO <sub>2</sub>	0	0	0	0	0	0	0	0	0	0	0	0	0	0	0
BaO	0,017	0	0	0,005	0,011	0,033	0	0	0	0	0	0	0,002	0,003	0
PbO	0,042	0,041	0,306	0	0	0,471	0,039	0	0	0	0,015	0,03	0	0	0
ThO <sub>2</sub>	0,594	0,053	0,573	0,045	0,069	2,045	0,027	0,016	0,051	0,067	0	0,244	0,003	0,035	0,069
SrO	0	0,066	0,02	0,163	0,106	0,137	0,148	0,004	0,062	0,254	0	0	0	0,039	0,001
ZrO <sub>2</sub>	0	0	0	0,004	0	0	0,078	0,011	0	0	0	0,056	0	0,061	0,01
La <sub>2</sub> O <sub>3</sub>	1,395	0	0,561	0,048	0	9,218	0,044	0,029	0,055	0,055	0	0,601	0,014	0	1,169
Ce <sub>2</sub> O <sub>3</sub>	2,139	0,045	3,326	0,349	0,061	26,612	0,068	0,12	0,267	0,104	0,071	0,598	0,044	0,038	2,262
Pr <sub>2</sub> O <sub>3</sub>	0,45	0,014	0,269	0,025	0	2,618	0,054	0	0,031	0,027	0	0,164	0,028	0	0,176
Nd <sub>2</sub> O <sub>3</sub>	1,681	0,025	1,371	0,048	0	10,395	0,017	0,033	0,062	0,074	0,027	0,438	0,002	0,033	0,847
Sm <sub>2</sub> O <sub>3</sub>	0,643	0	0,222	0	0	2,465	0	0	0	0	0,025	0,054	0	0	0,133
Eu <sub>2</sub> O <sub>3</sub>	0,065	0,009	0,035	0,028	0,075	0,458	0	0	0,029	0,009	0,043	0	0,023	0,004	0,006
Gd <sub>2</sub> O <sub>3</sub>	0,622	0	0,286	0	0,009	2,166	0,014	0,036	0,04	0,037	0	0,041	0,002	0,024	0,318
Tb <sub>2</sub> O <sub>3</sub>	0	0	0	0	0	0	0	0	0	0	0,001	0	0	0,018	0
Dy <sub>2</sub> O <sub>3</sub>	0,649	0,059	0,259	0	0	1,53	0	0	0	0,109	0,059	0,063	0	0	0,062
Ho <sub>2</sub> O <sub>3</sub>	0,086	0,048	0,031	0,011	0,032	0,19	0,054	0,072	0	0,125	0,072	0,094	0,095	0,058	0
Er <sub>2</sub> O <sub>3</sub>	0,249	0,065	0,059	0,045	0,062	0,561	0,059	0,018	0,012	0,057	0,029	0,048	0,013	0,063	0,137
Tm <sub>2</sub> O <sub>3</sub>	0,08	0	0,033	0	0,063	0,173	0	0	0	0	0,017	0	0	0	0,017
Yb <sub>2</sub> O <sub>3</sub>	0	0,033	0,074	0,167	0,077	0,235	0	0,061	0,092	0,017	0,006	0,034	0,024	0,104	0,107
Lu <sub>2</sub> O <sub>3</sub>	0,058	0,029	0	0,009	0	0,112	0	0	0	0	0,028	0,013	0,024	0	0,049

<b>Total</b>	111,791	107,665	102,224	92,811	110,996	103,486	111,394	82,323	102,696	101,81	101,336	98,232	106,384	108,199	105,53
<b>O=F</b>	-18,165	-18,959	-17,585	-15,189	-20,569	-19,116	-8,770	-13,319	-19,612	-19,058	-19,121	-16,970	-18,749	-21,437	-20,807
<b>Total</b>	93,626	88,706	84,639	77,622	90,427	84,370	102,624	69,004	83,084	82,752	82,215	81,262	87,635	86,762	84,723
<b>REE</b>	8,117	0,327	6,526	0,73	0,379	56,733	0,31	0,369	0,588	0,614	0,378	2,148	0,269	0,342	5,283
<b>REY</b>	8,979	0,866	8,156	1,426	0,832	59,087	0,515	0,924	1,609	2,366	0,654	2,766	1,12	1,565	5,464
<b>LREE</b>	6,373	0,093	5,784	0,498	0,136	51,766	0,183	0,182	0,444	0,269	0,166	1,855	0,111	0,075	4,593
<b>HREE</b>	1,744	0,234	0,742	0,232	0,243	4,967	0,127	0,187	0,144	0,345	0,212	0,293	0,158	0,267	0,69
<b>HREY</b>	2,606	0,773	2,372	0,928	0,696	7,321	0,332	0,742	1,165	2,097	0,488	0,911	1,009	1,49	0,871

---

## Oxifluoretos

---

### Oxifluoretos – Biotita granito

---

(%)	NC3A																			
-----	------	------	------	------	------	------	------	------	------	------	------	------	------	------	------	------	------	------	------	------

	1	2	3	4	5	6	7	8	9	10	11	12	13	14	15	16	17	18	19	20
<b>F</b>	8,445	9,065	7,445	7,441	8,068	5,491	10,261	7,607	7,233	8,126	7,952	10,788	9,218	8,145	8,636	7,256	8,071	7,761	8,408	7,634
<b>SiO<sub>2</sub></b>	0,202	0,541	0,241	0	0,055	0,044	0,01	0	3,559	9,576	0	0,313	3,759	0	5,584	0,059	0,676	0	0	0
<b>Al<sub>2</sub>O<sub>3</sub></b>	0,352	0,079	0,07	1,47	0,105	0,345	0,094	0,073	2,677	2,731	0,141	0,354	1,309	0,268	2,571	0,085	0,161	0,037	0,043	0
<b>FeO</b>	1,003	0,193	0,275	0,011	0,126	0,151	0,402	0,122	0,781	2,663	0,046	1,718	2,351	0,08	10,918	0,342	2,39	1,53	0,119	0,079
<b>CaO</b>	1,041	0,609	1,001	0,272	0,724	0,173	4,692	1,073	0,279	0,336	1,025	9,59	37,821	0,7	17,322	1,136	1,814	1,041	0,489	0,398
<b>Na<sub>2</sub>O</b>	0	0	0,058	0	0,033	0	0,039	0,077	0	0	0,096	0,052	0,049	0,022	0,086	0,034	0	0	0	0
<b>TiO<sub>2</sub></b>	0,136	0,195	0	0,114	0,098	0,137	0,222	0,011	0	0,105	0	0	1,831	0,092	0,672	0,466	1,02	0,168	0	0
<b>MnO</b>	0	0	0	0,081	0,096	0	0	0,045	0	0,012	0	0,069	0,047	0	0	0,111	0,156	0,06	0,16	0
<b>K<sub>2</sub>O</b>	0,026	0,043	0,128	0,03	0,027	0,057	0,031	0,02	0,07	0,051	0,069	0,027	0	0,061	0,034	0,095	0,132	0,026	0,03	0,01
<b>P<sub>2</sub>O<sub>5</sub></b>	0,033	0	0,08	0,026	0,021	0,035	0,055	0	0	0,02	0	0,085	0,092	0,003	0,113	0,02	0,049	0,089	0	0,056
<b>Nb<sub>2</sub>O<sub>5</sub></b>	0,097	1,718	0	0	0	0	0	0	0	0,208	0	0	0	0	0,76	0,291	0,743	0,054	0	0
<b>HfO<sub>2</sub></b>	0	0	0,183	0	0	0,034	0	0	0	0,189	0,045	0	0,108	0	0	0	0,068	0,019	0,014	0,116
<b>Y<sub>2</sub>O<sub>3</sub></b>	6,486	3,294	3,806	4,162	4,002	2,474	6,09	3,075	4,085	4,295	5,014	3,89	0,531	3,958	4,477	3,796	4,3	4,929	3,45	3,807
<b>Ta<sub>2</sub>O<sub>5</sub></b>	0,332	0	0,051	0	0,194	0	0,028	0	0	0	0,061	0	0,096	0,22	0	0	0	0	0,096	0
<b>UO<sub>2</sub></b>	0,016	0	0,032	0,006	0,024	0,019	0,04	0	0	0,025	0	0	0	0	0	0,111	0,029	0,006	0,076	0
<b>BaO</b>	0,016	0,006	0,018	0,032	0,02	0	0,031	0,022	0,017	0,027	0,031	0	0,014	0,044	0,038	0,036	0,056	0	0,009	0,048
<b>PbO</b>	0,407	0,548	0,762	0,38	0,198	0	0,498	0,265	1,074	0,624	0,152	0,308	0,04	0,4	0,065	1,4	1,167	0,787	0,098	0,359
<b>ThO<sub>2</sub></b>	1,895	1,798	5,016	1,401	1,625	1,263	4,333	2,086	1,32	1,192	0,673	0,739	0,045	1,894	0,033	1,3	1,472	1,333	0,909	0,871
<b>SrO</b>	0,123	0,141	0,266	0,035	0	0,029	0,064	0,121	0	0,006	0,024	0,058	0,12	0,054	0,042	0,015	0,117	0	0	0
<b>ZrO<sub>2</sub></b>	0	0	0	0	0	0	0	0	0	0	0	0	0	0	0	0	0	0	0,099	0
<b>La<sub>2</sub>O<sub>3</sub></b>	8,746	10,834	11,36	10,959	11,807	10,404	5,891	2,556	9,915	8,859	9,269	3,088	0,164	6,364	0,016	11,651	12,216	11,974	11,651	11,746
<b>Ce<sub>2</sub>O<sub>3</sub></b>	24,982	39,82	31,719	31,715	33,78	32,994	12,331	7,185	29,919	29,427	28,862	11,03	0,169	18,295	0,739	22,445	24,318	22,856	21,591	22,429
<b>Pr<sub>2</sub>O<sub>3</sub></b>	2,589	2,181	2,569	3,102	3,075	3,17	1,723	0,93	2,775	2,978	2,616	0,954	0,025	1,761	0,02	2,945	2,944	3,285	3,179	3,422
<b>Nd<sub>2</sub>O<sub>3</sub></b>	10,866	7,695	9,532	12,829	12,942	13,445	6,97	3,941	11,039	12,873	10,756	2,954	0,036	7,222	0,052	11,626	11,599	13,558	12,57	14,245
<b>Sm<sub>2</sub>O<sub>3</sub></b>	2,875	1,257	1,798	3,034	3,001	3,69	1,893	1,025	3,262	3,532	2,478	0,685	0,01	1,85	0	3,049	2,729	3,167	3,154	3,792
<b>Eu<sub>2</sub>O<sub>3</sub></b>	0,482	0,207	0,411	0,549	0,457	0,527	0,164	0,063	0,384	0,37	0,477	0,192	0	0,24	0	0,414	0,3	0,389	0,297	0,424
<b>Gd<sub>2</sub>O<sub>3</sub></b>	2,931	1,188	1,407	3,052	3,061	3,643	1,948	1,083	2,866	4,142	2,074	0,26	0,05	1,482	0,069	0,474	0,572	0,097	0,389	1,963
<b>Tb<sub>2</sub>O<sub>3</sub></b>	0	0	0	0,124	0,317	0,031	0,236	0,092	0,124	0,543	0	0	0	0	0	0	0	0	0,045	0,774
<b>Dy<sub>2</sub>O<sub>3</sub></b>	2,247	0,894	0,799	2,142	1,168	1,592	1,683	1,089	1,495	2,566	1,03	0,275	0,018	1,1	0,08	2,584	2,393	1,042	1,195	2,552
<b>Ho<sub>2</sub>O<sub>3</sub></b>	0,011	0,001	0,184	0,19	0,141	0,195	0,266	0,073	0,239	0,196	0,248	0,105	0,093	0,158	0,137	0,208	0,539	0,265	0,311	0,416
<b>Er<sub>2</sub>O<sub>3</sub></b>	0,465	0,312	0,318	0,231	0,132	0,146	0,425	0,284	0,208	0,23	0,214	0,085	0,013	0,231	0,058	0,632	0,51	0,276	0,364	0,3
<b>Tm<sub>2</sub>O<sub>3</sub></b>	0,227	0,06	0,123	0,123	0,124	0,108	0,16	0,116	0,111	0,261	0,143	0,087	0,017	0,05	0	0,108	0,163	0,136	0,099	0,163
<b>Yb<sub>2</sub>O<sub>3</sub></b>	0,174	0,177	0,047	0,133	0,032	0	0,157	0,229	0	0,07	0,073	0,094	0,003	0,098	0,067	0,34	0,267	0	0,274	0,116
<b>Lu<sub>2</sub>O<sub>3</sub></b>	0,263	0,114	0,101	0,072	0,022	0,126	0,106	0,088	0,021	0,021	0,079	0,008	0	0,075	0,002	0,199	0,091	0,091	0,117	0,188
<b>Total</b>	77,468	82,97	79,8	83,716	85,475	80,323	60,843	33,351	83,453	96,254	73,648	47,808	58,029	54,867	52,591	73,228	81,062	74,976	69,236	75,908
<b>O=F</b>	<b>-3,556</b>	<b>-3,817</b>	<b>-3,135</b>	<b>-3,133</b>	<b>-3,397</b>	<b>-2,312</b>	<b>-4,321</b>	<b>-3,203</b>	<b>-3,046</b>	<b>-3,422</b>	<b>-3,349</b>	<b>-4,543</b>	<b>-3,882</b>	<b>-3,430</b>	<b>-3,637</b>	<b>-3,056</b>	<b>-3,399</b>	<b>-3,268</b>	<b>-3,541</b>	<b>-3,215</b>
<b>Total</b>	73,912	79,153	76,665	80,583	82,078	78,011	56,522	30,148	80,407	92,832	70,299	43,265	54,147	51,437	48,954	70,172	77,663	71,708	65,695	72,693

<b>REE</b>	56,858	64,74	60,368	68,255	70,059	70,071	33,953	18,754	62,358	66,068	58,319	19,817	0,598	38,926	1,24	56,675	58,641	57,136	55,236	62,53
<b>REEY</b>	63,344	68,034	64,174	72,417	74,061	72,545	40,043	21,829	66,443	70,363	63,333	23,707	1,129	42,884	5,717	60,471	62,941	62,065	58,686	66,337
<b>LREE</b>	50,54	61,994	57,389	62,188	65,062	64,23	28,972	15,7	57,294	58,039	54,458	18,903	0,404	35,732	0,827	52,13	54,106	55,229	52,442	56,058
<b>HREE</b>	6,318	2,746	2,979	6,067	4,997	5,841	4,981	3,054	5,064	8,029	3,861	0,914	0,194	3,194	0,413	4,545	4,535	1,907	2,794	6,472
<b>HREEY</b>	12,804	6,04	6,785	10,229	8,999	8,315	11,071	6,129	9,149	12,324	8,875	4,804	0,725	7,152	4,89	8,341	8,835	6,836	6,244	10,279

<b>Oxifluoretos – granito greisenizado</b>					
<b>(%)</b>	<b>NC11A 1</b>	<b>NC11A 2</b>	<b>NC11A 3</b>	<b>NC11A 4</b>	<b>NC11A 5</b>
F	8,199	6,1	8,627	6,332	5,836
SiO <sub>2</sub>	0,108	0	0,175	0	0,108
Al <sub>2</sub> O <sub>3</sub>	0,049	0,008	0,004	0,013	0,026
FeO	2,137	0,643	5,877	0,059	0,245
CaO	3,991	0,209	10,155	0,086	0
Na <sub>2</sub> O	0	0	0,042	0	0
TiO <sub>2</sub>	0	0,131	0	0	0,12
MnO	0,145	0,03	0,116	0	0
K <sub>2</sub> O	0,15	0,026	0,062	0,01	0,255
P <sub>2</sub> O <sub>5</sub>	0	0,073	0	0,04	0,012
Nb <sub>2</sub> O <sub>5</sub>	0,062	0	0,066	0	0
HfO <sub>2</sub>	0	0	0	0,145	0,191
Y <sub>2</sub> O <sub>3</sub>	0,707	0,545	0,978	0,416	0,436
Ta <sub>2</sub> O <sub>5</sub>	0	0	0	0,053	0
UO <sub>2</sub>	0	0	0,02	0,001	0
BaO	0	0,022	0,028	0	0,067
PbO	0,025	0	0	0,002	0
ThO <sub>2</sub>	0,794	0,945	1,669	0,173	1,046
SrO	0,09	0,082	0,296	0	0,016
ZrO <sub>2</sub>	0	0	0	0	0
La <sub>2</sub> O <sub>3</sub>	12,731	16,867	11,075	25,729	15,632
Ce <sub>2</sub> O <sub>3</sub>	25,868	25,913	20,277	24,067	25,068
Pr <sub>2</sub> O <sub>3</sub>	3,144	3,349	2,703	2,341	3,46
Nd <sub>2</sub> O <sub>3</sub>	11,606	13,123	10,752	8,366	13,622
Sm <sub>2</sub> O <sub>3</sub>	2,03	1,877	1,859	0,775	2,251
Eu <sub>2</sub> O <sub>3</sub>	0,381	0,457	0,457	0,258	0,472
Gd <sub>2</sub> O <sub>3</sub>	0	0	0	0	0
Tb <sub>2</sub> O <sub>3</sub>	0	0	0	0	0
Dy <sub>2</sub> O <sub>3</sub>	0	0	0,034	0,054	0,036
Ho <sub>2</sub> O <sub>3</sub>	0	0	0	0	0
Er <sub>2</sub> O <sub>3</sub>	0,18	0	0,065	0,077	0,015
Tm <sub>2</sub> O <sub>3</sub>	0	0,117	0	0	0,102
Yb <sub>2</sub> O <sub>3</sub>	0	0	0,021	0,065	0
Lu <sub>2</sub> O <sub>3</sub>	0,003	0	0,034	0	0
<b>Total</b>	<b>64,201</b>	<b>64,417</b>	<b>66,765</b>	<b>62,73</b>	<b>69,016</b>
<b>O=F</b>	<b>-3,453</b>	<b>-2,569</b>	<b>-3,633</b>	<b>-2,666</b>	<b>-2,458</b>
<b>Total</b>	<b>60,748</b>	<b>61,848</b>	<b>63,132</b>	<b>60,064</b>	<b>66,558</b>
REE	55,943	61,703	47,277	61,732	60,658
REEY	56,65	62,248	48,255	62,148	60,849
LREE	55,76	61,586	47,123	61,536	60,505
HREE	0,183	0,117	0,154	0,196	0,153
HREEY	0,89	0,662	1,132	0,612	0,344

